



EUROPEAN
COMMISSION

European
Research Area

Carbon-14 Source Term

CAST



Report on ^{14}C release speciation from carbon steel under alkaline reducing conditions (D2.7)

Author(s):

Frank Druyts, Sébastien Caes, Wouter Van Renterghem and Elie Valcke

Date of issue of this report: 12/06/2017

The project has received funding from the European Union's Seventh Framework Programme for research, technological development and demonstration under grant agreement no. 604779, the CAST project'		
Dissemination Level		
PU	Public	x
RE	Restricted to the partners of the CAST project	
CO	Confidential, only for specific distribution list defined on this document	

CAST – Project Overview

The CAST project (CARbon-14 Source Term) aims to develop understanding of the potential release mechanisms of carbon-14 from radioactive waste materials under conditions relevant to waste packaging and disposal to underground geological disposal facilities. The project focuses on the release of carbon-14 as dissolved and gaseous species from irradiated metals (steels, Zircalloys), irradiated graphite and from ion-exchange materials as dissolved and gaseous species.

The CAST consortium brings together 33 partners with a range of skills and competencies in the management of radioactive wastes containing carbon-14, geological disposal research, safety case development and experimental work on gas generation. The consortium consists of national waste management organisations, research institutes, universities and commercial organisations.

The objectives of the CAST project are to gain new scientific understanding of the rate of release of carbon-14 from the corrosion of irradiated steels and Zircalloys and from the leaching of ion-exchange resins and irradiated graphites under geological disposal conditions, its speciation and how these relate to carbon-14 inventory and aqueous conditions. These results will be evaluated in the context of national safety assessments and disseminated to interested stakeholders. The new understanding should be of relevance to national safety assessment stakeholders and will also provide an opportunity for training for early career researchers.

For more information, please visit the CAST website at:

<http://www.projectcast.eu>

CAST

Report on ^{14}C release speciation from carbon steel under alkaline reducing conditions

(D2.7)

CAST		
Work Package: 2	CAST Document no. :	Document type:
Task: 2.3	CAST-2017-D2.7	R
Issued by: SCK•CEN		Document status:
Internal no. : SCK•CEN/RDW/2017/Pub-12		Final

Document title
Report on ^{14}C release speciation from carbon steel under alkaline reducing conditions

Executive Summary

The aim of the work at SCK•CEN in the framework of Work Package 2 of the CAST project was to investigate the release of ^{14}C from carbon steels representative for the reactor pressure vessel (RPV) steel of Belgian nuclear power plants and the ^{14}C speciation in a cementitious environment, which is relevant for the Belgian geological disposal concept, which involves placing the RPV steel in a concrete monolith. To achieve this, we designed static and accelerated corrosion tests, and we obtained irradiated reference material representative for the RPV steel at end-of-life in the Belgian power plants. The static tests consisted of exposing the sample to a representative environment (anaerobic, high pH) for several months without imposing a potential, while in the shorter accelerated tests an electrochemical setup was used to fix the potential of the sample at a more anodic value than the corrosion potential (in order to accelerate the corrosion). In order to determine the speciation of carbonaceous compounds, we used gas chromatography. In addition, we applied liquid scintillation counting to measure the total activity of ^{14}C , total (in)organic analysis, and ion chromatography.

The unirradiated sample was a Charpy-V specimen which was cut into smaller pieces. The nitrogen content in the unirradiated material was measured to be approximately $19 \mu\text{g/g}$, which is at the lower end of the $20\text{-}30 \mu\text{g/g}$ range mentioned in the literature. Calculations showed that this would lead, after irradiation, to a ^{14}C activity of 175 Bq/g in the JRQ steel.

Metallographic analysis was performed on both unirradiated and irradiated material in order to investigate the influence of irradiation on the metallic structure. The grain structure is that

of a ferritic-bainitic steel, which is the expected grain structure for a RPV steel. The main defects present in both the unirradiated and irradiated material are line dislocations, with the dislocation density diminishing by irradiation. Another effect of irradiation is the formation of a small amount of dislocation loops. Two types of carbides were found in both materials: Fe₃C and Mo₂C. The concentration of Fe₃C is increased by irradiation.

Measurements of the ⁶⁰Co release of JRQ carbon steel in pure portlandite water showed that the corrosion rate seems to obey a parabolic law, as reported in literature. The obtained corrosion rates however are very low, below 10 nm/year. This can be explained by experimental artefacts such as precipitation in the portlandite solution.

To obtain information on the behaviour of JRQ carbon steel in simulated geological disposal conditions, long-running leaching corrosion tests were performed. Accelerated (polarised) corrosion tests were performed to obtain some indication of the corrosion mechanism and the formation of lower carbon molecules in a shorter reaction time. The electrolyte used was a saturated portlandite Ca(OH)₂ aqueous solution of pH 12.5, representative of the geological disposal conditions. In addition, for a second batch of accelerated tests, 0.5 M of CaCl₂ was added to the portlandite solution, stimulating pitting corrosion in order to obtain a higher yield of corrosion products.

The accelerated tests were performed in glass test cells equipped with a standard three-electrode setup, using a house-made Ag/AgCl electrode as reference electrode, a platinum mesh as counter electrode, and an embedded and polished JRQ carbon steel sample as working electrode. Gas chromatography after the tests in saturated portlandite water showed no carbon-containing corrosion products. Tests in a portlandite solution with added CaCl₂ revealed a hydrogen peak due to pitting corrosion but no carbon-based molecules were formed.

The static (leaching) tests were performed in PEEK-lined steel vials with an internal volume of 50 cm³ filled with 35 cm³ of electrolyte under a nitrogen atmosphere. After closing the cell gastight with a lid, the whole setup was left behind a lead wall for 231 days. Gas chromatography revealed that during the static tests, hydrogen, methane, ethene, and ethane

CAST

Report on ^{14}C release speciation from carbon steel under alkaline reducing conditions

(D2.7)

were produced. Assuming that all carbon released from the metal is transformed into gaseous carbon compounds, this yields a corrosion rate of 68 to 117 nm/year.

List of Contents

Executive Summary	i
List of Contents	v
1 Introduction	1
2 Experimental	3
2.1 Materials	3
2.1.1 Description of the unirradiated samples	3
2.1.2 Irradiated samples	4
2.2 Nitrogen content analysis	5
2.3 γ -ray spectrometry	6
2.4 Metallographic analysis	6
2.4.1 Sample preparation	6
2.4.2 Grain size determination	7
2.5 Corrosion experiments	8
2.5.1 Choice of the electrolyte	8
2.5.2 Description of corrosion setups and sampling	9
2.5.2.1 Static corrosion tests	9
2.5.2.2 Accelerated corrosion tests	11
2.6 Determination of the carbon speciation	15
2.6.1 Gas chromatography	15
2.6.1.1 Identification of peaks	19
2.6.1.2 Determination of the detection limits	22
2.6.2 Total (In)Organic Carbon	23
2.6.3 Ion Chromatography (carboxylic acid analysis)	24
2.6.4 Liquid Scintillation Counting	24
3 Results and discussion	25
3.1 Nitrogen analysis	25
3.2 Metallographic analysis	25
3.2.1 Unirradiated sample	25
3.2.2 Active sample	33
3.3 γ -ray spectrometry	37
3.4 Estimation of the ^{14}C content of irradiated samples	37
3.5 Corrosion rate determination from ^{60}Co measurements	39
3.5.1 Description of the test	39
3.5.2 Results and discussion	39
3.6 Polarisation curves for JRQ C-steel	42
3.6.1 Unirradiated samples	43
3.6.2 Irradiated samples	44
3.7 Carbon speciation after leaching and polarised corrosion	46
3.7.1 Analysis of the gas phase by gas chromatography	46
3.7.1.1 Accelerated corrosion tests	46
3.7.1.2 Static corrosion tests	56
3.7.2 Analysis of the liquid samples	59

3.7.2.1 Carbon speciation by total organic/inorganic carbon analysis and by ion chromatography	59
3.7.3 ^{14}C activity detection by Liquid Scintillation Counting	64
4 Conclusions	65
References	67
Appendix 1: Precipitation probability of CaCO_3 (calcite) at a pH of 12.5	70
Appendix 2: Validation of the measurement of methane, carbon dioxide, ethene, ethane, propene and propane in gas samples by the <i>GC-2010 Plus</i> gas chromatograph	71
Appendix 3. Corrosion rate calculation from the I vs. t plot	85
Appendix 4. Corrosion rate calculation from the carbon-based gas production during the leaching tests	87
Appendix 5. Total inorganic / organic carbon content and ion chromatography results	90

1 Introduction

In the safety assessment of the geological disposal of high level nuclear waste, ^{14}C is a critical radionuclide because of its long half-life (5730 years) and its high mobility in the geosphere and biosphere. It is possible for ^{14}C to be released as the result of corrosion or waste degradation processes. The speciation of ^{14}C will depend on the speciation of its precursor (it is generally assumed that the main precursor of ^{14}C in irradiated ferrous materials is ^{14}N , but there are ^{14}C production pathways with ^{13}C and ^{17}O as precursors) and the chemical conditions in the repository. The question also arises whether the chemical bond of the precursor is maintained during irradiation.

The international project CAST (Carbon-14 Source Term), which is partially funded through the Euratom Seventh Framework Programme, aims at understanding the generation and release of ^{14}C containing species in conditions relevant for waste packaging and geological disposal. The project is focusing on ^{14}C releases from irradiated metals (steels and zirconium alloys), irradiated graphite, and spent ion-exchange resins, as dissolved and gaseous species. The results of these studies will be transferred to the national programmes where they will be used for further development of the national safety cases. Within the CAST project, Work Package 2 focuses on irradiated steels – both stainless steels representative for reactor internals and carbon steels representative for the reactor pressure vessel material.

The aim of the work at SCK•CEN in the framework of Work Package 2 of the CAST project was to investigate the release of ^{14}C from carbon steels representative for the reactor pressure vessel (RPV) steel of Belgian nuclear power plants and the ^{14}C speciation in a cementitious environment, which is relevant for the Belgian geological disposal concept, which involves placing the RPV steel in a concrete monolith. To achieve this, we designed static and accelerated corrosion tests, and we obtained irradiated reference material representative for the RPV steel at end-of-life in the Belgian power plants. The static tests consisted of exposing the sample to a representative environment (anaerobic, high pH) for several months without imposing a potential, while in the shorter accelerated tests an

electrochemical setup was used to fix the potential of the sample at a more anodic value than the corrosion potential (in order to accelerate the corrosion). It is well known that in highly alkaline environments carbon steel develops a thin, coherent passive film leading to very low corrosion rates, in the order of 0.1 $\mu\text{m}/\text{year}$ [DIOMIDIS, 2014; FUJISAWA, 1997; FUJIWARA, 2002; GRAUER, 1991a; GRAUER, 1991b; HONDA, 2009; KREIS, 1993; KANEKO, 2004; KURSTEN, 2014; MIHARA, 2002; NAISH, 1990; NAISH, 1993; NAISH, 2001; NEWMAN, 2010; NEWMAN, 2015; NISHIMURA, 2003; RWMC, 1998; SMART, 2002; SMART, 2009]. Therefore, we expect a very low release of carbon species through corrosion of the carbon steel.

This report gives an overview of the entire experimental programme carried out at SCK•CEN in the framework of WP2 of the CAST project. It contains information on the samples (both unirradiated and irradiated), the properties of the samples, the results from corrosion tests, and the results from speciation studies.

2 Experimental

2.1 Materials

The material of choice for this study was JRQ steel, which is an internationally accepted reference material representative for RPV steels. Its manufacturing process and general properties are described elsewhere [IAEA, 2001]. JRQ is the IAEA designation for the ASTM A533 grade B class 1 steel.

2.1.1 Description of the unirradiated samples

The unirradiated sample we received was a Charpy-V specimen. It was cut as shown in Figure 1 and prepared for accelerated testing in an electrochemical setup (for information on the manufacturing of the electrodes, see Section 2.3.2). The nominal composition for JRQ steel is given in Table 1.



Figure 1. General view of the cut JRQ Charpy-V sample.

Table 1. Nominal composition of JRQ C-steel (ASTM A533).

Element	C	Si	Mn	P	S	Cr	Mo	Ni
wt. %	0.10-0.17	0.60-0.90	0.50-0.80	0.025	0.035	0.50-0.75	0.15-0.25	<0.25

2.1.2 Irradiated samples

The irradiated material was representative for end-of-life conditions in nuclear power plants and as such offered the advantage of providing realistic input data on ¹⁴C release into the national safety cases (WP6). The samples we received were irradiated in 1993 in the BR2 reactor at SCK•CEN in the Vestale irradiation loop (290 ± 15 °C ; 150 bar). There were different samples for the static and the accelerated tests. The sample for the static tests was rectangular with original dimensions 1 x 10 x 26 mm and had the code 16-6-18/1R. This was cut into three subsamples with the dimensions and contact dose rates given in Table 2. The sample for accelerated tests originally was a ½ Charpy-V specimen from which the fissured edge had been cut away. The dimensions of the sample were 10 x 26.1 x 4.5 mm (Figure 2) and its dose rate was 3.6 mSv/h in contact. The sample was manually cut with a metallic handsaw to dimensions fit for the manufacturing of an electrode (the inner cross section of the electrode holder was approximately 25 mm). The final dimensions of the sample for accelerated testing were 10 x 6 x 4.5 mm (Figure 3) and the sample had the code JRQ 16-6-18/AT1. It had a contact dose rate of 920 µSv/h.

Table 2. Dimensions and contact dose rates for the subsamples used for static tests.

Sample identification	Dimensions (mm)	Contact dose (µSv/h)
16-6-18/1RA	8.06 x 10 x 1	350
16-6-18/1RB	8.11 x 10 x 1	360
16-6-18/1RC	8.10 x 10 x 1	350

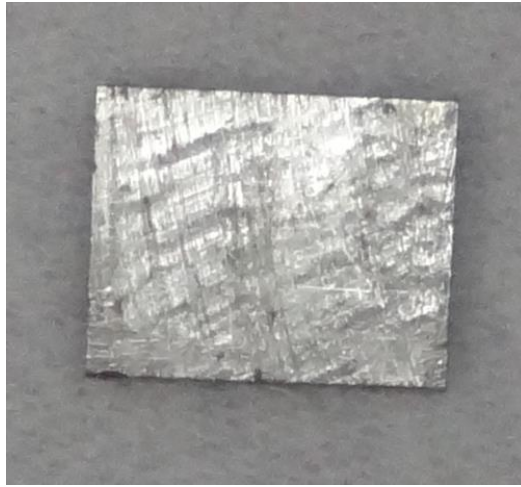


Figure 2. Sample 16-6-18/1RA (for static testing).

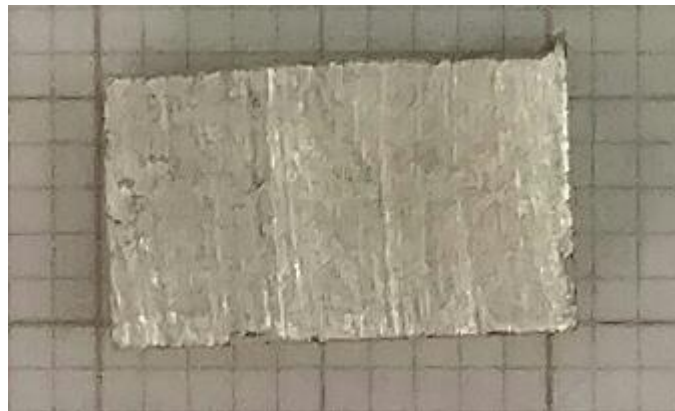


Figure 3. Sample JRQ 16-6-18/AT1 for accelerated testing.

2.2 Nitrogen content analysis

The nitrogen content of the unirradiated samples was measured by using an inert gas fusion method with a LECO TC436 model analyser. The sample was cut into a small cube of ~0.5 g and stored in acetone until the analysis. Before the sample analysis, at least 3 nitrogen blanks were measured and the average was subtracted from the result. The instrument was calibrated using two certified reference materials of different nitrogen concentrations: AR668 with a nitrogen concentration of 29 $\mu\text{g/g}$ (Alpha Resources) and AR660 with a nitrogen concentration of 61 $\mu\text{g/g}$ (Alpha Resources). With these references, the lowest

point, the linearity of the calibration and the calibration factor to apply were checked. The reported lower limit of detection of the method is approximately 1 $\mu\text{g/g}$ for N.

For the analysis, the sample was placed inside a graphite crucible and held between the upper and lower electrodes of an impulse furnace. A high current passed through the crucible, increasing the inner temperature ($> 2500\text{ }^\circ\text{C}$), and leading eventually to the melting of the sample. Gaseous compounds generated in the furnace were released into a flowing inert gas stream (argon or helium). The gas stream was sent to the appropriate infrared detector: a thermal conductivity detector for the analysis of nitrogen. At least three replicate measurements were realised.

2.3 γ -ray spectrometry

For γ -ray spectrometry, two HPGe detectors were used, one from Canberra and one from Ortec. The HPGe-detectors were energy- and efficiency-calibrated over an energy range of 60 to 2000 keV using a γ -ray reference solution with a mixture of 10 different radionuclides. The ORT1 detector was calibrated using a 9ML01ELMA60 (2014) standard solution from LEA (Laboratoire Etalons d'Activité). The CAN2 detector was calibrated using a 12ML01ELMA60 standard source from LEA.

2.4 Metallographic analysis

2.4.1 Sample preparation

Microstructure analysis was performed on unirradiated sample JRQ 12-4A-X17 and irradiated sample JRQ 16-6-18/2RA representative for the leaching tests.

The activity of the irradiated sample was relatively low and its preparation was performed in a fume hood.

A rectangular slice of about 0.6 mm thick was cut from the sample with a Struers Accutom 50 instrument. This slice was mechanically polished on SiC paper with grit sizes 500, 1200, and 4000. When the thickness of the slice was reduced to below 0.3 mm, five discs of 3 mm in diameter were punched out. These discs were polished again on SiC paper until the

thickness was reduced to 0.1 mm. The final step in the sample preparation was electrochemical double jet polishing with a Struers Tenupol-3 instrument. The electrolyte used consisted of 5% perchloric acid and 95% methanol. The polishing solution was cooled to $-50\text{ }^{\circ}\text{C}$ and a voltage of 40 V was applied. Two samples were polished until perforation and one sample was only polished for 10 s. The other two discs were held in reserve.

The first two samples were used for the TEM investigation in a JEOL 3010 microscope operating at 300 kV. Bright field, dark field, and selected area electron diffraction were used to determine the defect structure and precipitates. Energy dispersive X-ray spectroscopy (EDS) was applied for the qualitative determination of the composition of the precipitates. It should be noted that during the EDS measurement a small amount of carbon was deposited on the surface of the sample. Moreover, when analysing small precipitates, it could not be avoided that part of the signal was generated in the steel adjacent to or on top or below the precipitate. Therefore, it was not possible to obtain a quantitative composition of the observed precipitates and carbides, but qualitative statements were possible.

The third sample was used during the SEM investigation in order to determine the grain size. Even though polishing conditions may not have been optimal to reveal the grain structure, it was possible to observe the grain structure under the electron beam of the SEM. The best results were obtained in the back-scattered electron (BSE) images, where the contrast was mainly induced by the atomic weight. Light elements scattered fewer electrons than heavy elements and therefore were darker in the BSE images.

2.4.2 Grain size determination

The grain size of each material was determined from the BSE images of the samples after electrochemical polishing for 10 s. The grain size was determined in accordance with the ASTM standard E112-95, which defines the grain size number (G) as:

$$N = 2^{G-1} \quad (1)$$

Where N is the number of grains per square inch at a magnification of $100\times$ which equals the number of grains per mm^2 at a magnification of $1\times$ divided by 15.50. This number is

obtained by placing a circle of known diameter on the BSE images and by counting the number of grains within the circle. The grains that intersect the circle count for half a grain. Because the SEM images were calibrated the actual diameter of the circle could be determined and the average size of the grains could be calculated. This value was used to calculate the number of grains per mm^2 and the grain size number.

2.5 Corrosion experiments

Two types of corrosion tests have been performed: (i) static corrosion tests (leaching tests) to allow for a realistic corrosion behaviour and associated ^{14}C release and speciation, and (ii) accelerated corrosion tests (polarised tests) with an applied potential, which mainly served for preliminary speciation determination. These corrosion tests were performed under anaerobic and highly alkaline conditions representative for geological disposal.

2.5.1 Choice of the electrolyte

During the WP2 and WP3 technical meeting in Switzerland (27-28 May 2015), a solution of NaOH at pH 12 at room temperature was recommended for the leaching tests. However, all participants were allowed to use their own electrolyte. SCK•CEN decided to use a saturated portlandite $\text{Ca}(\text{OH})_2$ solution for its experiments (pH 12.5). The main reason is that portlandite is more representative for the Belgian waste repository design. The artificial pore water was prepared in a glove box under anaerobic conditions and degassed with nitrogen to reduce the risk of dissolving environmental $^{14}\text{CO}_2$, which would lead to an artefact. The risk of calcite (CaCO_3) precipitation cannot be excluded, as shown in our calculations (see Appendix 1). A mere $18.6 \mu\text{g/L}$ of CO_3^{2-} is enough to provoke CaCO_3 precipitation.

A second type of electrolyte was used exclusively for the accelerated (polarised) corrosion tests in addition to the pure portlandite pore water. This electrolyte was the same as described above, but with the addition of 0.5 M of CaCl_2 (1 M of chloride) in order to increase the corrosion rate by inducing pitting corrosion. By using this electrolyte, we hoped to increase the production of carbon species and make their detection easier.

2.5.2 Description of corrosion setups and sampling

2.5.2.1 Static corrosion tests

Static tests, or leaching tests, were carried out with irradiated samples, in order to have a realistic view on the ^{14}C release rate and ^{14}C speciation.

Figure 4 shows the schematic of the experimental setup. The JRQ carbon steel sample was placed in contact with saturated portlandite pore water (pH ~12.5) inside a steel vial equipped with a PEEK insert. Figure 5 shows photographs of the steel vials before and after assembly. The internal volume of the steel vials was 50 cm³. The vials were each filled with 35 mL of saturated portlandite (Ca(OH)₂) pore water before adding the JRQ carbon steel sample. Afterwards, the lid was screwed to the vial to make it airtight. All these manipulations were performed in a glove bag in a nitrogen atmosphere to ensure that the leaching test took place under anaerobic conditions. The glove bag is shown in Figure 6.

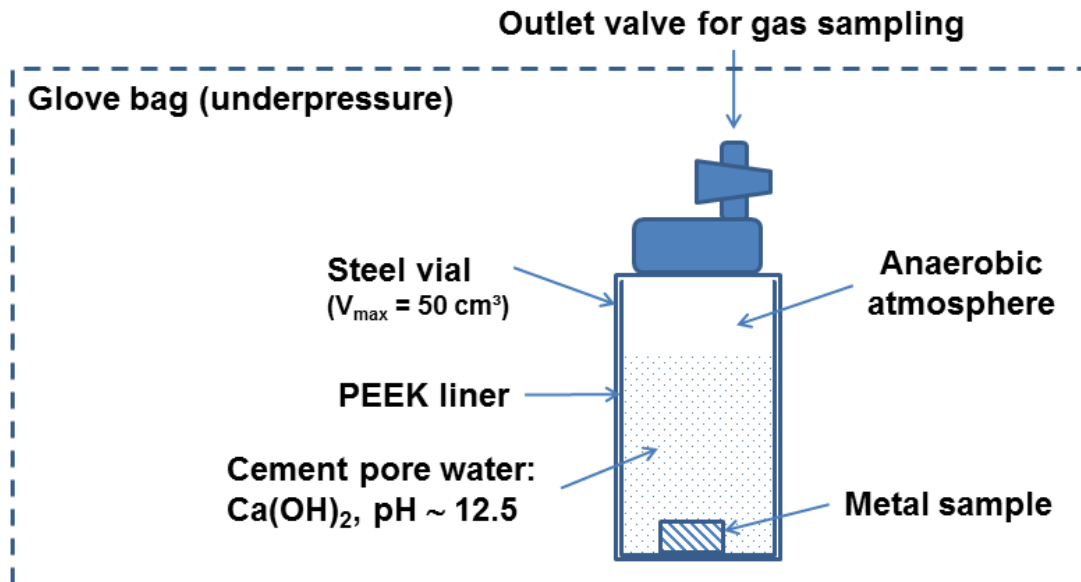


Figure 4. Schematic of the static corrosion test experimental setup.



Figure 5. Picture of the static test setups (A) before assembly and (B) after assembly.



Figure 6. View of the glove bag placed in a fume hood.

After the leaching tests, which lasted for approximately 7.5 months (231 days), gas and liquid samples were taken and analysed for carbon species. The gas sampling was performed with a 500 μL gas tight syringe with a 5 cm long needle (Figure 7). After sampling 500 μL of gaseous phase from the test cell, the needle was stuck into a septum and the syringe was placed in a small solid transport box, in order to avoid displacement of the

syringe's piston. The syringe was then transferred to a gas chromatograph for analysis (for a description of the gas chromatograph, see Section 2.6.1). After taking the gas samples, the lid of the test cell was removed and liquid samples were taken for further analyses (liquid scintillation counting, ion chromatography, TIC/TOC).



Figure 7. Gas tight syringe with removable needle.

2.5.2.2 Accelerated corrosion tests

Accelerated corrosion tests were performed with both unirradiated and irradiated samples. The tests consisted of two parts. In a first phase, polarisation curves were recorded in order to examine the E-i behaviour of the samples in the investigated environment. Then, in a second phase, a pre-determined potential (derived from the polarisation curve) that would result in accelerated, active corrosion, was imposed on the sample.

Manufacturing of the electrodes

The working electrode was manufactured by gluing a steel wire, serving as an electrical connection, to the back of the cut JRQ C-steel sample. The glue used was a conductive silver epoxy (type CW2400, Circuitworks). The specimens were embedded in an epoxy resin and mechanically wet-ground, with successively finer SiC papers, down to 500 grit, and then cleaned with double distilled water and finally left to dry in an argon atmosphere. Figure 8 shows the different steps in the preparation of the electrode.

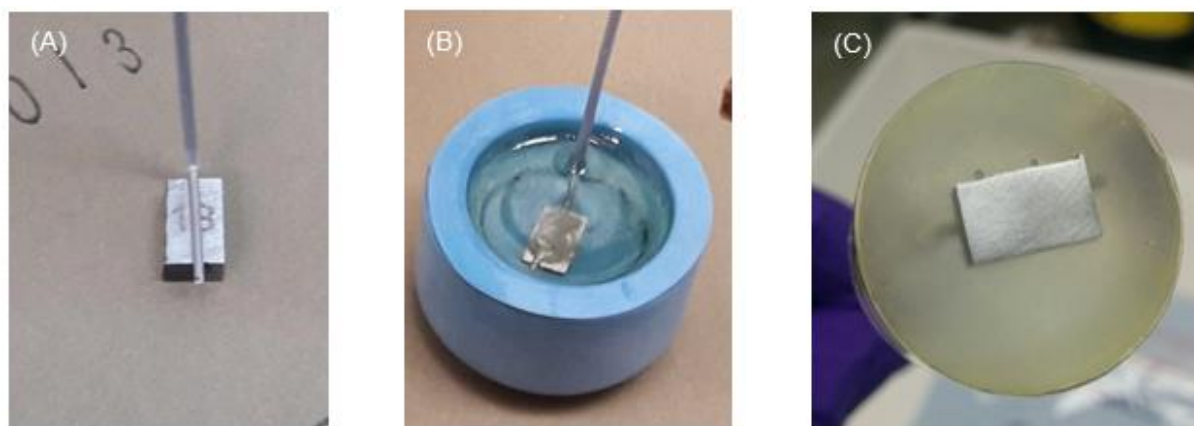


Figure 8. Preparation of the irradiated JRQ C-steel sample (16-6-18/AT1) for the accelerated corrosion test after (A) the gluing step, (B) the embedding step, and (C) the polishing step.

Electrochemical cells

The test cell consisted of a glass vial with an internal volume of approximately 1450 mL and containing three electrodes attached to the lid: (1) the working electrode (carbon steel sample), (2) the platinum counter electrode, and (3) the in-house made Ag/AgCl reference electrode. These electrodes constitute a traditional three-electrode setup described in the general literature on electrochemistry [TAIT, 1994]. Figure 9 shows a schematic representation of the test setup and Figure 10 shows a photograph of the test cell equipped with the three electrodes.

The gas tightness of the cell was determined by using rubber sealing between the cell lid and cell body and filling the cell with helium. The pressure in the glass cell was set to 1.1 bar. During the tightness test, which lasted for two months, the cell pressure and ambient pressure and temperature were monitored (experimental setup in Figure 11). The results are shown in Figure 12. After two months, the pressure inside the cell had decreased from 1.10 to 1.07 bar, which is negligible, given the short actual duration (a few hours up to a week) of the accelerated tests. The sharp intermediate drop in pressure indicates the moment at which the sensors were replaced.

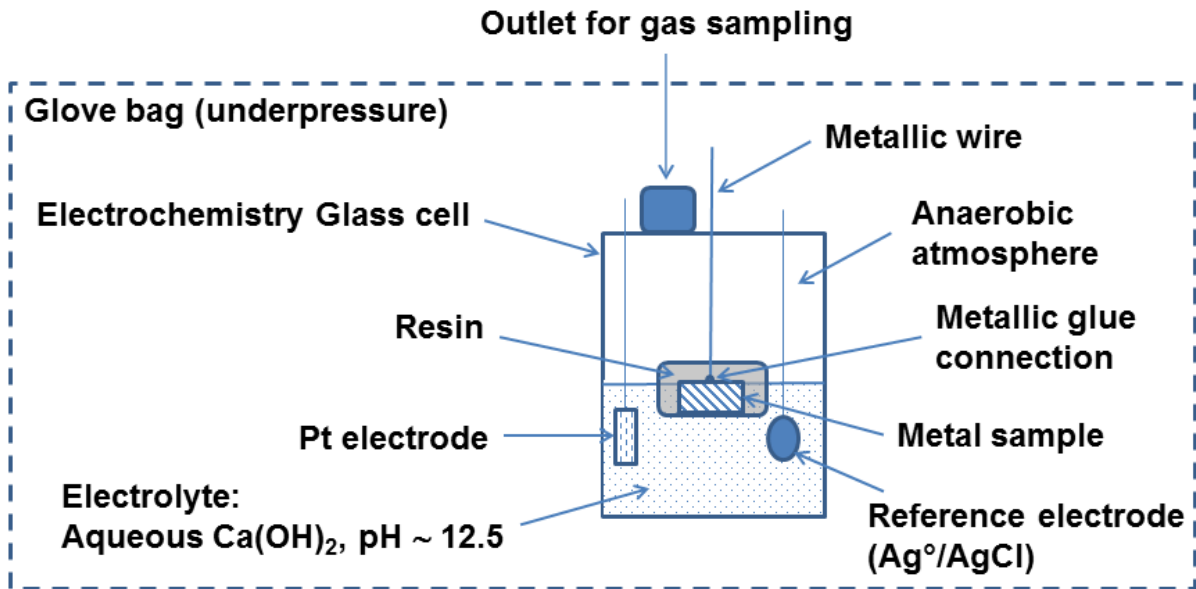


Figure 9. Schematic of the electrochemical cell for accelerated testing.

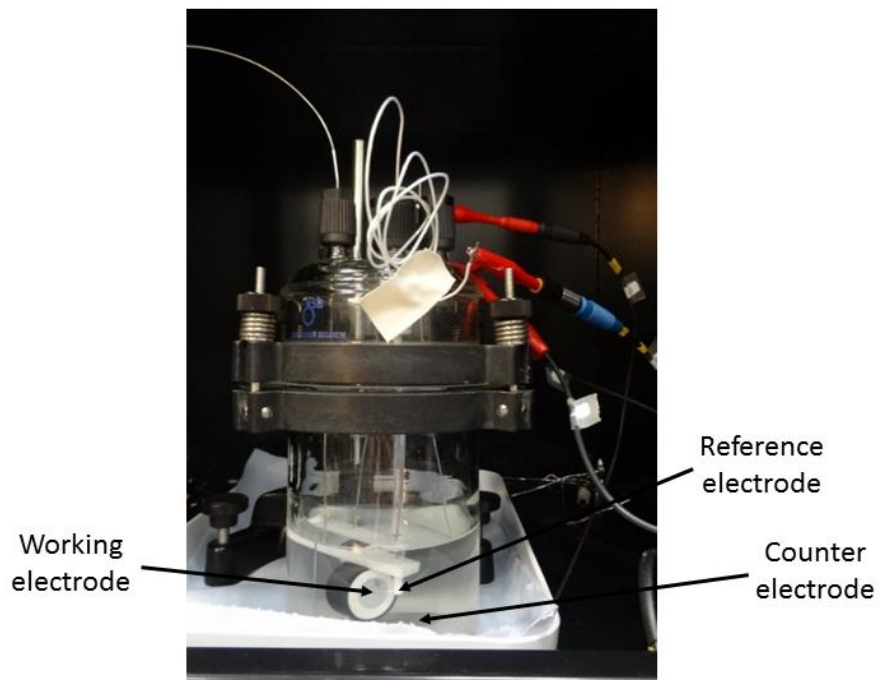


Figure 10. View of the electrochemical cell for accelerated testing.

CAST
Report on ^{14}C release speciation from carbon steel under alkaline reducing conditions
(D2.7)

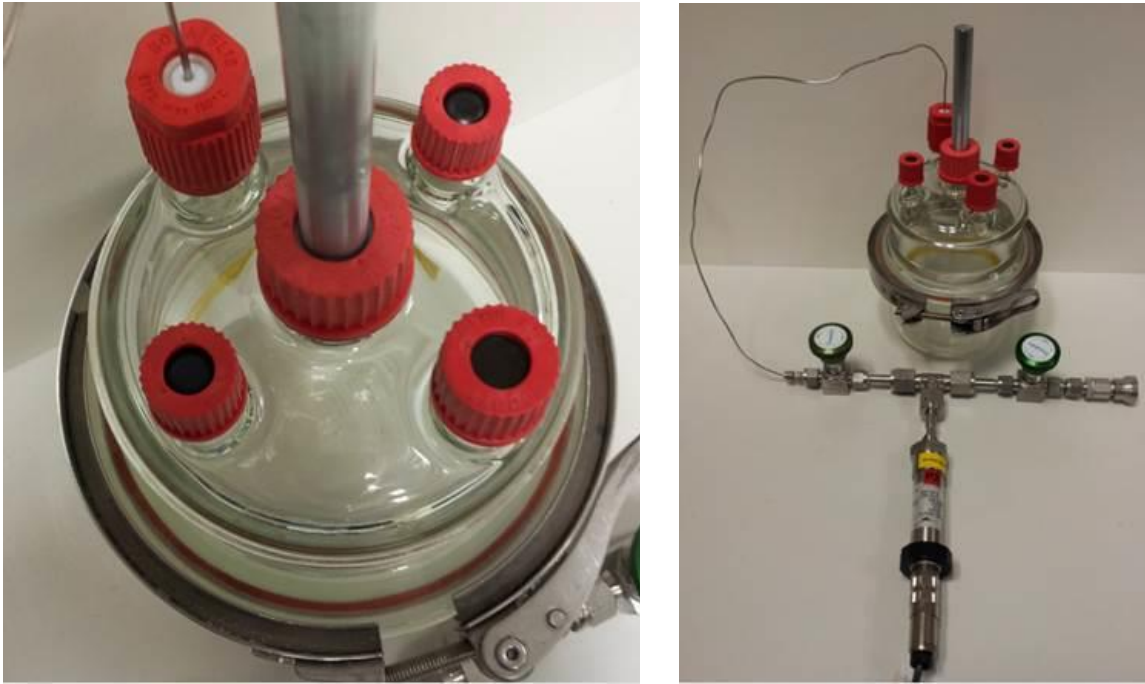


Figure 11. Setup for gas tightness testing of the electrochemical cell.

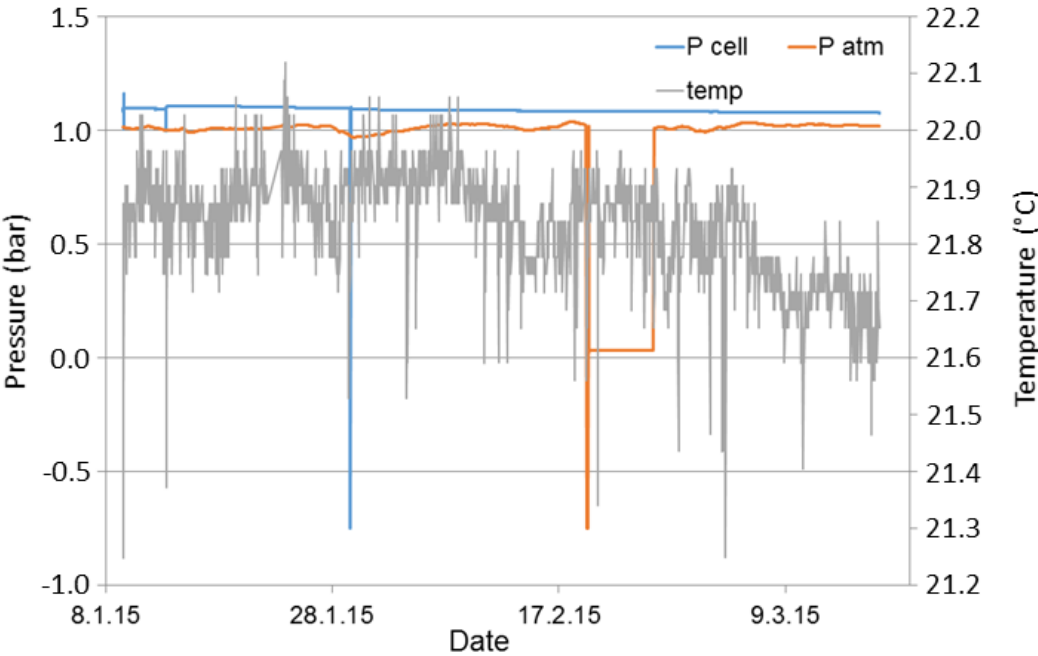


Figure 12. Results from gas tightness testing.

2.6 Determination of the carbon speciation

2.6.1 Gas chromatography

For the determination of the ^{14}C speciation, a gas chromatography system type Shimadzu GC-2010 Plus, tailor-made to our needs, was used (Figure 13). The gas sample can be injected manually (1 on Figure 13) or automatically (2 on Figure 13). In general, the main components of a GC system are an injector, a column and a detector (Figure 14), while the injected sample is transported through the system by a carrier gas.



Figure 13. General view of the gas chromatograph.

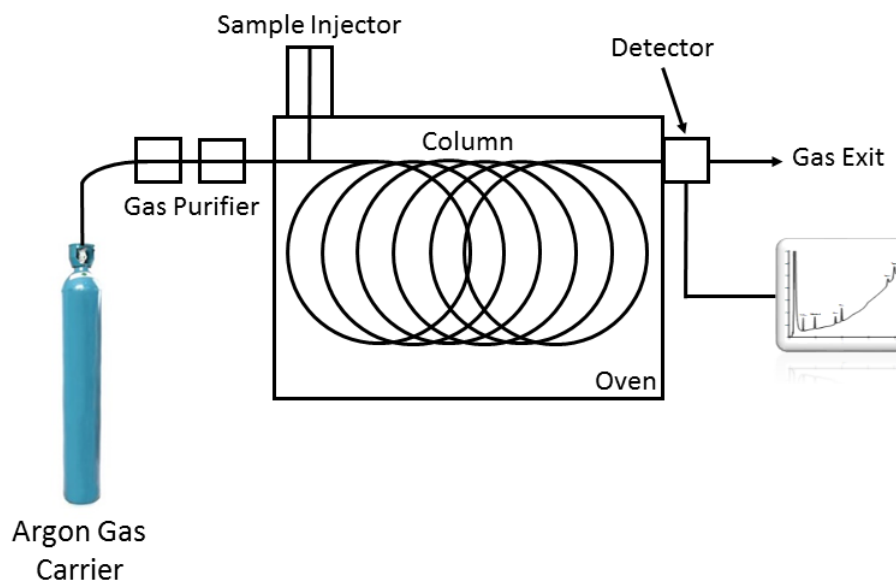


Figure 14. General scheme of a gas chromatograph.

The carrier gas used in our system is pure Argon (N7.5, Air Products). To remove any residual impurities (H_2O , H_2 , O_2 , N_2 , NO , NH_3 , CO , CO_2 , and CH_4), this gas passes through two gas purifiers (VICI Valco Instruments Co. Inc.) before entering the GC column.

The injector used is a split/splitless injector (Figure 15). The gas sample is introduced into the quartz liner of the injector with a syringe and through a septum. At the same time, the carrier gas flows through the column, out of the septum purge and out of the split when the split mode is used. In these conditions, only a fraction of the sample is injected into the column, depending on the split ratio (the split ratio is the ratio between the column flow and the total flow). In contrast, in splitless mode, the entirety of the sample reaches the column.

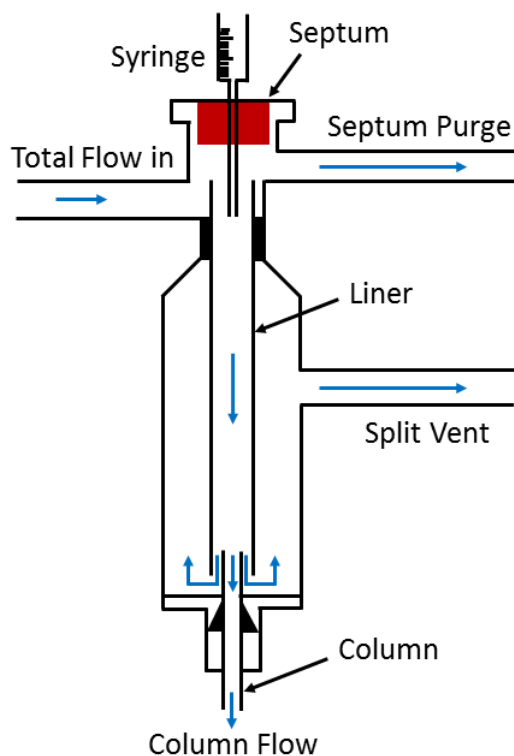


Figure 15. General scheme of a split/splitless GC injector.

Two columns are currently available at SCK•CEN: a ShinCarbon ST composed of a high surface area carbon molecular sieve (Figure 16) and a SH-RTX-1, which is a non-polar column composed of dimethyl polysiloxane. The first column has been developed for separating permanent gases, such as N_2 , O_2 , CO or CO_2 , and mixtures of permanent gases and low hydrocarbons rapidly, without cryogenic cooling. It is a micropacked column with dimensions of 2 m length x 1.27 mm outer diameter x 1 mm inner diameter. The second column is a more universal one. It is a capillary column with dimensions of 30 m length x 0.53 mm inner diameter. The results presented in this report were obtained with the ShinCarbon ST column.

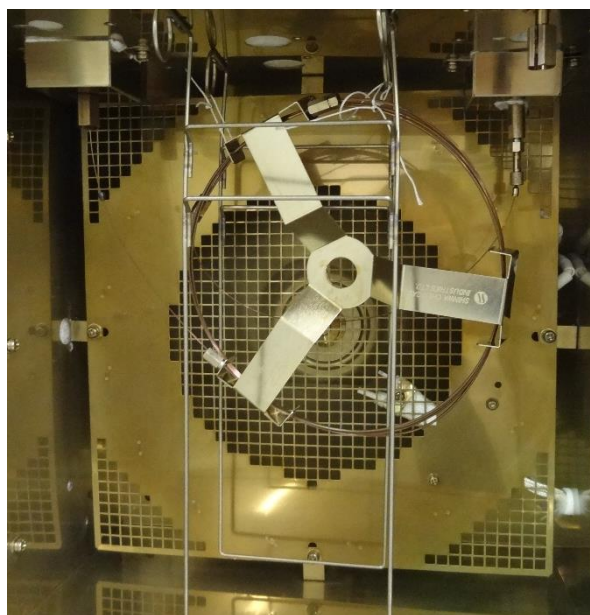


Figure 16. Picture of the ShinCarbon ST column in the furnace of the GC.

Detectors include a Flame Ionisation Detector (FID), a Barrier Discharge Ionisation Detector (BID), and a Pulsed Discharge Helium Ionisation Detector (PDHID). The operation of the FID is based on the detection of ions formed during combustion of organic compounds in a hydrogen flame. The generation of these ions is proportional to the concentration of organic species in the sample gas stream. The response of a FID is semi-universal: all hydrocarbons can be detected. The FID has a detection limit of approximately $1\ \mu\text{g/L}$. In a BID detector, a plasma is generated by applying a high voltage to a quartz dielectric chamber, in the presence of helium. Compounds that elute from the GC column are ionised by this He plasma, then captured with collection electrodes and described as peaks. The limit of detection of the BID is approximately $500\ \text{ng/L}$. The most sensitive sensor available is the PDHID, which is shown schematically in Figure 17. The PDHID uses a stable, low powered, pulsed DC discharge in helium as an ionisation source. Compounds coming from the GC are ionised by high-energy photons from the helium discharge. These photons have enough energy ($13.5 - 17.5\ \text{eV}$) to ionise all elements and compounds, with the exception of neon. The electrons resulting from this ionisation are focused towards the collector electrode by the bias electrodes. Changes in the measured current constitute the

detector response. The helium must be 99.9995 % pure, otherwise impurities quench the ionisation of the helium atoms. The limit of detection of the PDHID is 50 ng/L.

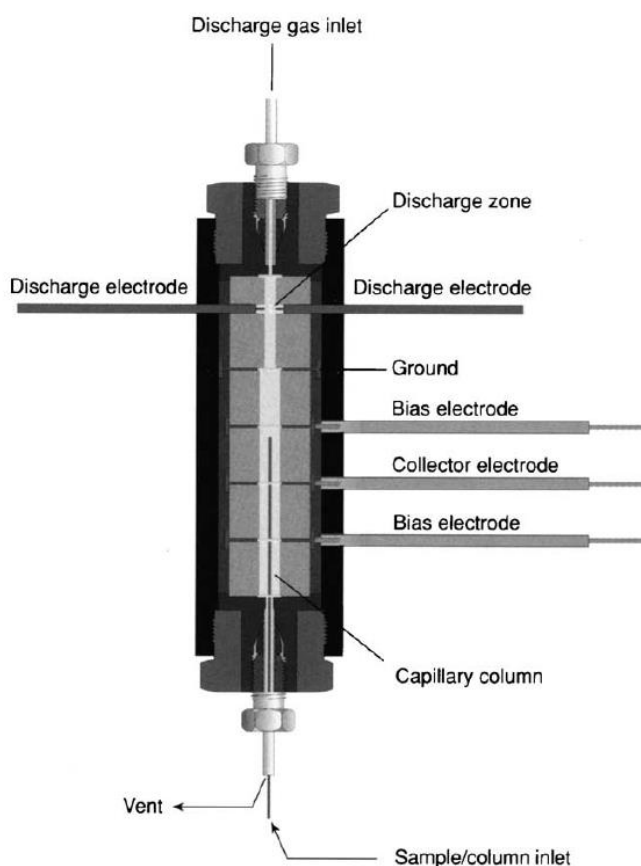


Figure 17. Scheme of a Pulse Discharge Helium Ionisation Detector (PDHID).

2.6.1.1 Identification of peaks

The calibration of the GC consisted of two parts: (i) determination of the retention time of the most probable carbon compounds, and (ii) determination of the detection limit for each compound. The retention time is dependent on, among other parameters, the type of column and the temperature of the furnace and therefore must be determined with calibration gases for each type of column (and furnace temperature). We focused on the most probable carbon-containing products obtained from the carbon steel corrosion: methane, ethane, ethene, propane, propene and carbon dioxide. As both retention time and peak separation depend on the experimental parameters, we conducted preliminary tests to optimise the peak

definition for the above compounds. The results, i.e. the parameter values used for our analyses, are shown in Table 3.

Table 3. Parameters used for GC analysis.

Parameters	Values
Carrier gas pressure	350.5 kPa
Total flow	47.1 mL/min
Column flow	14.38 mL/min
Linear velocity	44.2 cm/sec
Purge flow	4.0 mL/min
Split ratio	2
Detector temperature	200°C
Initial column temperature	35°C
Ramp of temperature	15°C/min until 175°C 10°C/min until 200°C 5°C/min until 215°C 2.5°C/min until 235°C 10 min at 235°C

Figure 18 shows a chromatogram indicating the peaks of the most probable carbon compounds. The broad peak present at a lower retention time than methane can be attributed to nitrogen (matrix gas), to argon (carrier gas), and partially to oxygen (present in air during the injection). The slope in the background signal is due to an increase of temperature of the column.

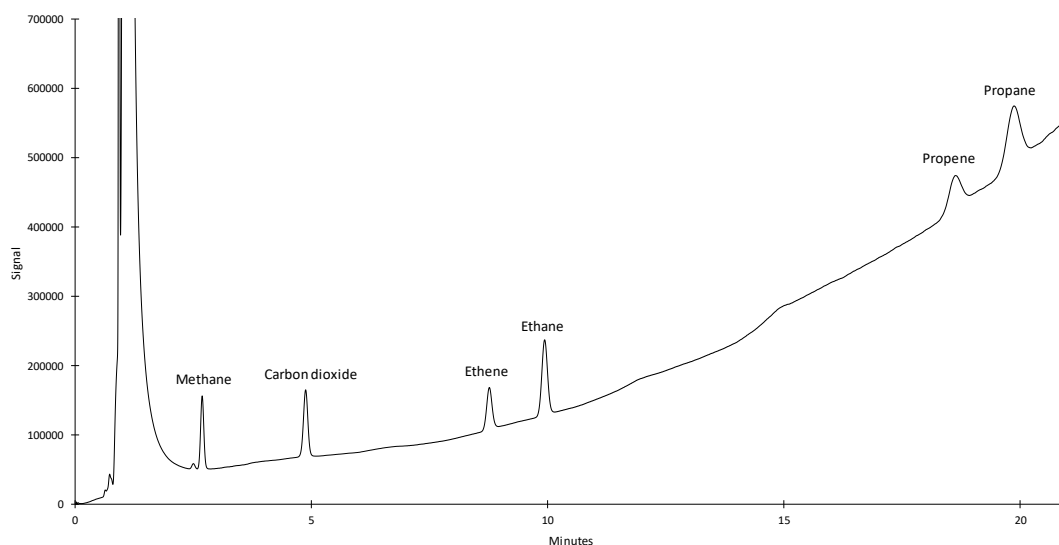


Figure 18. Gas chromatogram of a mixture of methane, carbon dioxide, ethene, ethane, propene and propane at a concentration of 10 $\mu\text{g/g}$.

Some peaks, besides methane, remain present at retention times between 2 and 3 minutes even when pure nitrogen is injected into the GC, as shown in Figure 19. Those peaks are ghost peaks coming from pressure changes in the injector and one of them appears at the same retention time as methane. To try to remove these peaks, the sample injection was performed exactly 20 seconds after piercing the septum of the injector with the syringe and 20 seconds before removing the syringe from the injector. This procedure resulted in a decrease of the intensity of the ghost peaks. Nevertheless they were still present, leading to an increase of the detection limit of methane. In addition, this procedure created new peaks close to 0.7 minutes of retention. These correspond to peaks of O_2 and N_2 from air accidentally injected during the piercing of the septum.

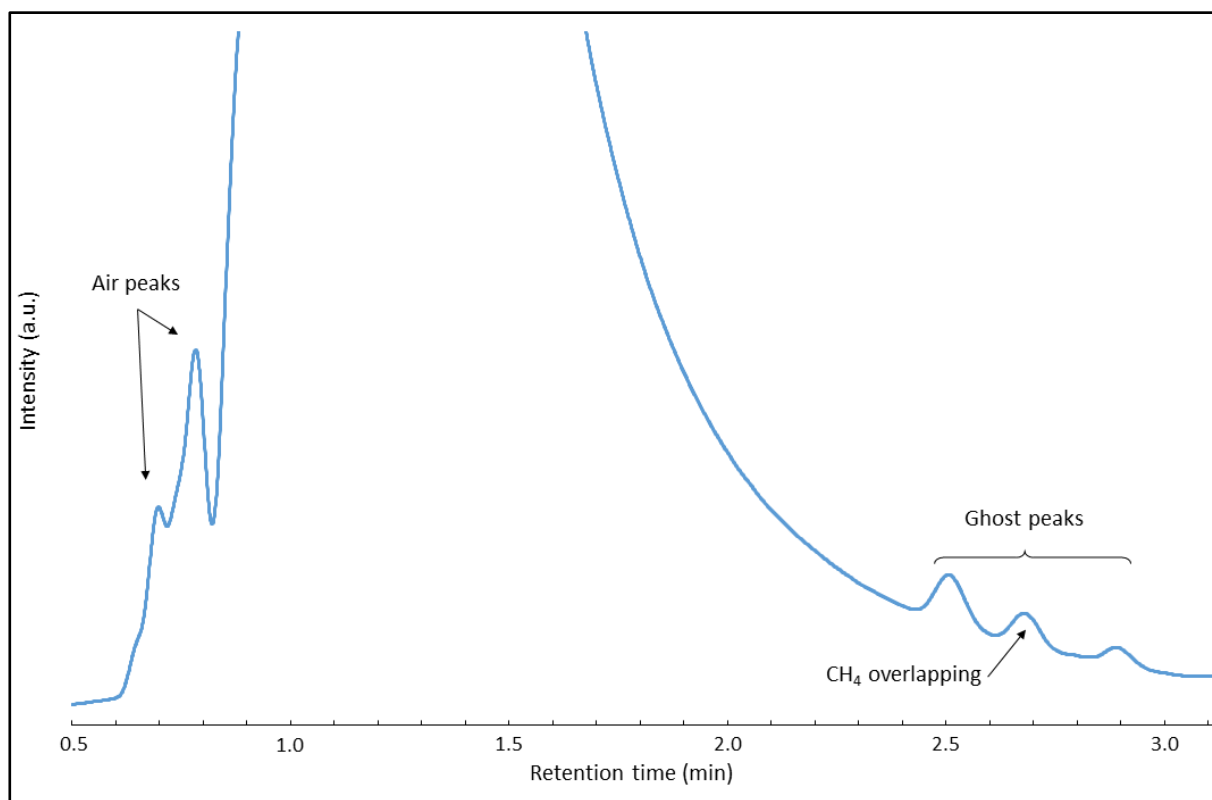


Figure 19. Magnification of the gas chromatogram between 0.5 and 3.1 minutes showing ‘ghost peaks’.

2.6.1.2 Determination of the detection limits

The detection limits for the most probable carbon compounds were determined in two ways: (i) by means of the noise in the vicinity of the peak of interest, and (ii) by measuring standards of successive lower concentration until no (clear) peak was observed anymore. More details on the determination of the detection limits can be found in Appendix 2. Table 4 shows the reported limits, taken as the average value (rounded up) of the detection limits determined by means of both methods. The value for carbon dioxide however seems to be extremely high and has to be considered with care. Because a direct injection technique of the sample is used, some ambient air will inevitably enter the column (and the detector), which results in carbon dioxide contamination. So, 3 $\mu\text{g/g}$ is the practical detection limit of CO_2 when this injection technique is used, although the detection limit of the instrument itself is much lower.

Table 4. Detection limits for common carbon compounds, measured with the Shimadzu GC-2010 Plus.

Gasses	Reporting limits ($\mu\text{g/g}$)
Methane	0.4
Carbon dioxide	3
Ethene	0.2
Ethane	0.2
Propene	1.5
Propane	0.75

2.6.2 Total (In)Organic Carbon

TOC (Total Organic Carbon) analysis is usually carried out by measuring total carbon (TC) and total inorganic carbon (TIC). Total organic carbon is then obtained by subtraction of TIC from TC. Total carbon is determined by injection of a small aliquot of sample into a furnace filled with a catalyst. All carbon products are oxidized to carbon dioxide which is detected by an infrared (IR) detector after purification of the gases leaving the furnace. Total inorganic carbon is determined by injection of a small aliquot in a reactor filled with dilute phosphoric acid. All inorganic carbon species are converted to carbon dioxide. These are purged from the reactor and detected by the IR detector.

Instead of TOC one could also measure NPOC (non-purgeable organic carbon). This is carried out by acidifying and purging the sample with gas so that all carbonates in the samples are converted to carbon dioxide which is then purged. The carbon compounds that remain in solution are supposed to be organic and can be measured directly as TC. This assumption is only true if no volatile organic compounds are present in the solution as these could also be purged from the sample. This approach is very useful for samples with high pH values because these can quickly absorb carbon dioxide to produce carbonates. This gives rise to unstable TIC levels and makes accurate determination of TIC and TOC impossible.

For TIC analysis the samples were not diluted prior to analysis. Because the samples have high pH values, NPOC measurement is preferred. Samples were acidified and purged and then analyzed for TC.

All measurements were carried out with a Skalar Formacs HTi TOC analyzer. This instrument is able to analyze liquid aqueous samples with a carbon content of 0.5 mg/l or higher. Calibration of the instrument was carried out in the concentration range 0.5 to 10 mg/l and 10 to 100 mg/l. The appropriate calibration was used for the samples. The injection volume for both TC and TIC was 100 μl and repeated measurements were carried out until the relative standard deviation (RSD) on the replicates was better than 2%.

2.6.3 Ion Chromatography (carboxylic acid analysis)

Ion chromatography was realized to measure the concentration of carboxylic acids, such as formate, acetate and oxalate, using a Dionex IC-25 machine with potassium hydroxide eluent generator. The IC-25 Ion Chromatograph performs isocratic ion analyses using conductivity detection. The IC25 integrates pump and detector functions in a single instrument. 25 μL of sample was injected on a dionex AS15 column at room temperature.

2.6.4 Liquid Scintillation Counting

The ^{14}C activity was determined by Liquid Scintillation Counting using a Quantulus 1220 counter. The cocktail used was Optiphase Hisafe 3 (Perkin Elmer) which handles a broad range of solutes. It combines good counting efficiency with a very high level of sample acceptance, particularly for high ionic strength solutes. 17 ml of the cocktail was mixed with 2.5 ml sample in super polyethylene vials of 20 ml (Perkin Elmer).

3 Results and discussion

3.1 Nitrogen analysis

Table 5 shows the result of the nitrogen analysis measurement. The obtained concentration was slightly lower than the values mentioned in literature, which fall in the range 20-30 $\mu\text{g/g}$ [IAEA, 2009]. This result leads to a decrease of the expected amount of ^{14}C inside the sample after irradiation. Indeed, the activation of ^{14}N ($^{14}\text{N}(\text{n,p})^{14}\text{C}$) is the most probable production of ^{14}C in Carbon Steel.

Table 5. Nitrogen content of the unirradiated JRQ steel.

Sample ID	N_{avg} ($\mu\text{g/g}$)
JRQ 12-4A-X17	19 ± 0.4

3.2 Metallographic analysis

3.2.1 Unirradiated sample

The grain structure of the RPV steel is shown in the BSE micrograph of Figure 20. The black spots in the image are probably the result of the oxidation of the sample after the electrochemical polishing and will not be considered further. The grain structure is that of a ferritic-bainitic steel, which is the expected grain structure for a RPV steel. Many grains have a lath-like morphology which is characteristic for the bainite structure and these laths are parallel within the boundaries of the larger ferrite grain structure. Other grains do not show the lath structure. Considering the ferrite grains, the grain size determination gave a grain size number of 8.4, which corresponds to an average grain surface of $380 \mu\text{m}^2$ or a grain size of $19.5 \mu\text{m}$. The average width of the bainite laths is $2 \mu\text{m}$.

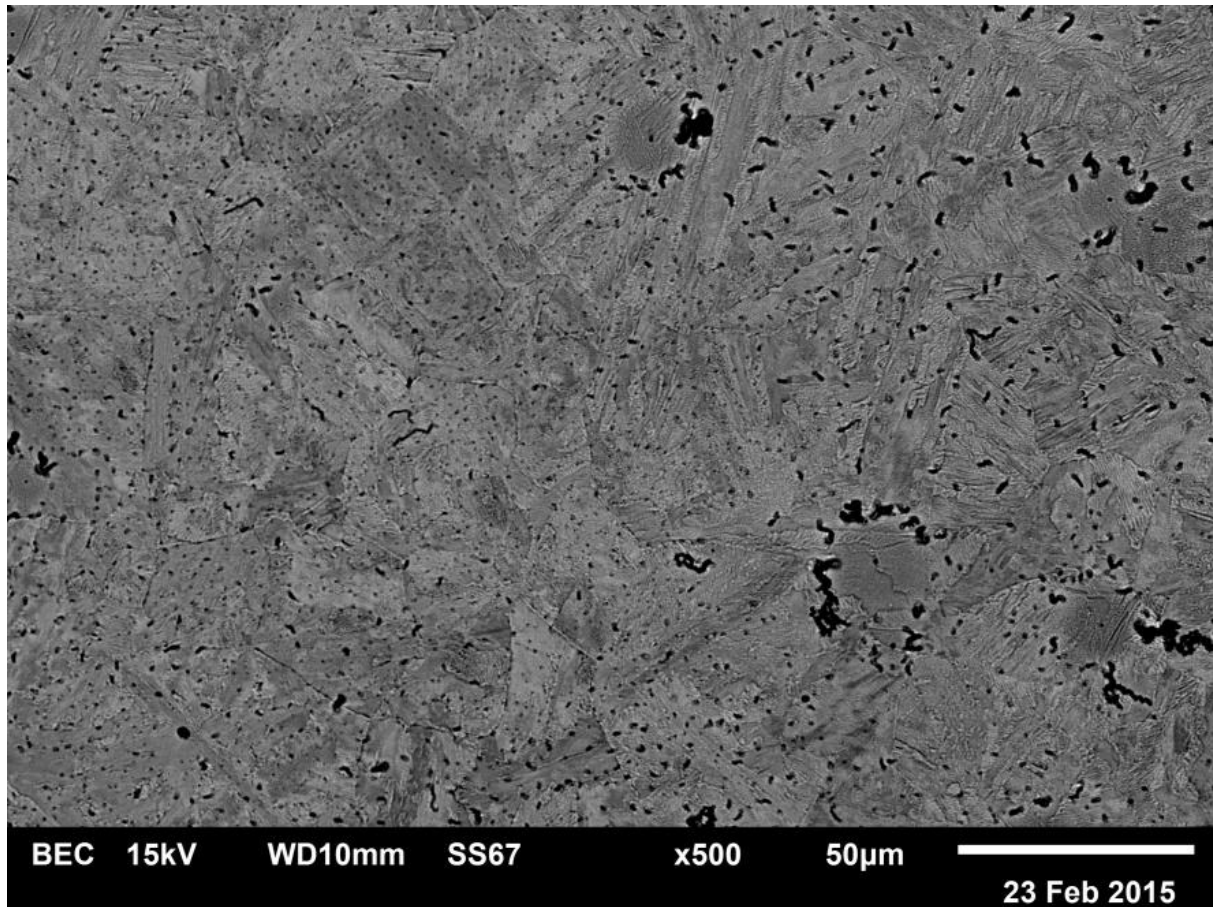


Figure 20. BSE micrograph revealing the grain structure of the unirradiated JRQ RPV steel sample JRQ 12-4A-X17 2.

The bright field TEM micrographs of Figure 21 are given to confirm the grain structure. Because the field of view of the TEM camera is limited, 4 micrographs were recorded and stitched. It can be observed that several grain boundaries are present, creating the lath-like grain structure which is typical for the bainite phase. Orientation differences between two laths on both sides of a grain boundary are often very small, which means that these boundaries are small angle grain boundaries.

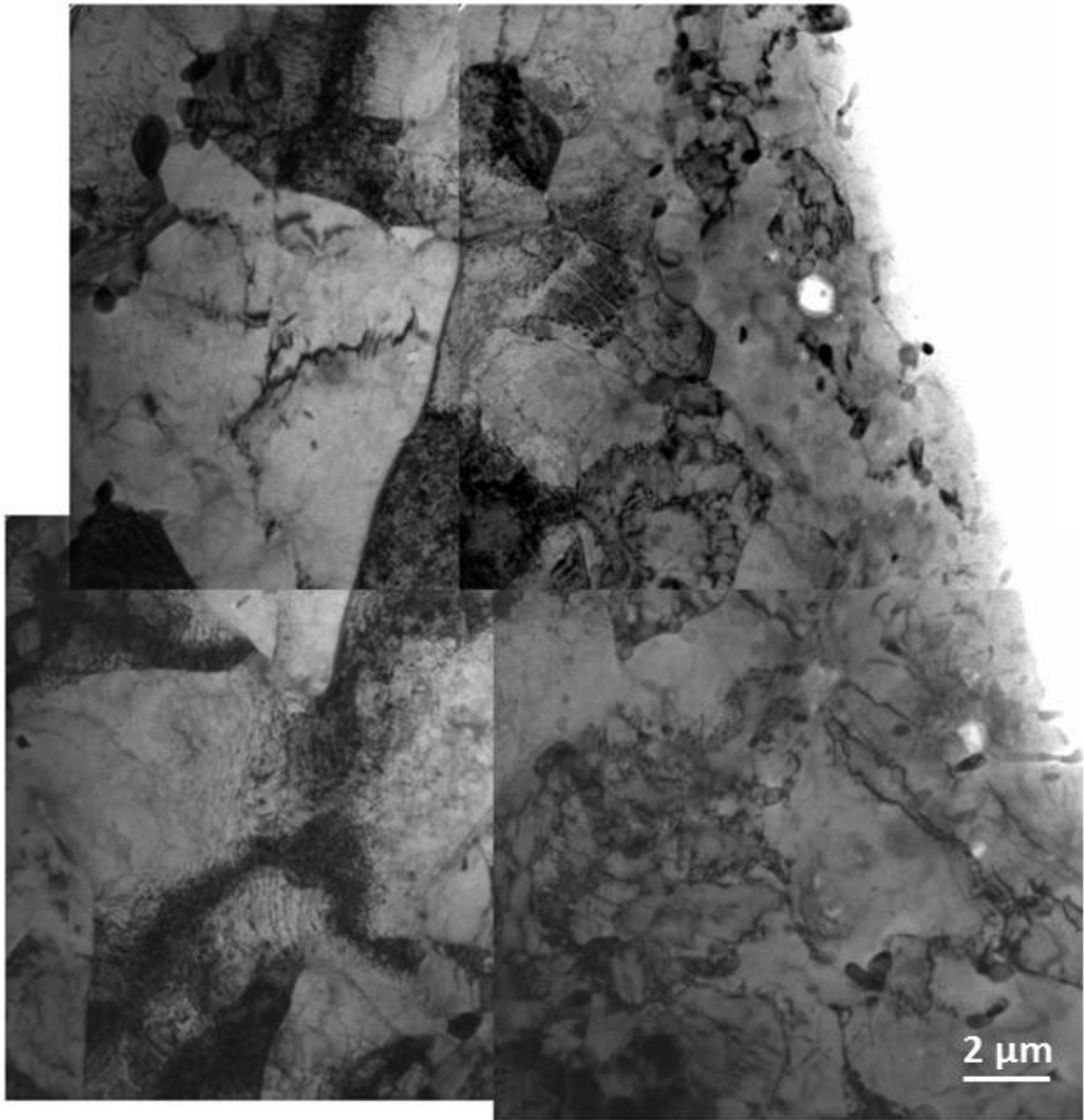


Figure 21. Collage of bright field TEM micrographs of the unirradiated JRQ RPV steel sample showing the grain structure in more detail.

The defect structure at higher magnification is shown in Figure 22. Mainly line dislocations were observed with a dislocation density of $1.3 \times 10^{14}/\text{m}^2$. Locally, as for example in Figure 22(B), the dislocation density is higher and dislocation networks are formed. Similar networks were also found at the grain boundaries of the bainitic laths. There they are formed

to compensate for the small lattice mismatch between the grains on both side of the grain boundary.

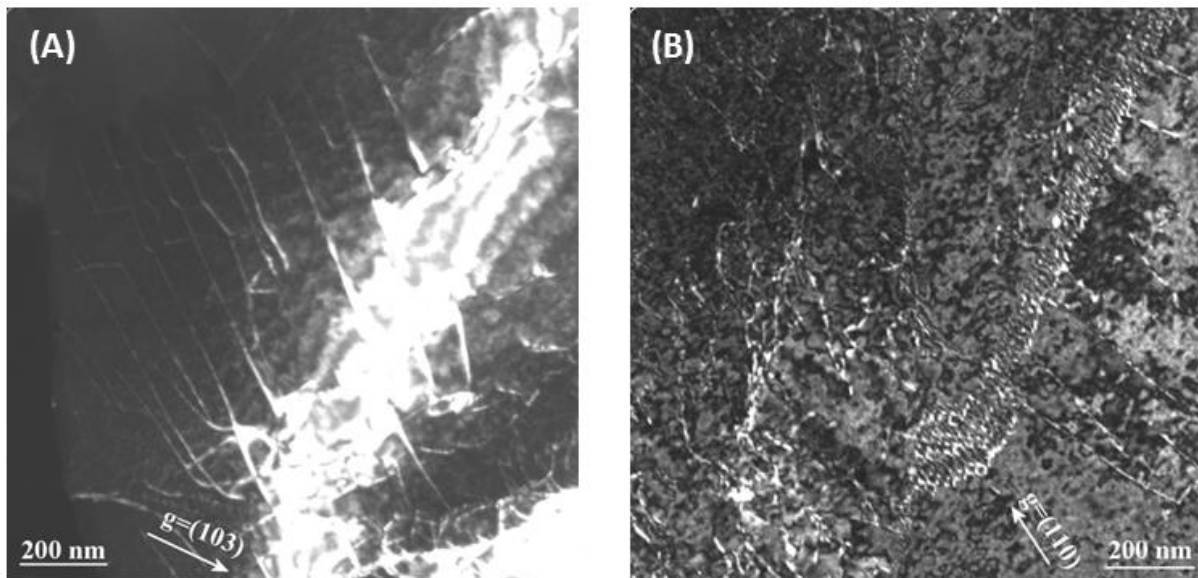


Figure 22. (A) and (B) Dark field micrographs of the defect structure of the unirradiated JRQ RPV steel.

The carbides that are formed in the steel are of particular interest. Two different types of carbides were identified and examples of each type are given in Figure 23 and Figure 24. The carbides that occur most frequently are carbides with a cementite structure as shown in Figure 23. The bright field micrograph shows 3 carbides, but the discussion is focused on the carbide in the middle of the picture.

The diffraction pattern in Figure 23(B) reveals the crystallographic structure of the carbide. Ferritic iron has a body centred cubic lattice with a lattice parameter of 2.886 \AA . Fe_3C has a orthorhombic lattice with lattice parameters $a= 5.0825 \text{ \AA}$, $b= 6.733 \text{ \AA}$ and $c=4.5119 \text{ \AA}$. The diffraction pattern was identified as $[-2,4,-1]$ zone of Fe_3C .

The EDS spectra in Figure 23(C) give a qualitative indication of the composition of the carbide. The blue curve is the spectrum of the bulk steel. It is dominated by the Fe peaks, but small amounts of Mn and Ni are present as well. A small concentration of Mn and Ni was added to the steel during manufacturing and the small peaks are in agreement with this

concentration. A small carbon peak can be observed as well, but this peak is the result of carbon deposition on the sample during the EDS analysis. The red curve was obtained by focusing the electron beam on the carbide. To correct for difference in beam intensity or recording time, the spectrum is renormalized such that the total number of counts of both spectra is equal. Because of the size of the carbide, the contribution to the spectrum from the surrounding bulk material will be small and the result will be representative for the carbide concentration. In this spectrum, iron is still the main element, but the Mn signal has increased. Moreover, small amounts of Cr and Mo are detected as well. Also the carbon signal has increased. Even though different amounts of carbon can be deposited under different measuring conditions, it is a strong indication that the precipitate contains carbon. So the EDS analysis confirms on a qualitative level that the precipitate is a Fe_3C carbide and it shows that the carbide is enriched in Mn, Cr and Mo.

These carbides were frequently found to occur at the grain boundaries of the bainite laths as well as the ferrite grains, but some are formed in the interior of the grain. The carbides are inhomogeneously distributed over the sample as can be seen in the overview image of Figure 21, which contains both areas of high carbide density, like in the lower left corner of the picture, and areas of low carbide density, like in the upper right corner. Also the morphology and size are very inhomogeneous. The carbide morphology changes from almost spherical carbides to elongated, needle shaped structures. The size is on average of the order of a few 100 nm, but the elongated carbides can reach a length of more than 1 μm for a width of about 100 nm.

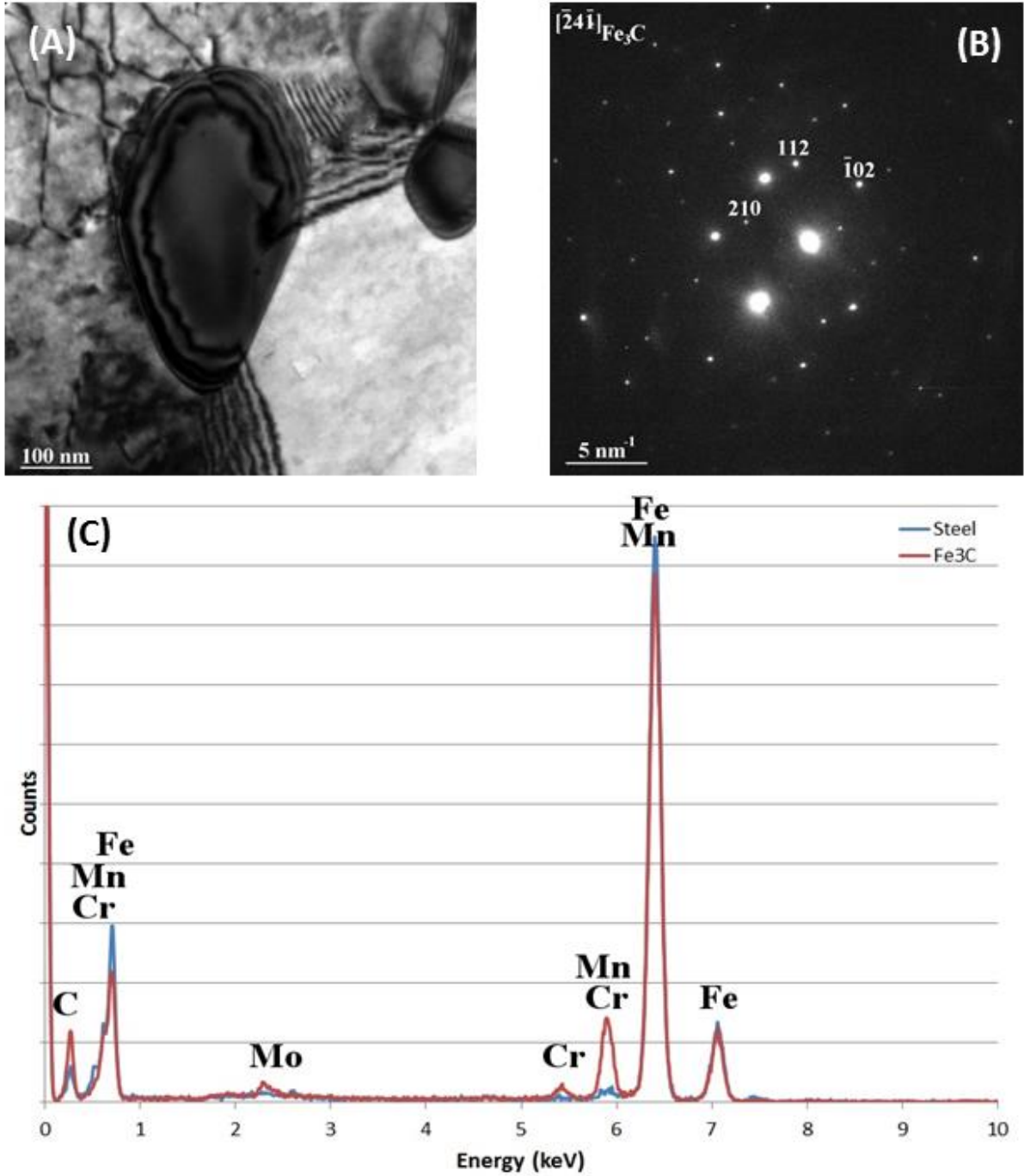


Figure 23. (A) Bright field micrograph of a Fe₃C carbide, (B) the corresponding diffraction pattern revealing the cementite crystal structure and (C) the EDX spectrum of the carbide (red line) compared to the composition of the bulk steel (blue line).

The second type of carbide is shown in Figure 24(A). These carbides were only found in the grain interior and they do not occur as frequently as the Fe_3C carbides. These carbides have a rectangular shape in the projected images with a length of about 100 nm and a width of about 20 nm. On average, they are much smaller than the Fe_3C carbides. The diffraction pattern in Figure 24(B) gives an indication about the crystallographic structure of the carbide. Because of the small size, also reflections of the bulk metal appear in the diffraction pattern and these reflections are indicated by a subscript Fe. The other reflections can be identified as the $[-3, 3, 2]$ zone of Mo_2C . Mo_2C has a face centred cubic structure with a lattice parameter of 4.273 Å.

The EDS spectrum of the carbide is given in Figure 24(C). Because of the small size of this precipitate, it should be considered that the bulk metal gives a contribution to the spectrum and increases the Fe signal. The spectrum shows a high Mo signal and small amounts of Mn, Al, Si and Cr. The carbon signal is higher than in the measurement of the bulk steel, which indicates again that the precipitate is a carbide and in combination with the diffraction data, it is concluded that the second type of carbides are Mo_2C type carbides.

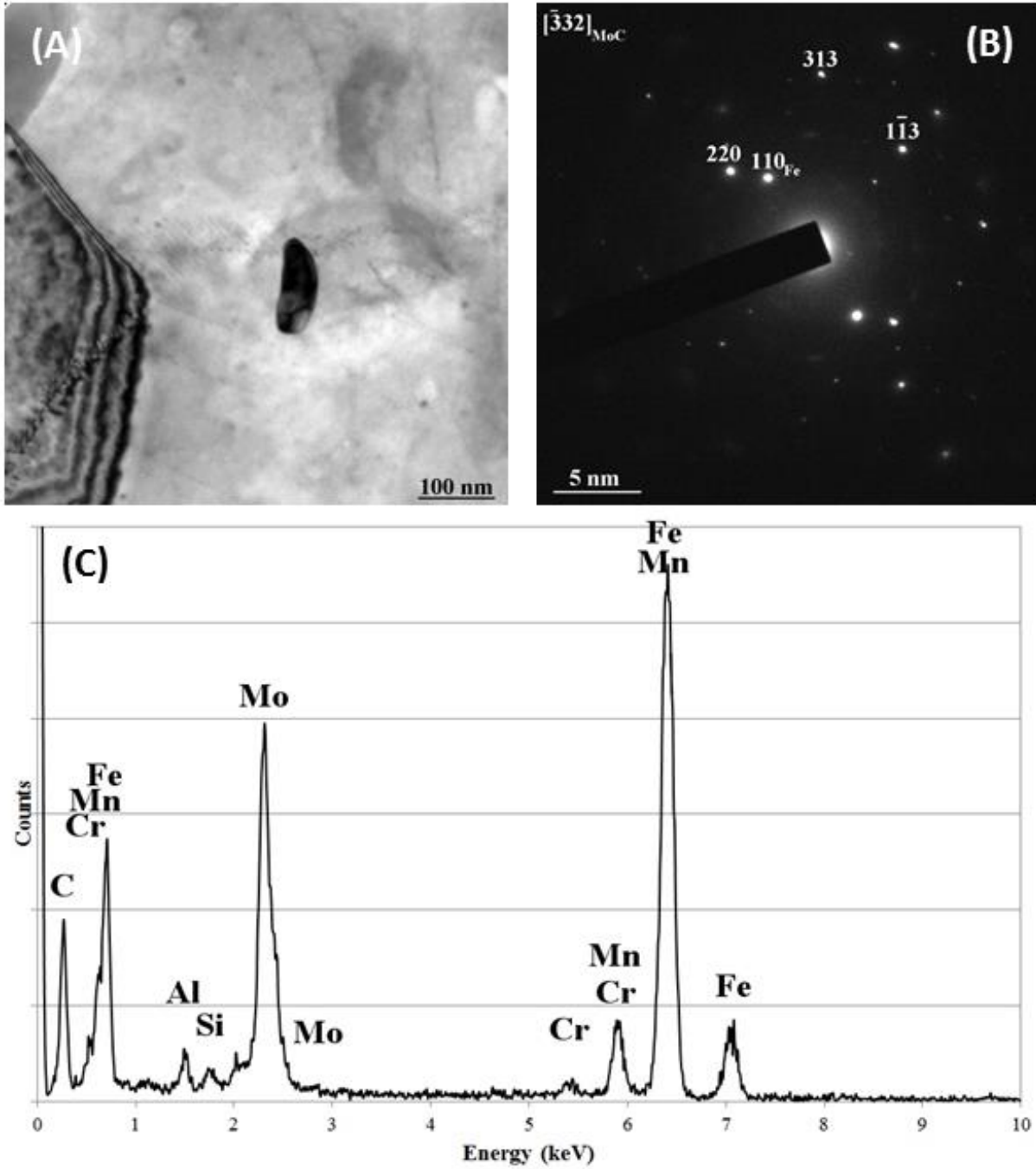


Figure 24. (A) Bright field micrograph of the Mo_2C type carbide, (B) the corresponding diffraction pattern of Mo_2C type carbide and (C) the EDX spectrum giving a qualitative indication of the composition of the carbide.

3.2.2 Active sample

After the study of the material before irradiation, the analysis of the microstructure of the irradiated carbon steel used for leaching tests was done. These properties were only studied by Transmission Electron Microscopy.

Similar results than the ones obtained for unirradiated sample were found in the irradiated JRQ carbon steel sample. Figure 25 shows a collage of bright field micrographs revealing the grain structure. The large holes in the material are the result of the electrochemical polishing. In between the bainitic grain structure is visible. A significant amount of elongated carbides is present, which will be analysed later.

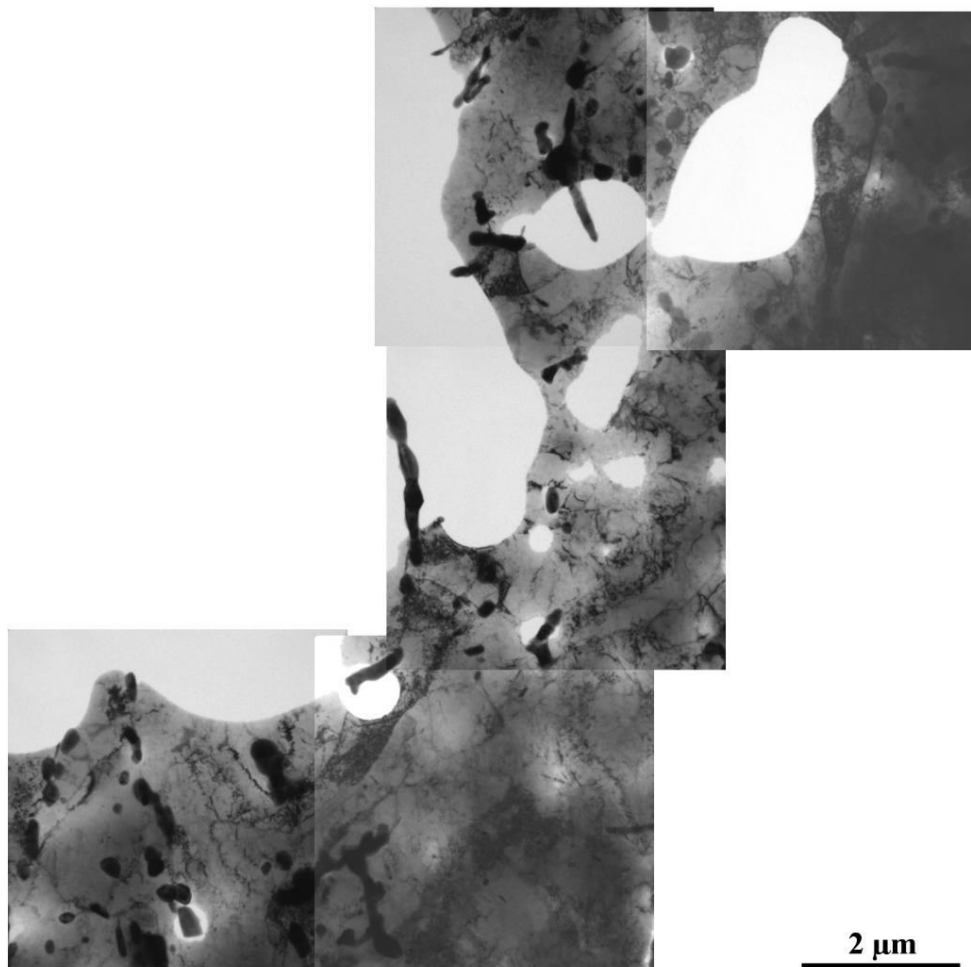


Figure 25. Collage of bright field micrographs showing the grain structure and carbide distribution.

The defect structure is analysed in more detail in Figure 26. The main defects that are present are line dislocations. The dislocation density was determined from micrographs like Figure 26(C) and 26(D), taken at five different locations in the sample. The result was a dislocation density of $(3.7 \pm 0.8) \times 10^{14} / \text{m}^2$. This value is higher than in the carbon steel that was studied before irradiation. In general, neutron irradiation decreases the amount of line dislocations, and the higher density observed here is probably related to a difference in mechanical or thermal treatment prior to irradiation. The neutron irradiation has only a minimal effect on the visible defect structure. The only effect is the formation of a limited number of small dislocation loops. A few examples are indicated by the white arrows in Figure 26(B).

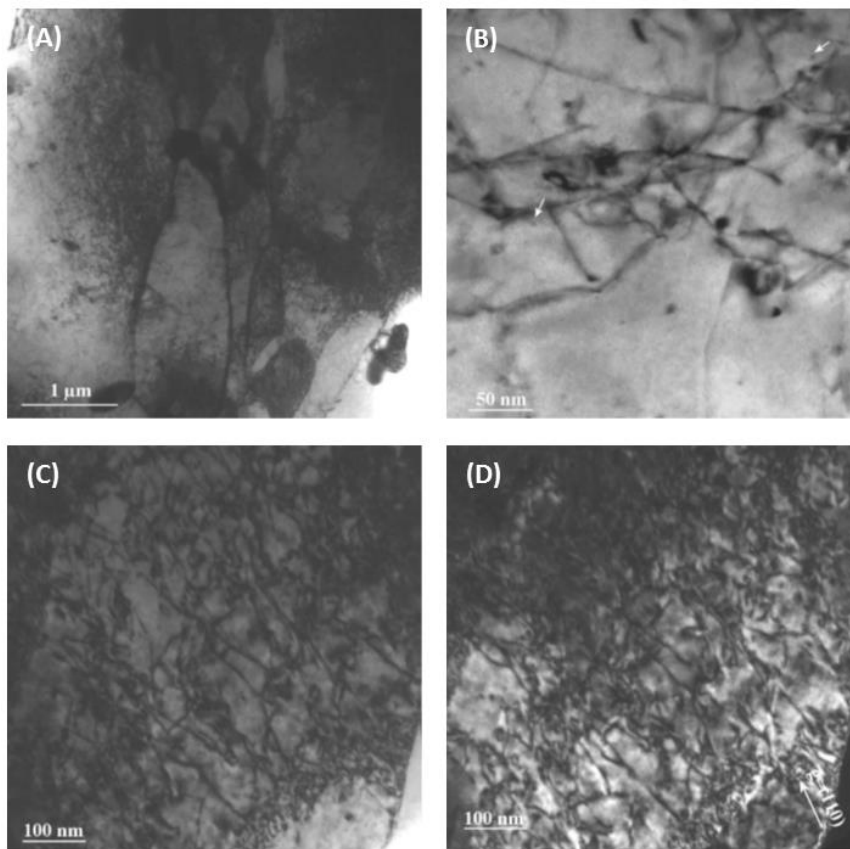


Figure 26. (A) Bright field micrograph of the bainitic grain structure, (B) bright field micrograph showing a limited amount of radiation induced defects, two are indicated by the white arrows, (C) bright field and (D) dark field micrographs of a high-density of line dislocations.

Also after irradiation, two types of carbides were found. The majority of the carbides, like the ones in Figure 27, are Fe_3C type. The diffraction pattern of Figure 27(B) agrees with the crystallographic structure of this type of carbide. The EDS spectrum of Figure 27(C) confirms that the carbide has a higher Mn content than the matrix, which is typical for this kind of carbide. It appears that the amount of carbides has increased in comparison with the sample before irradiation. It is, however, difficult to quantify their amount and it should be considered that the carbides are not soluble for the electrolyte that was used. Therefore the density of carbides that remains on the TEM samples is higher than the actual volume density.

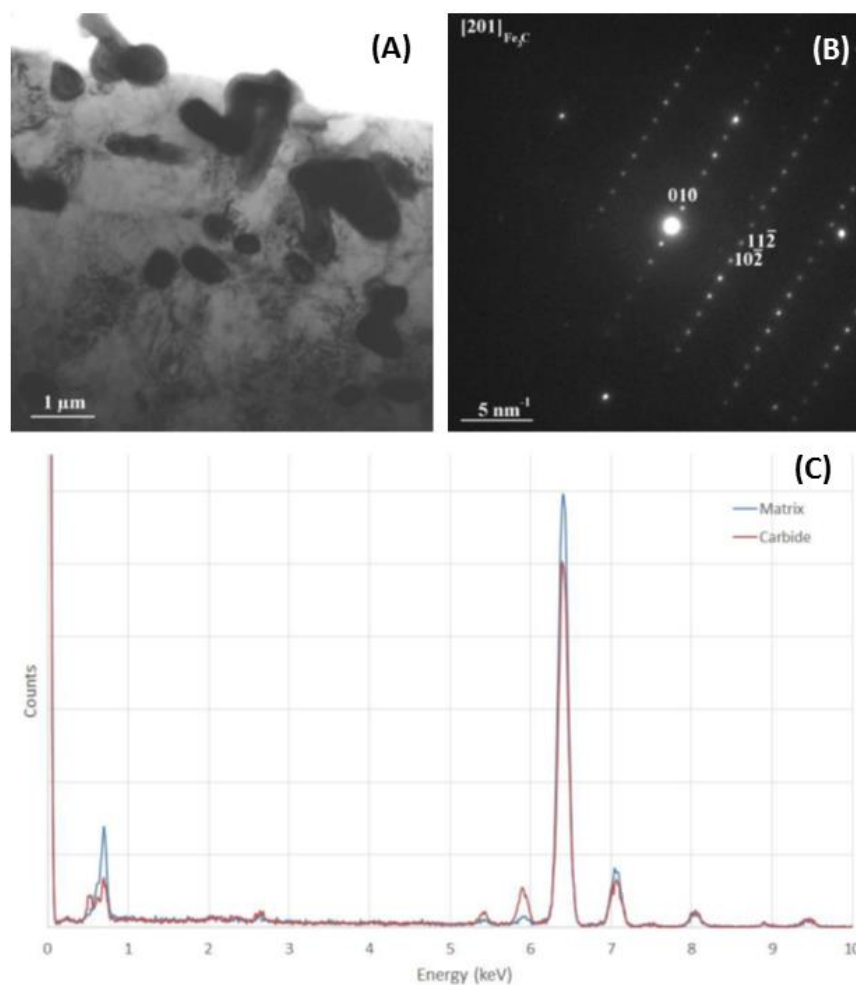


Figure 27. (A) Bright field micrograph of an assembly of cementite carbides, (B) typical diffraction pattern, confirming the Fe_3C crystal structure and (C) qualitative EDS-spectra of the matrix and Fe_3C carbide.

Figure 28 shows that also the Mo_2C type carbides are still present in the irradiated steel. They are still smaller than the Fe_3C carbides and only occur in the interior of the grains. The EDS-spectrum shows the presence of the Mo in the carbide. The small Mn peak results from the neutron activation of Fe. The iron signal itself is generated in the surrounding steel matrix and its presence in the EDS spectrum cannot be avoided. It is not clear, however, if Fe is present in the carbide or not. Some carbides appear to have elongated, but others have not.

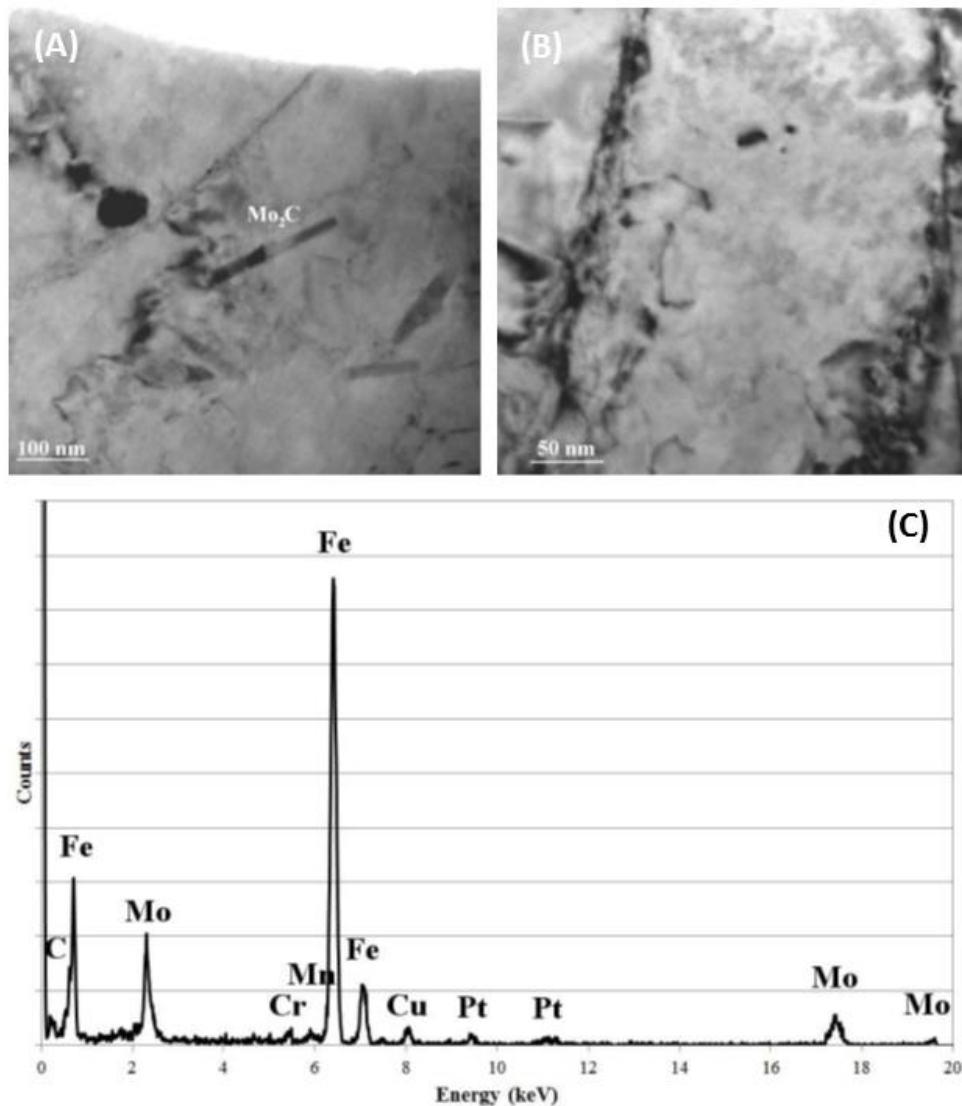


Figure 28. (A and B) Bright field micrographs of Mo_2C carbides and (C) EDS spectrum proving the higher Mo concentration.

3.3 γ -ray spectrometry

Table 6 shows the results from γ -ray spectrometry for the irradiated JRQ sample for static testing. In this sample, both ^{60}Co and ^{106}Ru were detected. Table 7 shows the results for the sample for accelerated testing. The only γ -emitter detected was ^{60}Co .

Table 6. Results from γ -ray spectrometry for the irradiated JRQ samples for static testing.

Nuclide	Activity (Bq)	2 σ (Bq)
^{60}Co	9.1×10^5	2.3×10^5
^{106}Ru	3.3×10^4	0.8×10^4

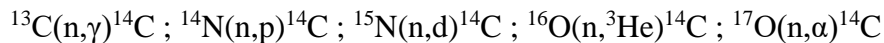
Table 7. Results from γ -ray spectrometry for the irradiated JRQ sample for accelerated testing.

Nuclide	Activity (Bq)	2 σ (Bq)
^{60}Co	6.5×10^5	1.6×10^5

3.4 Estimation of the ^{14}C content of irradiated samples

Thanks to the measurement of the nitrogen content in unirradiated carbon steel sample, an estimation of the ^{14}C amount after irradiation of the metal was obtained using a computer modelling calculation.

The production of ^{14}C through nuclear reaction on nitrogen, carbon and oxygen was evaluated for a PWR representative neutron spectrum, as a literature review shows [WALLACE, 1977] that the following reactions may provide ^{14}C build-up:



Among these, $^{14}\text{N}(n,p)^{14}\text{C}$ would bring the dominant contribution.

A simple, single cell model was therefore developed in the SCALE-6.1 code using the ‘Triton’ depletion sequence. The sample composition was taken as standard carbon steel. Taking the irradiation history, a total neutron fluence of 5×10^{19} n/cm² was calculated.

CAST
 Report on ¹⁴C release speciation from carbon steel under alkaline reducing conditions
 (D2.7)

The calculations were then repeated with a small change in the carbon steel composition, where nitrogen, carbon or oxygen is added at a concentration of 1000 wt. µg/g, with an isotopic composition reflecting natural abundances. It is an overestimation, although from this calculation, results can be proportionally descaled to any lower concentration.

Differences in ¹⁴C compared to the reference case then provide the ¹⁴C build-up associated to the sole presence of 1000 wt. µg/g of the considered element, in conditions representative of a PWR neutron spectrum. Considering the low concentration of these trace elements in the carbon steel sample, second order effects due to the presence of the trace elements or ¹⁴C may be neglected; the ¹⁴C concentrations obtained can then be rescaled to reflect the actual material composition and fluence.

From the calculations, it appears that the only significant ¹⁴C production arises with the presence of nitrogen: the addition of 1000 µg/g of N (natural abundances) leads to the production of 60 ng/g of ¹⁴C at the end of irradiation. The value can be rescaled to other N content in view of the linear build-up of ¹⁴C over the irradiation history.

Table 8 shows the concentration of ¹⁴C of carbon steel samples, and its corresponding activity, obtained from the computer simulation depending on the nitrogen concentration previously measured. The corrosion of 1 g of carbon steel will lead to the release of ~1 ng of ¹⁴C. Unfortunately, the total activity of the irradiated carbon steel used at SCK•CEN couldn't be measured and no comparison with the calculation could be done.

Table 8. ¹⁴C activity of the irradiated Carbon Steel obtained from the computer simulation and its initial nitrogen content.

Sample ID	C _N (wt. µg/g)	Fluence (n/cm ²)	Concentration of ¹⁴ C (wt. µg/g)	¹⁴ C activity (Bq/g)
JRQ	19 ± 0.4	5 x10 ¹⁹	1.069 x10 ⁻³	175

3.5 Corrosion rate determination from ^{60}Co measurements

The measurement of the corrosion rate of carbon steel in a highly alkaline environment is a difficult task, because of the extremely low values. Therefore, we investigated whether the corrosion rate could be determined radiometrically by measuring the release of activation products, like ^{60}Co , when an irradiated steel sample is in contact with artificial portlandite pore water (saturated $\text{Ca}(\text{OH})_2$, see Section 3.1). This approach assumes a homogeneous distribution of ^{60}Co in the material and the same leaching rate as Fe under alkaline conditions.

3.5.1 Description of the test

A sample of irradiated JRQ carbon steel was immersed in a Teflon test cell containing approximately 20 mL of 0.01 M $\text{Ca}(\text{OH})_2$. After pre-defined time periods, 10 mL of liquid was taken from the cell during each sampling, and transferred into a 20 mL HDPE liquid scintillation vial. The released ^{60}Co activity was determined with γ -ray spectrometry. After each measurement, which lasted two to three days because of the low ^{60}Co activity, the liquid sample was poured back into the original test cell to continue the corrosion experiment and let ^{60}Co accumulate in the portlandite solution. The total duration of the leaching test was 50 days. It has to be noted that even if the sampling was realised carefully, this procedure could have an impact on the precision of the measure since small amount of the ^{60}Co could be lost at every measurement.

3.5.2 Results and discussion

The corrosion mechanism of carbon steel in highly alkaline conditions consists of three steps: oxidation of iron at the metal/passive film interface, diffusion of iron through the passive film, and dissolution of the metal ions at the passive film/solution interface. The diffusion through the passive film is the rate-determining step, and the corrosion rate obeys a parabolic law [KURSTEN, 2014]. This behaviour is our basic assumption for the interpretation of the results from the ^{60}Co determination. Table 9 summarises the results from γ -ray spectrometry, corrected to the full 20 mL of the test cell. The result at 50 days is clearly an outlier, being two orders of magnitude higher than the other values. This might be

caused by an accidental transfer of a very small piece of irradiated metal into the liquid scintillation vial. Therefore, we omitted this data point from subsequent analyses.

The scatter on the results is high. This might be due to the precipitation of small sized particles which are visible in the solution. Indeed, under alkaline conditions the released ^{60}Co can precipitate as a hydroxide. It is difficult to completely homogenise the solution, which makes it difficult to take representative samples. Another source of error might be that these precipitates adsorbed on the wall of the test cell. The third source of error may lie in the γ -ray spectrometry itself. In order to obtain a reliable measurement, a prerequisite is that ^{60}Co is homogeneously distributed throughout the solution, while in our case the precipitates may have (partially) settled on the bottom of the vial. In this case, the calibration factor can differ by a factor of two. Furthermore, the amount of precipitates in the vial may be different for each sampling and is not possible to quantify retroactively.

Figure 29 shows a linear fit of the ^{60}Co release data versus the square root of the elapsed time of the experiment, with the fit line forced through the zero point. A fit with $R^2 = 0.90$ is obtained. The parabolic rate law is

$$R_{\text{Co-60}} = (0.12 \pm 0.02)\sqrt{t} \quad (2)$$

Where $R_{\text{Co-60}}$ is the total released ^{60}Co activity in Bq at time t , and t is the elapsed time in days. Even if large uncertainties were observed, this result seems to corroborate that the release of ^{60}Co is controlled by diffusion through the passive layer formed under highly alkaline conditions.

After 365 days, according to equation (2), 2.3 Bq will have dissolved. The original carbon steel specimen had dimensions of 2 x 2 x 35 mm and a total activity of 1.6×10^5 Bq. This means that the dissolved fraction of the specimen (assuming that ^{60}Co was distributed evenly throughout the carbon steel sample) was $2.3 / 160000 = 1.4 \times 10^{-5}$. On a total initial volume of 140 mm^3 this results in $2 \times 10^{-3} \text{ mm}^3$ of dissolved carbon steel. The exposed surface of the sample is 288 mm^2 . This yields a corrosion depth, after one year of exposure, of 7 nm. A corrosion rate of 7 nm/y is very low compared to the reference value of $0.1 \text{ }\mu\text{m}/\text{y}$

[KURSTEN, 2014], but this may be explained by the observed precipitation. Also, it is unlikely that the diffusion behaviour of cobalt through the passive film is the same as that of iron. It probably also means that ^{60}Co measurements are not the perfect way to determine the corrosion rate of carbon steel. Further in this report, an approximation of the corrosion rate was estimated thanks to the carbon-based molecule release concentration after static corrosion (see section 3.7.1.2).

After the leaching test, we measured the ^{14}C release of the test solution by adding OptiPhase HiSafe3 LSC cocktail to the solution and using a Quantulus liquid scintillation counter. This showed that the ^{14}C activity in the original 20 mL volume after 50 days of leaching was 1.05 ± 0.7 Bq. This low quantity predicted that the detection of ^{14}C and determination of ^{14}C speciation would be very difficult for the subsequent corrosion tests.

Table 9. Total ^{60}Co activity released in the test cell.

Elapsed time (days)	Activity (Bq)	2σ (Bq)
2	0.236	0.040
9	0.556	0.058
16	0.316	0.044
23	0.826	0.074
30	0.580	0.056
50	230	16

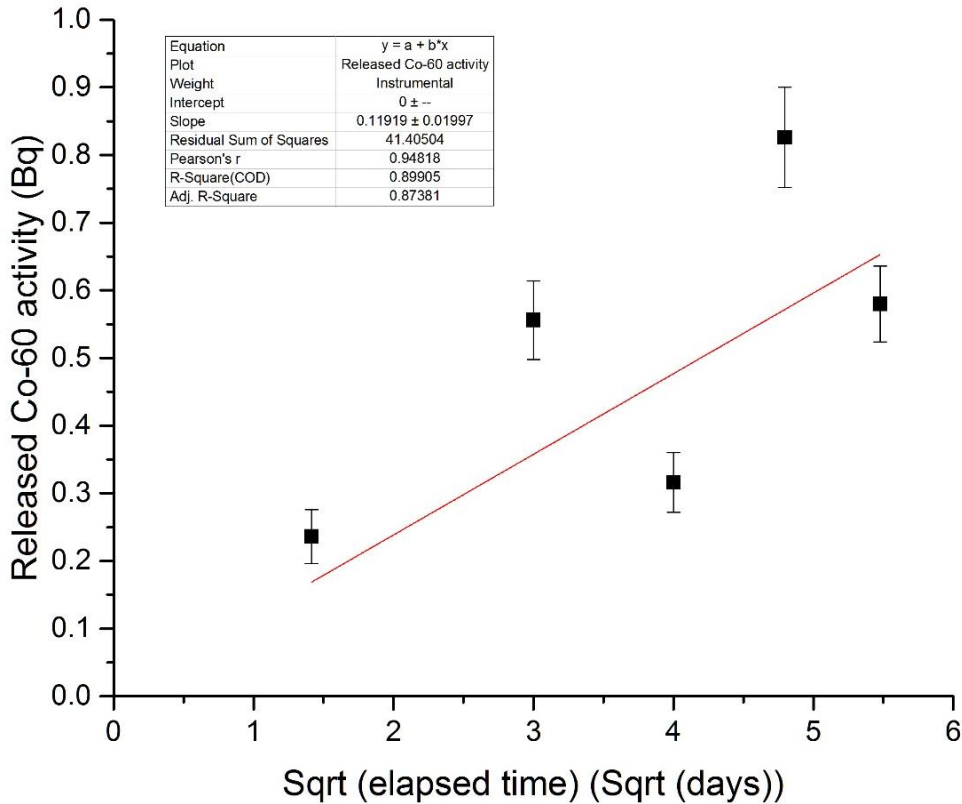


Figure 29. Linear fit of the released ⁶⁰Co activity as a function of the square root of the elapsed time.

3.6 Polarisation curves for JRQ C-steel

In preparation of the accelerated corrosion tests, we first determined a potential corresponding to an increased corrosion rate (with respect to the corrosion rate at the corrosion potential). Therefore we recorded potentiodynamic polarisation curves, which consisted in scanning the potential from the cathodic to the anodic region and recording the current (which is proportional to the corrosion rate). Polarisation curves are a powerful tool to investigate the behaviour of metals as a function of the potential and show the active to passive and/or the passive to transpassive transitions.

As explained earlier (Section 2.5.1), polarised corrosion tests were performed in two different electrolytes. First, a saturated portlandite pore water solution with a pH of approximately 12.5 was used. In a second phase, chlorides were added to the portlandite

pore water in order to induce pitting corrosion and thus artificially increase the corrosion rate. All polarisation curves were recorded under an anaerobic nitrogen atmosphere.

In this section, polarisation curves for both samples (unirradiated and irradiated) in both electrolytes (portlandite pore water without and with chlorides) are presented.

3.6.1 Unirradiated samples

The polarisation curve of the unirradiated JRQ C-steel sample in pure portlandite pore water is shown in Figure 30. The potentials are in V versus Ag/AgCl. The appearance of the polarisation curve is typical for a passivating metal: there is an active to passive transition around -0.9 V, a broad passive region from -0.8 to 0.6 V, and a passive to transpassive transition from around 0.6 V. This electrochemical behaviour is expected for carbon steel in geological disposal conditions. From this curve, a potential of 0.62 V vs Ag/AgCl was selected for the accelerated tests. Although the gain in corrosion rate is rather modest, this potential was chosen because it is still inside the stability domain of water.

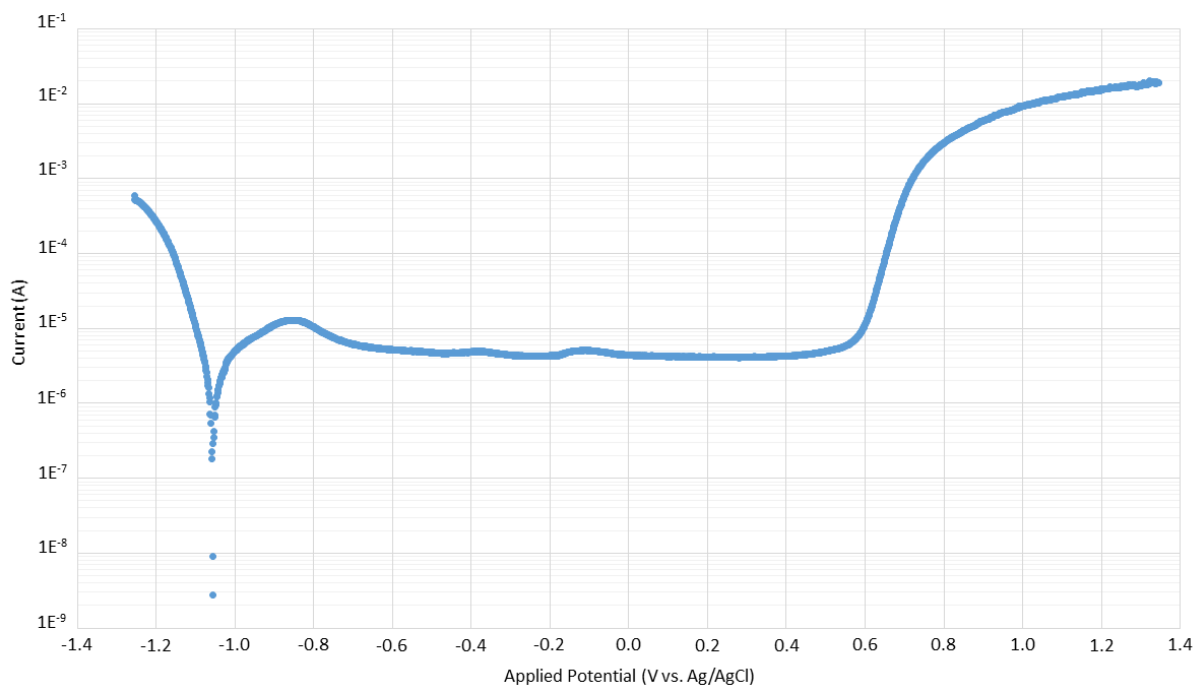


Figure 30. Polarisation curve for unirradiated JRQ C-steel in pure portlandite pore water.

Figure 31 shows the polarisation curve for unirradiated JRQ C-steel in portlandite pore water with 0.5 M CaCl_2 added. Again we observe an active to passive transition at around -0.9 V. At -0.3 V, however, there is now a sudden large increase in current, which is typical for the onset of pitting corrosion (for an overview of pitting corrosion, see e.g. [Sklarska-Smialowska 1986]). Above this potential, pitting corrosion will occur readily. Therefore, a potential of -0.2 V vs Ag/AgCl was chosen for the accelerated tests with chloride.

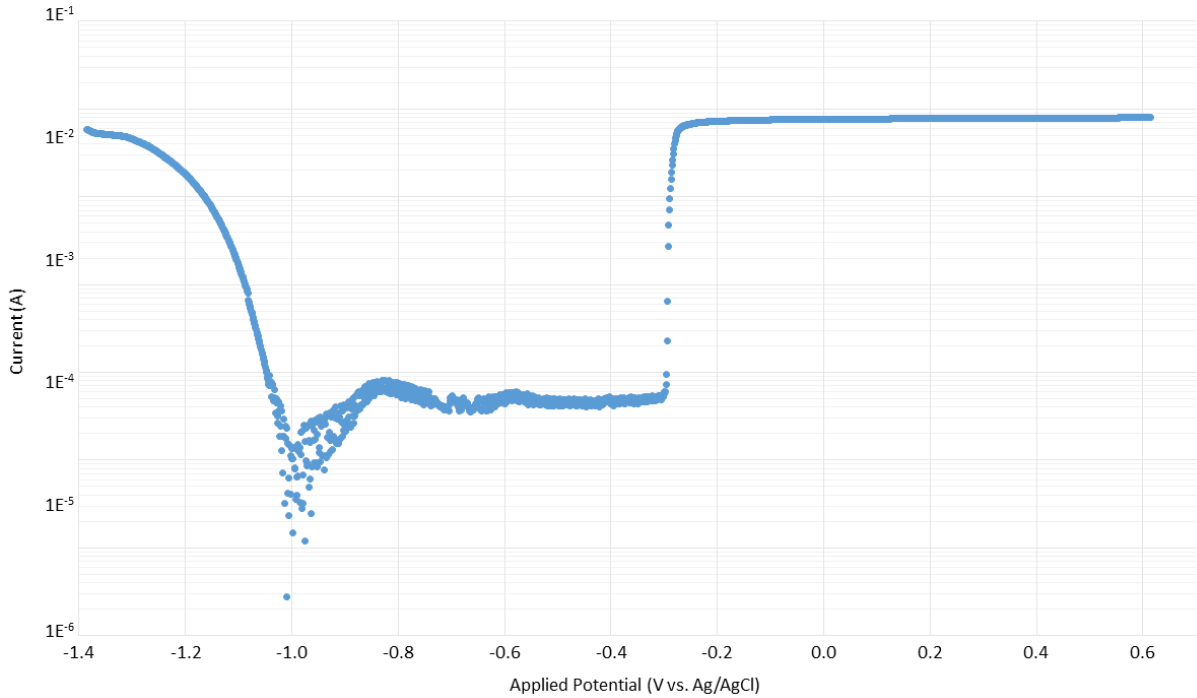


Figure 31. Polarisation curve for unirradiated JRQ C-steel in portlandite pore water with the addition of 0.5 M CaCl_2 .

3.6.2 Irradiated samples

Figure 32 shows the polarisation curve of irradiated JRQ C-steel in portlandite pore water. Again, the polarisation curve has the typical appearance for a passivating metal: an active to passive transition, a passive region, and a transpassive region. With respect to unirradiated material (Figure 30), the corrosion potential has shifted in the anodic direction (less negative potentials) by approximately 400 mV. As we ran the experiment only once, it is not possible to quantify the uncertainty on the value of the corrosion potential, but from previous experience we can state that the measurement uncertainty will be well below 400 mV. We

also see an improvement in the quality of the passive film, which is reflected in a decrease of the passive current by a factor 2-3. On the other hand, irradiation clearly had no influence on the breakdown potential of the passive film, which is still situated around 0.6 V vs Ag/AgCl. Therefore, as for the unirradiated material, a potential of 0.62 V vs Ag/AgCl was chosen for the accelerated tests. It has to be noted that polarisation curves of irradiated materials were recorded in the supervised area with another potentiostat possessing a higher current detection limit. This results in noise in the curves when the current is too low.

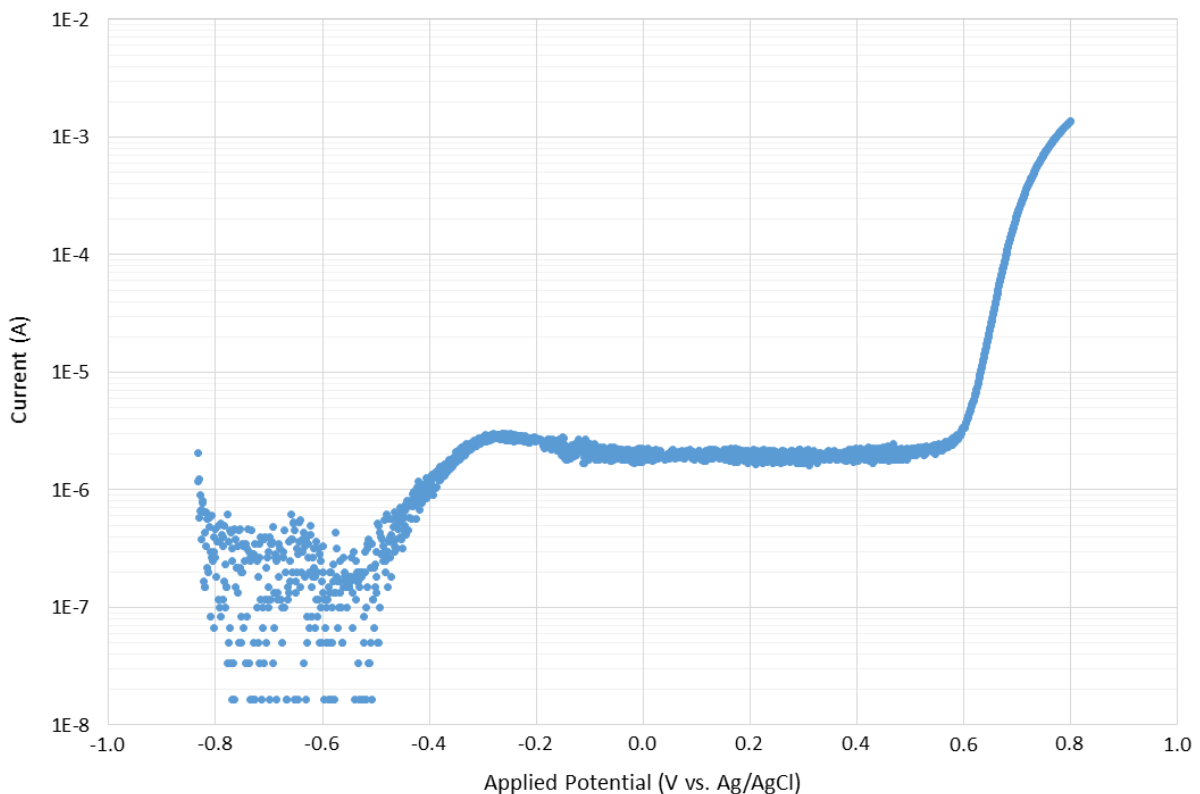


Figure 32. Polarisation curve for irradiated JRQ C-steel in portlandite pore water.

Figure 33 shows the polarisation curve for irradiated JRQ C-steel in portlandite pore water with 0.5 M CaCl_2 added. The active to passive transition appears in the same potential region compared to the polarisation without chloride. The onset of pitting corrosion appears close to -0.3 V, showing once again no influence of the irradiation (cfr. Figure 31).

Therefore, to compare both unirradiated and irradiated samples, a potential of -0.2 V vs Ag/AgCl was chosen for the accelerated tests with chloride.

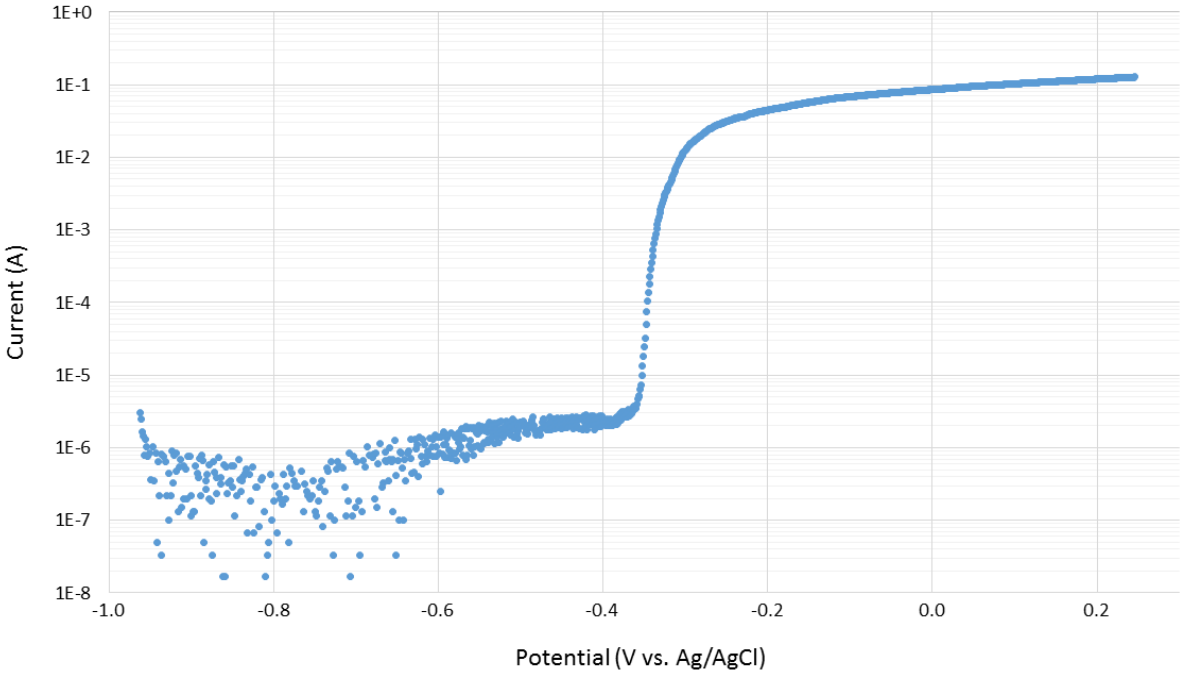


Figure 33. Polarisation curve for irradiated JRQ C-steel in portlandite pore water with the addition of 0.5 M CaCl₂.

3.7 Carbon speciation after leaching and polarised corrosion

3.7.1 Analysis of the gas phase by gas chromatography

3.7.1.1 Accelerated corrosion tests

Accelerated corrosion tests, also called polarised corrosion tests, are potentiostatic experiments where a fixed potential is imposed to the system during the analysis while the obtained current is recorded. This potential was chosen based on the outcome of the corresponding polarisation curve, as explained in the previous section.

Polarised corrosion tests were performed on both irradiated and unirradiated samples in two different electrolytes. The first electrolyte was the saturated portlandite Ca(OH)₂ solution simulating conditions met in an underground disposal environment. The second electrolyte was saturated portlandite Ca(OH)₂ solution with 0.5 M of CaCl₂ added. The presence of

chloride induces the pitting corrosion of metals, leading to higher corrosion rate. So, even if chemical conditions induced by this second electrolyte are farther from the real conditions than the first one and even if chloride could maybe influence the mechanism of the carbon-based molecule formation, some information on the production of these molecules could be obtained much faster.

Unirradiated samples

Figures 34 to 36 show the chromatograms for JRQ C-steel in pure portlandite pore water as a function of time. The applied potential was 620 mV vs. Ag/AgCl. This potential was chosen based on the corresponding polarisation curve (see Section 3.6.1). As explained earlier, this potential corresponds to the higher current in the transpassive zone of the curve, close to the upper limit of the stability domain of water.

The analysis of gas chromatograms presented in Figures 34 and 35 show the presence of ghost peaks (see more information in Section 2.6.1.1 and Appendix 2) at ~2.5 min of retention, overlapping with the expected methane peak. These peaks possess different intensities depending on the chromatogram. Despite their presence, there is no peak with a higher intensity than the detection limit, meaning that no or very little methane gas was produced during this test. The same conclusion can be made for other hydrocarbons gases analysed during the calibration of the column (CO_2 , ethene, ethane, propene and propane). Nevertheless, at ~0.4 minute of retention a peak resulting from the detection of H_2 is detected. The intensity of this peak increases with the corrosion time (Figure 35). This increase, however, doesn't (mainly) come from the production of hydrogen through the corrosion of the carbon steel sample. Indeed, Figure 36 shows that the intensity of the oxygen peak is also increasing with the corrosion time, meaning that water hydrolysis took place during the accelerated corrosion test.

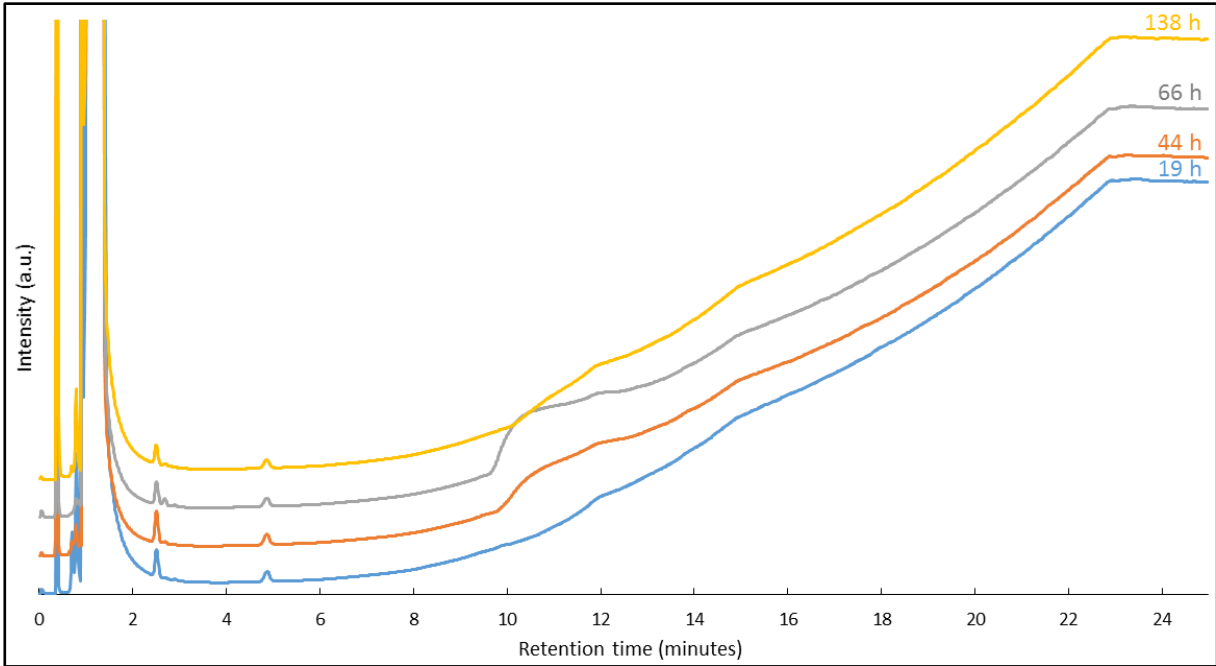


Figure 34. Gas chromatograms obtained for unirradiated JRQ C-steel in pure saturated portlandite pore water as a function of time.

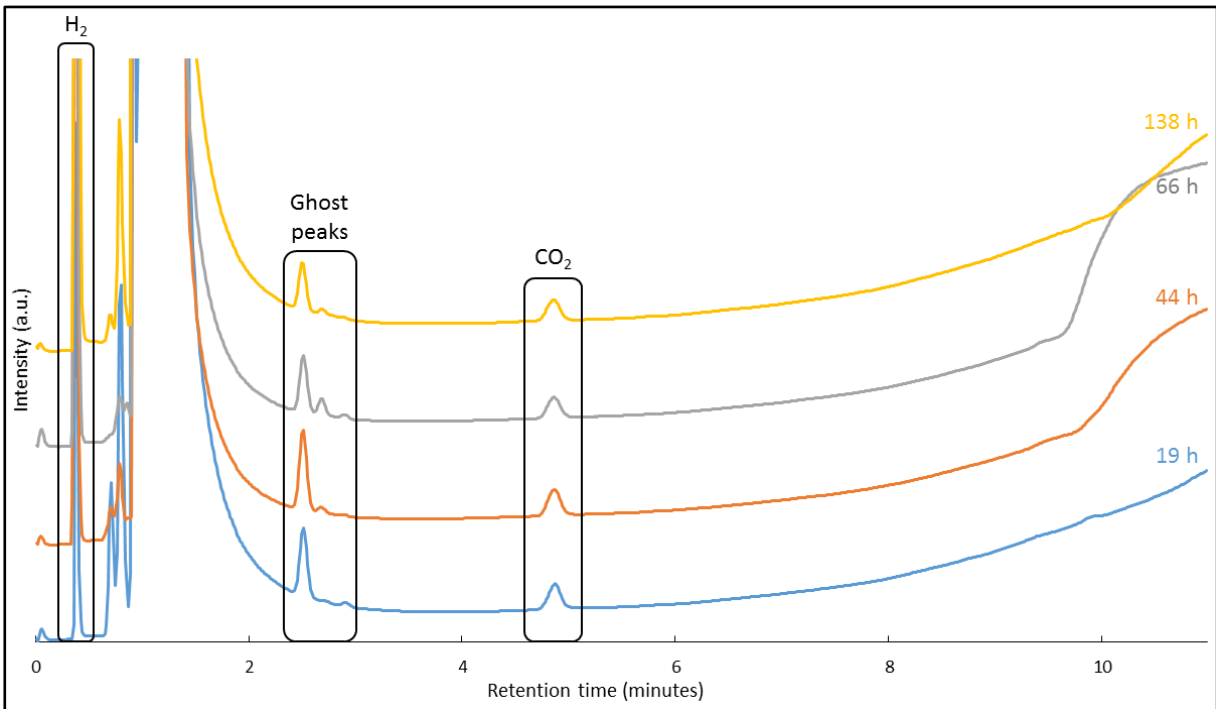


Figure 35. Gas chromatograms obtained for unirradiated JRQ C-steel in pure saturated portlandite pore water as a function of time (Zoom of Figure 34).

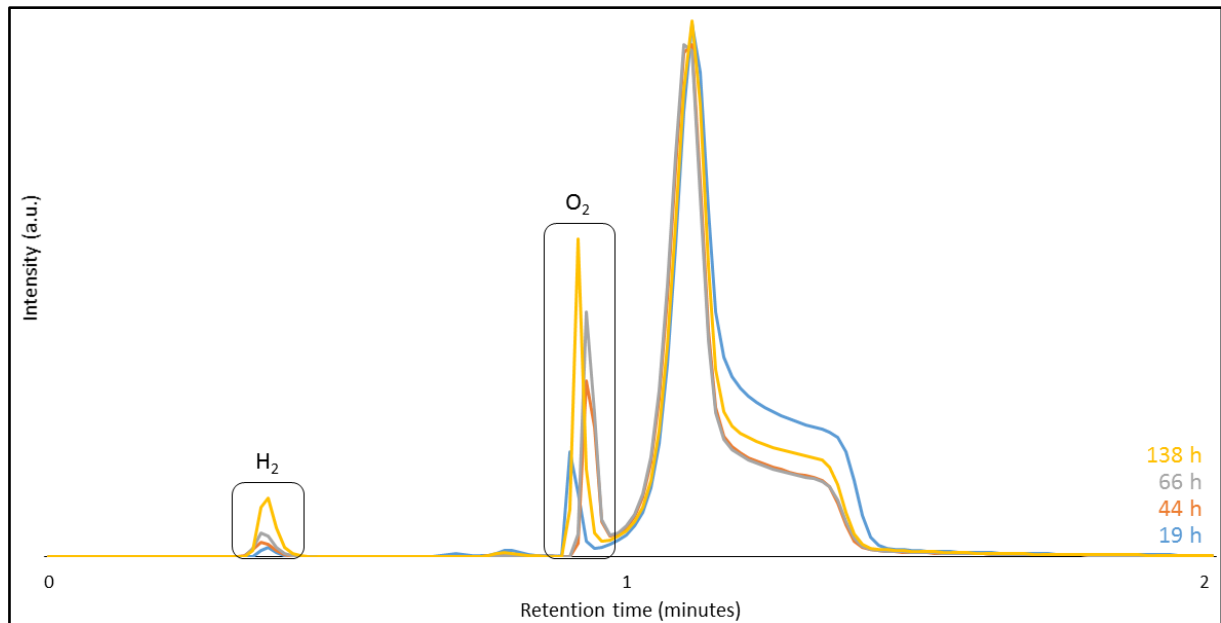


Figure 36. Gas chromatograms obtained for unirradiated JRQ C-steel in pure saturated portlandite pore water as a function of time (Zoom on H₂ and O₂ peaks).

Figure 37 shows the potentiostatic i vs. t plots. The obtained current is comparable with the value obtained during the recording of the polarisation curve (Figure 30). Moreover, thanks to this i vs. t curve, the total charge could be calculated as well as the amount of corroded metal (see calculation in Appendix 3). It appears that a corrosion rate of $\sim 150 \mu\text{m}/\text{year}$ is obtained if all the recorded current came from the corrosion of the carbon steel. This confirms that water hydrolysis took place during the accelerated corrosion test.

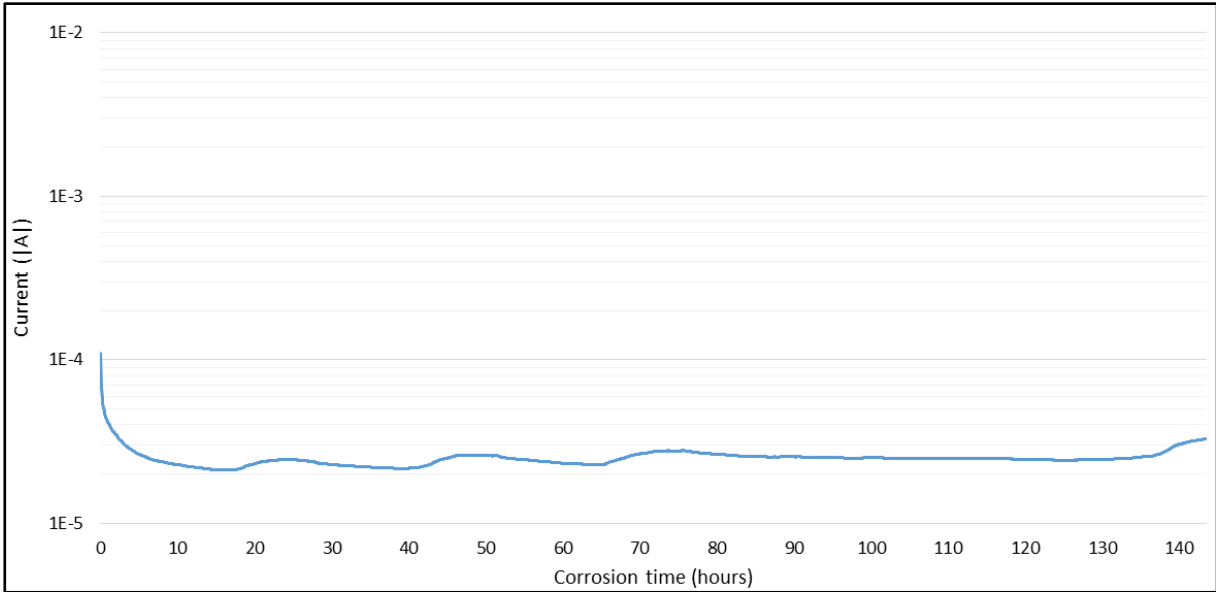


Figure 37. Current as a function of corrosion time of the unirradiated carbon steel sample in Ca(OH)₂.

Figure 38 and 39 show the chromatograms for JRQ C-steel in portlandite pore water with added CaCl₂ as a function of time. The addition of CaCl₂ leads to a decrease of the pH from ~12.5 to ~11.7. These conditions are harsher than the ones encountered during geological disposal but they offer the possibility to accelerate the corrosion rate by inducing pitting corrosion which should increase the gas formation.

The applied potential was -200 mV vs. Ag/AgCl. The potential was chosen based on the corresponding polarisation curve (see section 3.6.2) As explained earlier, pitting corrosion happens at this potential leading to a higher corrosion rate. Indeed, only a few seconds after the onset of the corrosion tests, pitting occurred and black precipitation products were formed in abundance.

Indeed the hydrogen peak is much higher than in pure portlandite pore water (without chloride) confirming that corrosion is accelerated by chlorides. Unfortunately, no other peaks could be distinguished from the chromatograms, except for a small hump at the retention time of ethene (between 8 and 9 minutes, see Figure 39) after 4h40 of testing. Unfortunately, the intensity of this peak corresponds to a concentration under the reporting limit of ethene.

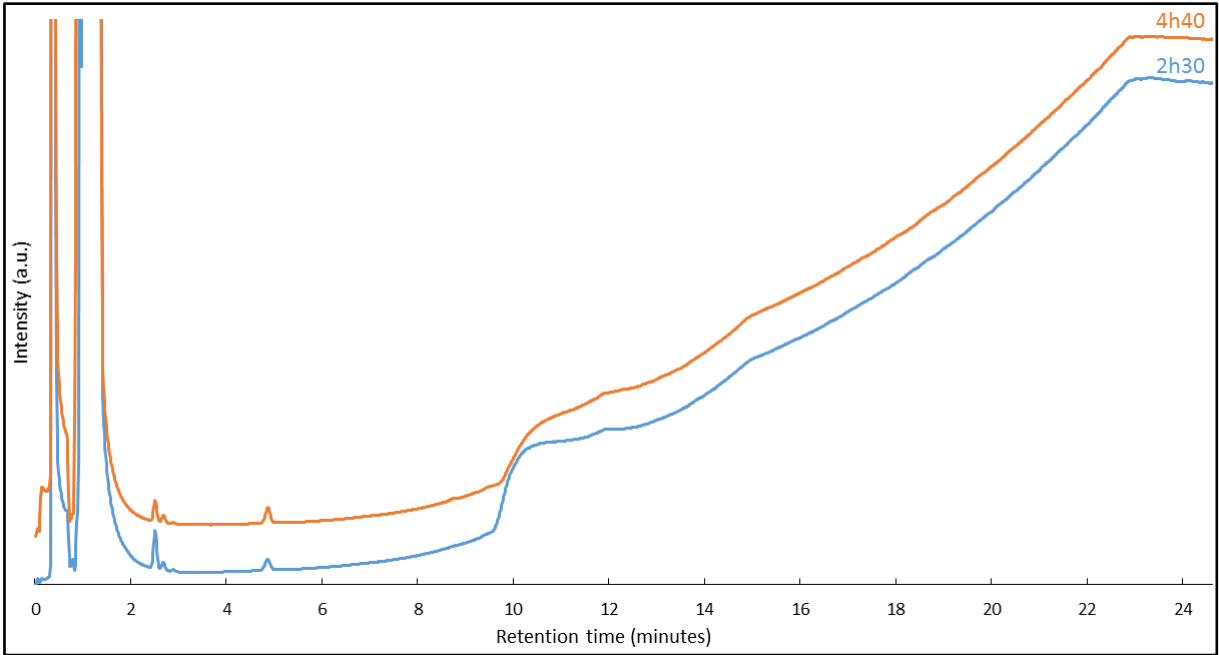


Figure 38. Gas chromatograms obtained for unirradiated JRQ C-steel in saturated portlandite water with added CaCl_2 as a function of time.

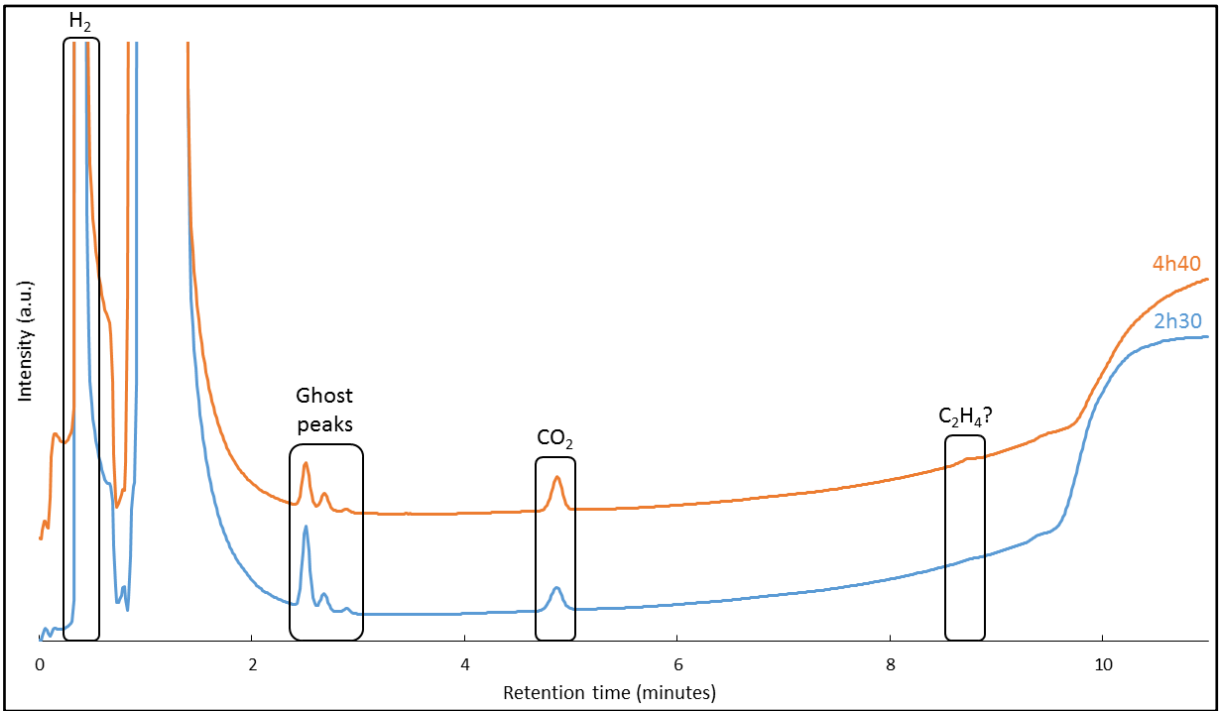


Figure 39. Gas chromatograms obtained for unirradiated JRQ C-steel in saturated portlandite water with added CaCl_2 as a function of time (Zoom of Figure 38).

Irradiated samples

The same kind of corrosion tests as the ones performed on unirradiated samples were performed on the irradiated one in order to investigate the effect of irradiation.

Figures 40 and 41 show the evolution of the chromatogram for irradiated samples in saturated portlandite pore water as a function of exposure time. As for the unirradiated sample, the applied potential is 620 mV. Due to the lower passive current in the irradiated sample (see Section 3.6.2), the corrosion current corresponding to 620 mV is also lower (5.9×10^{-6} A for the irradiated sample compared to 2.2×10^{-5} A for unirradiated one). This change leads to a lower water hydrolysis and as a consequence the presence of a lower hydrogen peak in the chromatograms. An increase of the carbon dioxide peak intensity is also present after 165 h (Figure 41). But, since no other peaks appear this could be due to a problem during the injection of the sample into the GC. Finally, as for the unirradiated sample, no other carbon compounds could be detected.

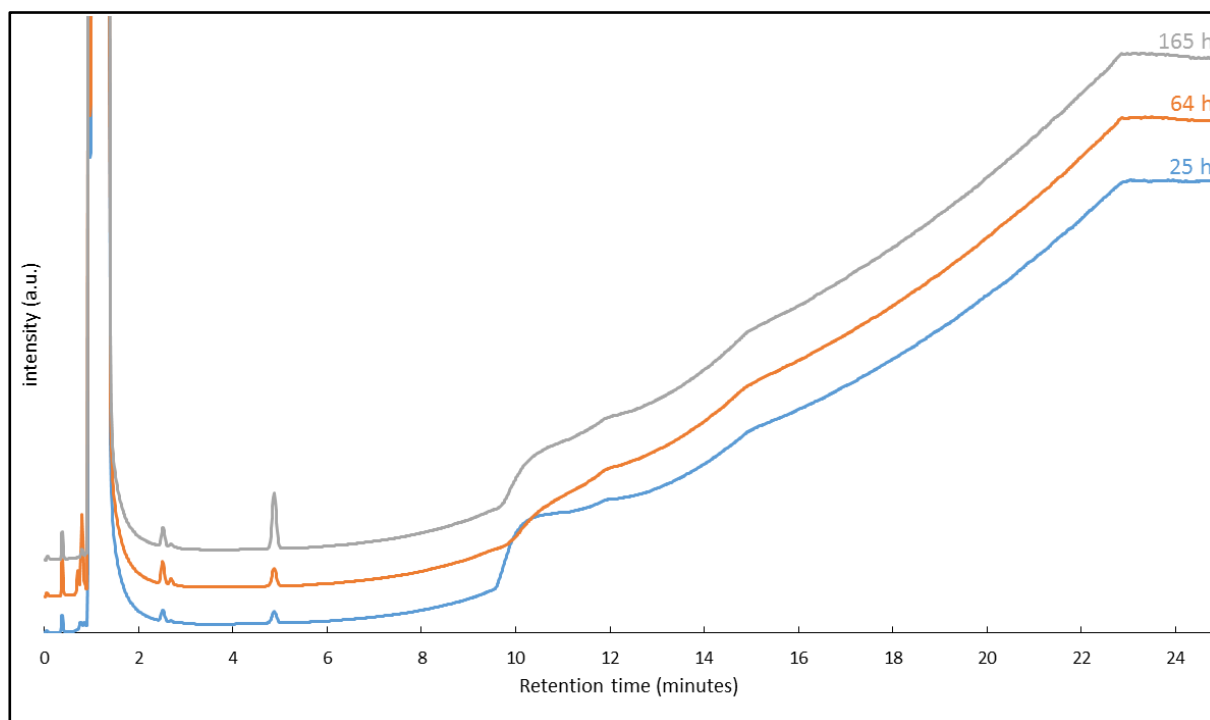


Figure 40. Gas chromatograms obtained for irradiated JRQ C-steel in pure saturated portlandite pore water as a function of time.

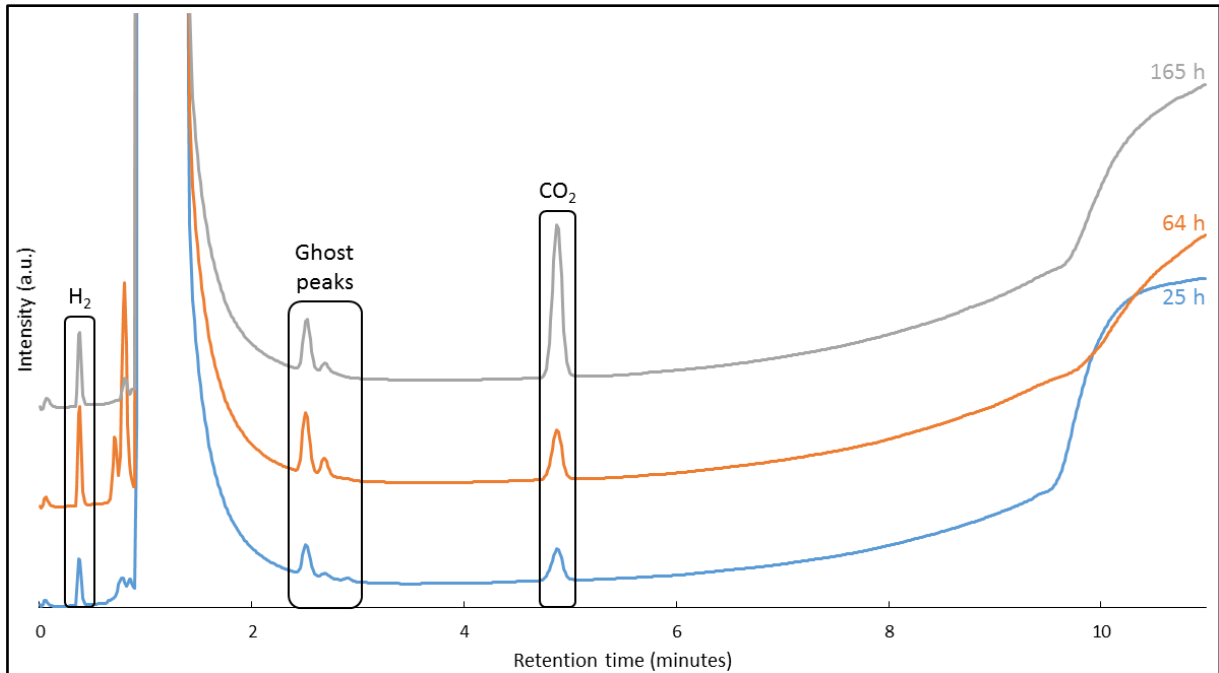


Figure 41. Gas chromatograms obtained for irradiated JRQ C-steel in pure saturated portlandite pore water as a function of time (Zoom of Figure 40).

As like as the current obtained from the corrosion of the unirradiated carbon steel, the recorded current obtained during the accelerated corrosion test of the irradiated sample (Figure 42) corresponds to the one expected from the polarisation curve (Figure 32). The total charge as well as the estimated corrosion rate were also calculated from the i vs. t curve. A corrosion rate of $\sim 63 \mu\text{m}/\text{year}$ is obtained if all the recorded current came from the corrosion of the carbon steel. So, even if the water hydrolysis seems to be lower than during the corrosion of the unirradiated sample, it is still present.

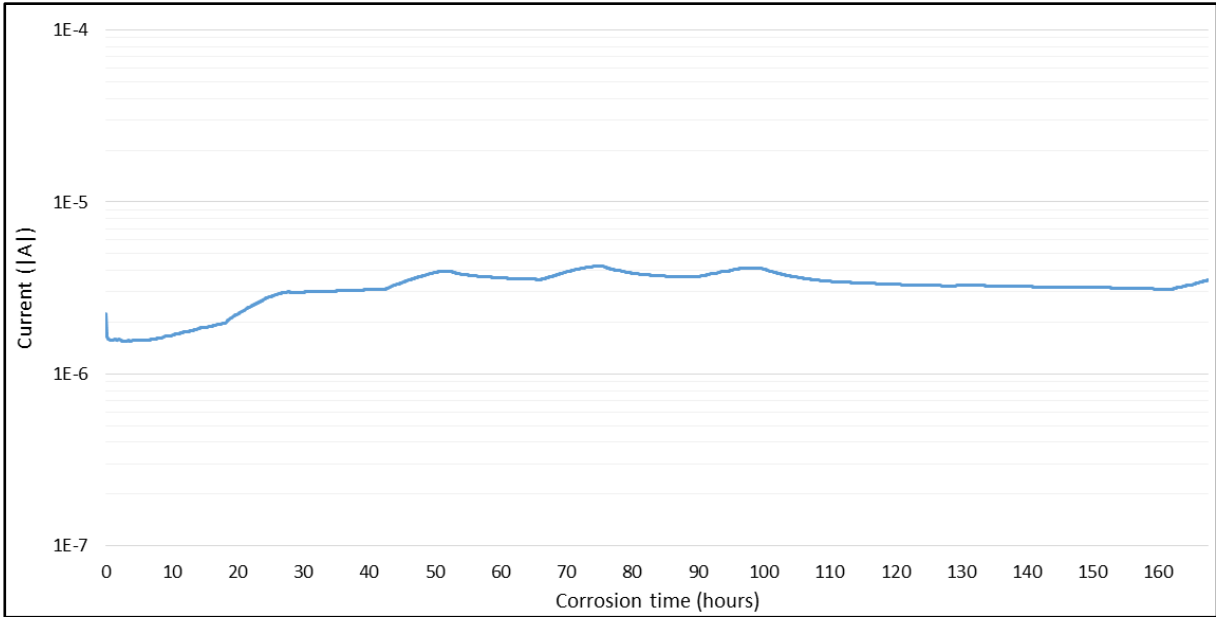


Figure 42. Current as a function of corrosion time of the irradiated carbon steel sample in $\text{Ca}(\text{OH})_2$.

Figures 43 and 44 show the chromatograms as a function of time for irradiated samples in portlandite pore water with added CaCl_2 . An applied potential of -200 mV was also chosen for the irradiated sample. The behaviour of the irradiated sample is similar to the one of the unirradiated sample with the production of hydrogen but without any other carbon-based gas production, even though pitting corrosion took place.

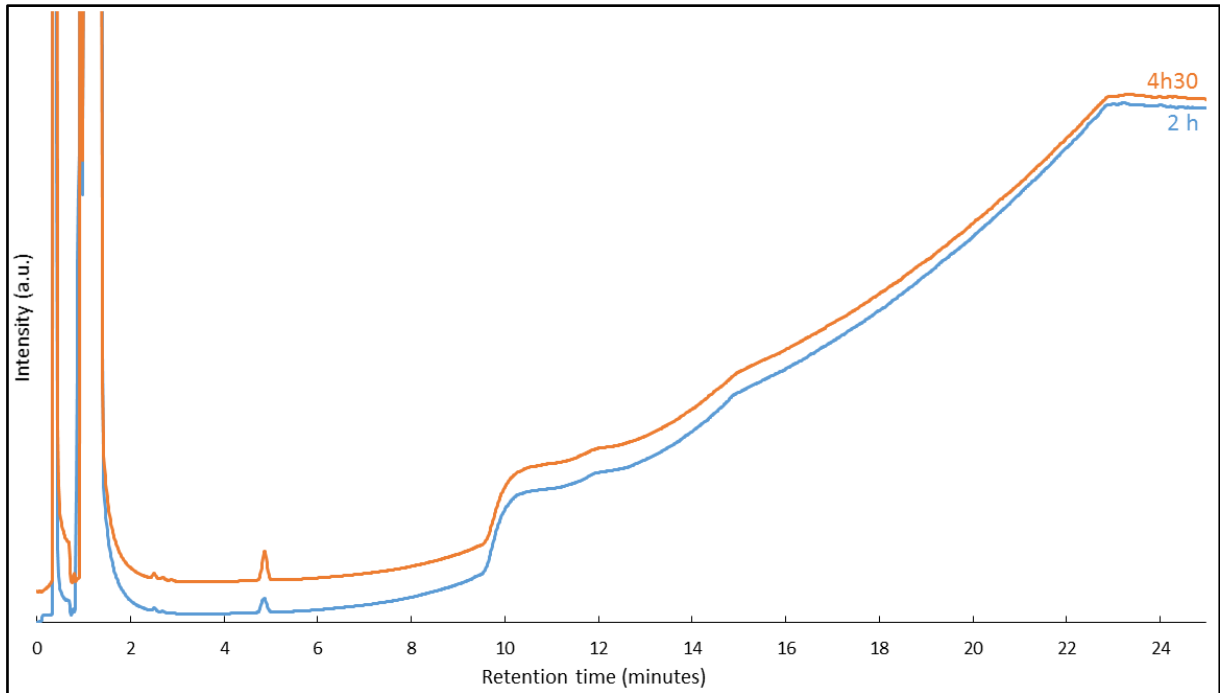


Figure 43. Gas chromatograms obtained for irradiated JRQ C-steel in saturated portlandite water with added CaCl_2 as a function of time.

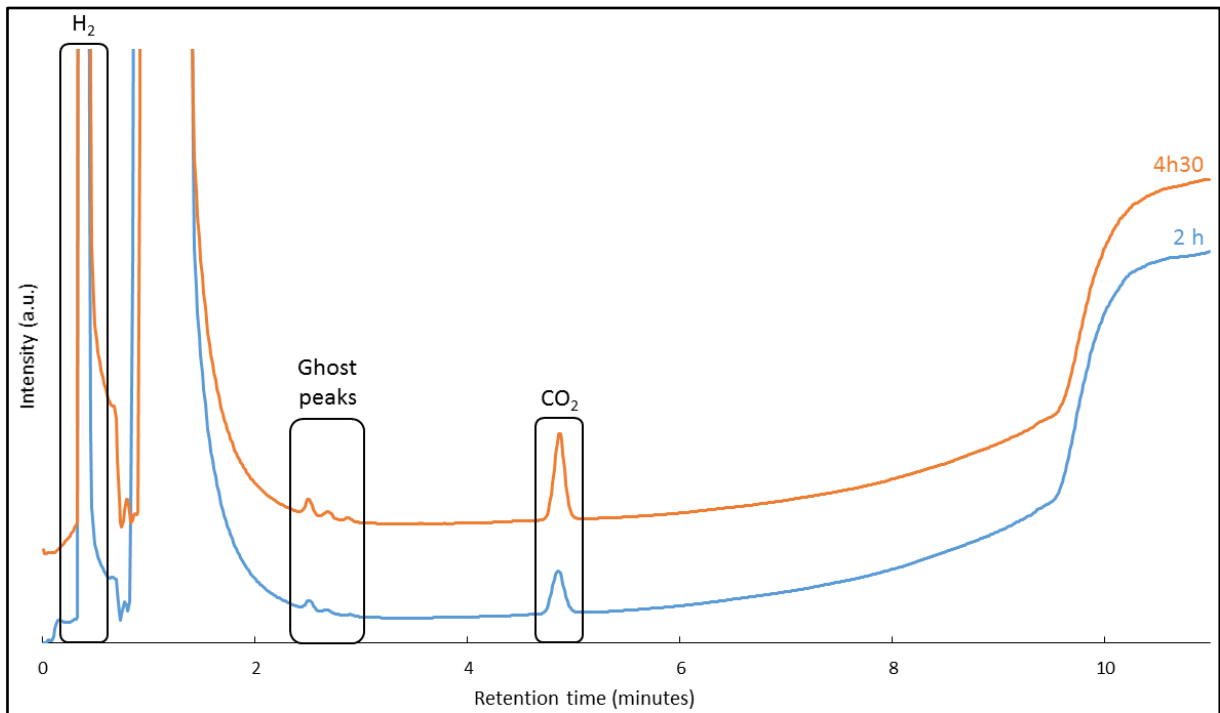


Figure 44. Gas chromatograms obtained for irradiated JRQ C-steel in saturated portlandite water with added CaCl_2 as a function of time (Zoom of Figure 43).

3.7.1.2 Static corrosion tests

Three static corrosion tests were started in July 2016 with irradiated samples 16-6-18/1RA, 16-6-18/1RB, and 16-6-18/1RC respectively. Unirradiated samples were not tested. After 231 days (~7.5 months), gas and liquid samples were taken. Gas samples were injected in the gas chromatograph. The corresponding chromatograms are compared in Figures 45 and 46. The liquid samples were reserved for liquid scintillation counting, TIC/TOC analysis, and ion chromatography

Figure 45 shows a broad peak due to the presence of oxygen. This high concentration didn't come from the accidental injection of air in the column because its presence is recurrent in the 3 samples. Moreover, it is not due to a leak in the leaching test vials because the intensity of the peak corresponding to the presence of CO_2 (Figure 46) is comparable to the intensities obtained during calibration. A third possibility is that the oxygen peak originates from the radiolysis of water by the irradiated carbon steel sample.

Figure 46 shows a zoom of Figure 44. Peaks can clearly be distinguished for hydrogen, methane, carbon dioxide, ethene and ethane. For two of the three chromatograms, the ethane peak is largely hidden by a broad peak, which could be attributed to water.

The signals for the carbon compounds were quantified using the calibration curves shown in Appendix 2. The results are shown in Table 10. The measured concentrations are low, but well above the detection limit.

No calibration curve was available for hydrogen and the concentration could not be determined quantitatively. But in comparison with the intensities of H_2 peaks obtained during the polarised tests, the hydrogen concentration seems very low compared to the amount of corroded material. This can be explained by its reaction with the O_2 present in the leaching vial to produce water. Another explanation could be the presence of residual oxygen at the beginning of the tests, leading to an aerobic/oxidizing condition and no/less hydrogen production. This hypothesis seems less likely. Indeed, gas chromatograms mainly show the production of hydrocarbon gas molecules during corrosion, while in oxic

conditions, oxidized carbon-based molecules, such as CO or CO₂, should be preferentially produced, which doesn't seem to happen.

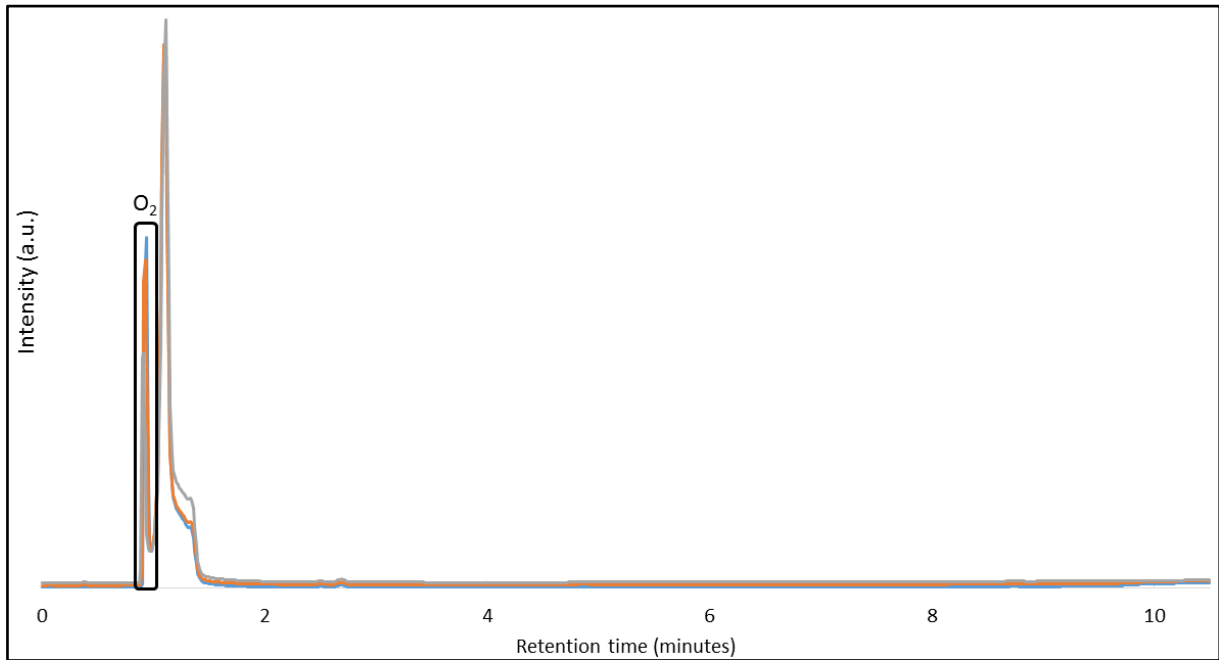


Figure 45. Gas chromatograms obtained after the static tests with JRQ carbon steel (duration 231 days).

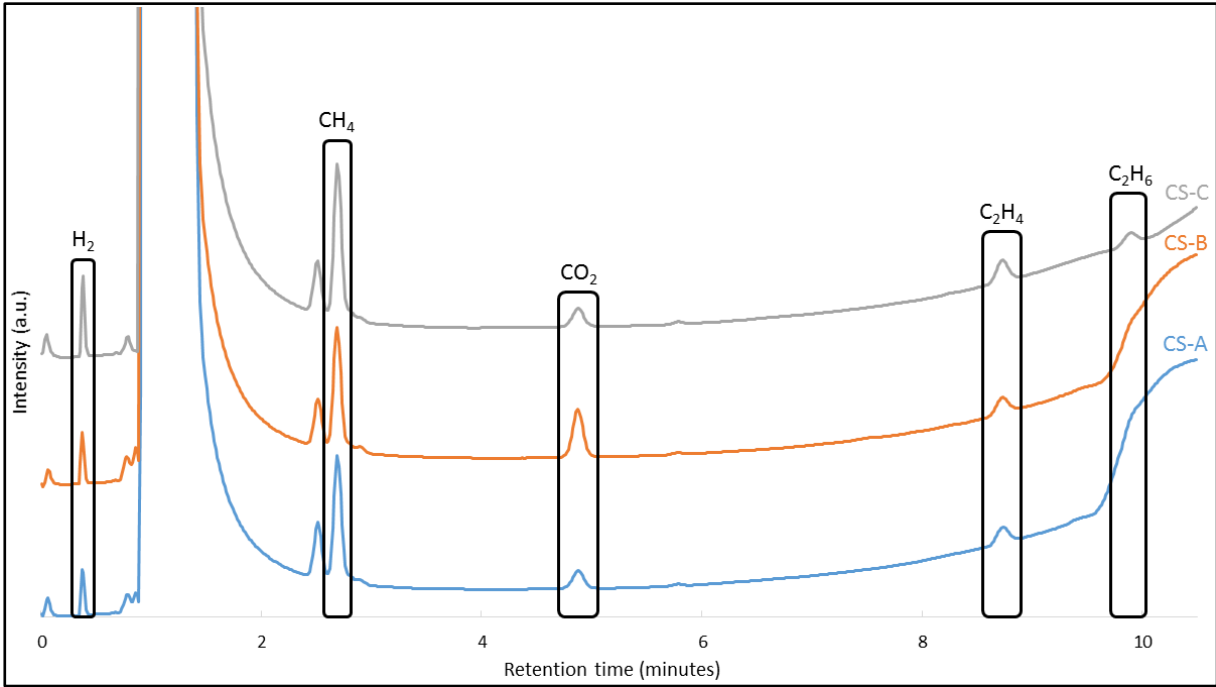


Figure 46. Gas chromatograms obtained after the static tests with JRQ carbon steel (duration 231 days) (Zoom of Figure 45).

Table 10. Calculated concentrations of methane, ethene and ethane in the gas phase after static tests with JRQ carbon steel in Portlandite pore water (duration 231 days).

ID	Methane			Ethene			Ethane		
	Peak area	Calculated concentration		Peak area	Calculated concentration		Peak area	Calculated concentration	
		μL/L	mol/L		μL/L	mol/L		μL/L	mol/L
CS-A	681880	9.9 ± 0.5	6.1 × 10 ⁻⁹	144299	1.6 ± 0.1	1.0 × 10 ⁻⁹	-	-	
CS-B	660379	9.6 ± 0.5	5.9 × 10 ⁻⁹	137950	1.5 ± 0.1	0.9 × 10 ⁻⁹	-	-	
CS-C	817457	11.9 ± 0.6	7.3 × 10 ⁻⁹	189461	2.1 ± 0.1	1.3 × 10 ⁻⁹	94967	0.6 ± 0.1	0.4 × 10 ⁻⁹
Mean value		10.4	6.4 × 10 ⁻⁹		1.7	1.1 × 10 ⁻⁹		0.6	0.4 × 10 ⁻⁹

Thanks to the calculated carbon-based gas production and the carbon concentration in the bulk, an approximation of the corrosion rate could be determined (details are given in Appendix 4). With the hypothesis that all the carbon present in the bulk is transformed in

carbon-based gas, the corrosion depth reaches 43 nm to 74 nm after 231 days, which means a corrosion rate of 68 to 117 nm per year, which is in good agreement with the 0.1 $\mu\text{m}/\text{year}$ given by Kursten et al. [KURSTEN, 2014].

3.7.2 Analysis of the liquid samples

In the previous section we gave an overview of the carbon speciation in the gas phase by means of results from gas chromatography. In this section, we discuss the analysis (carbon speciation) of the liquid phase by total organic / inorganic carbon analysis (TIC/TOC) and by ion chromatography (IC) to determine the presence of carboxylic acids. The ^{14}C determination was performed by liquid scintillation counting (LSC) while the whole activity of the solutions was measured by γ -ray spectrometry.

3.7.2.1 Carbon speciation by total organic/inorganic carbon analysis and by ion chromatography

The carbon speciation was determined by total organic/inorganic carbon analysis (TIC/TOC) on blank electrolytes and the leachate solutions after the static and accelerated tests (with both unirradiated and irradiated samples). The results of TIC/TOC analysis are shown in Table 11. TIC and TOC values of carbon steel leachate solutions were corrected for the TIC and TOC content present in the blank solution. Non corrected values are presented in Appendix 5. It has to be mentioned that the analysis of solutions obtained after the corrosion of active samples or inactive samples was performed with two different apparatus. To be able to compare all results, blank solutions were analysed by both TIC/TOC machines and gave very similar results.

Analysis of the blanks showed that some inorganic and organic carbon were already present in the solution before the start of the corrosion tests. Even if the solutions were prepared in a glove box under inert atmosphere, inorganic carbon could come from the reaction of CO_2 (still present in the glove box atmosphere, albeit in a very low concentration) with the high pH solution, producing carbonates. A small contamination with atmospheric CO_2 may also have happened during the measurement of the solution, although this should have led to a higher TIC concentration in the leachate solutions as well. However, the corrosion of carbon

steel released some Fe^{2+} ions in solution, even if in low concentration, which could have led to the precipitation of FeCO_3 . Indeed, the K_{sp} of FeCO_3 ($3.13 \times 10^{-11} \text{ M}^2$) is lower than the one of CaCO_3 ($4.95 \times 10^{-9} \text{ M}^2$) and its precipitation is favored compared to the one of CaCO_3 . This precipitation could then decrease the TIC content in the leachate solution, contrarily to the blank solution. The organic carbon probably came from the polypropylene recipient into which the solution was poured after its preparation in a glass recipient to avoid the increase of Si due to glass dissolution at high pH. It could maybe also come from a degradation of the sample holder resin due to a combination of the high pH of the solution and the radiation of the sample.

No inorganic carbon was found after the accelerated corrosion tests in saturated portlandite solution while approximately 4 mg/L of organic carbon was obtained for the accelerated corrosion of unirradiated samples and a approximately 23 mg/L of organic carbon for the accelerated corrosion of the irradiated sample in saturated portlandite solution. This last result is surprising because neither the GC analysis nor the current produced during the corrosion test could explain such a high concentration. Furthermore, this organic carbon should not come from a contamination of the electrolyte used for this analysis because electrolyte from the same batch was also used for the analysis of the blank (Blank- $\text{Ca}(\text{OH})_2$). As explained earlier, organic carbon could then come from the polypropylene recipient or sample holder resin.

The analysis of accelerated corrosion tests electrolyte in the presence of chloride showed the presence of inorganic and organic carbon after the corrosion of the unirradiated sample. This was expected due to the intense pitting corrosion. However, only a small amount of inorganic and organic carbon was detected after the corrosion of the irradiated material (see Table A5-1 in Appendix 5). Due to the intense pitting corrosion, heavy particles were released in the solution. Some carbon could maybe be adsorbed and/or precipitated with these particles.

Finally, after the static corrosion tests, no inorganic carbon was detected in the saturated portlandite solution while only little organic carbon was detected (under the blank level; Tables 11 and A5-1). These results were expected because of the low corrosion rate

expected for those tests. Moreover, the higher organic carbon concentration in the blank solution supports our hypothesis that organic carbon probably came from the polypropylene recipient. Indeed, for the static corrosion test, the solution was used directly after its preparation and hence it was not stored in plastic bottles for a long time in contrast to the blank solutions and the ones from the accelerated tests.

Table 11. Results from TIC/TOC analysis (blank value removed from leachate concentration).

Sample-ID	Electrolyte/Material	TIC		TOC	
		mg/L	mmol/L	mg/L	mmol/L
Blank-Ca(OH) ₂	Saturated portlandite water solution	6.4 ± 0.8	0.53 ± 0.07	4.4 ± 0.5	0.37 ± 0.04
Blank-CaCl ₂	Saturated Ca(OH) ₂ water solution + 0.5 M CaCl ₂	7.4 ± 0.7	0.62 ± 0.06	7.4 ± 0.7	0.62 ± 0.06
Inactive-CS_ Ca(OH) ₂	Unirradiated Carbon Steel / Polarised test / Ca(OH) ₂ water solution	< 0.5	-	4.1 ± 0.8	0.34 ± 0.07
Inactive-CS_ CaCl ₂	Unirradiated Carbon Steel / Polarised test / Ca(OH) ₂ + CaCl ₂ water solution	11.1 ± 0.5	0.92 ± 0.04	7.1 ± 1.4	0.59 ± 0.12
Active-CS_ Ca(OH) ₂	Irradiated Carbon Steel / Polarised test / Ca(OH) ₂ water solution	< 0.5	-	22.8 ± 2.8	1.90 ± 0.23
Active-CS_ CaCl ₂	Irradiated Carbon Steel / Polarised test / Ca(OH) ₂ + CaCl ₂ water solution	< 0.5	-	< 0.5	-
Sol-CS-A	Irradiated Carbon Steel / Leaching test / Ca(OH) ₂ water solution	< 0.5	-	< 0.5	-
Sol-CS-B	Irradiated Carbon Steel / Leaching test / Ca(OH) ₂ water solution	< 0.5	-	< 0.5	-
Sol-CS-C	Irradiated Carbon Steel / Leaching test / Ca(OH) ₂ water solution	< 0.5	-	< 0.5	-

Ion chromatography was used to determine the content of carboxylate acids such as formate, acetate and oxalate in blank and leachate solutions. The results are presented in Table 12.

The analyses of the blank solutions show that no carboxylic acids are detected in the presence of chlorides while formate and acetate are already present in the saturated

portlandite solution in small concentration. The presence of these molecules is strange because both electrolytes were prepared in the same conditions. One of the differences between both electrolytes is the higher pH obtained for the saturated portlandite solution (~12.5 compared to ~11.7 in the presence of chloride) which could maybe influence the solution stored in polypropylene bottles. The second difference is the presence of 0.5 M of Ca^{2+} , which could maybe bind formate and acetate, resulting in their precipitation, removed after filtration over 0.45 μm before the ion chromatography analysis. Finally, in none of the solutions oxalate was found. This maybe means that the formation of molecules with two carboxylic acid functions is less favourable in the conditions met during these corrosion tests.

After the accelerated corrosion tests in saturated portlandite solution (without chloride), formate and acetate were detected in some cases (Tables 12 and A5-2). This was unexpected for accelerated corrosion and therefore these molecules could also come from impurities, as the ones measured in the blank.

In the presence of chloride, no carboxylic acids are detected. The reason for this could be that either all the organic carbon-based compounds are present in the gas phase, even in low concentration, or they are present in the precipitate formed during pitting corrosion, or they could be adsorbed on the vial wall.

For the static corrosion tests, carboxylic acids are not detected except for some formate in sample Sol-CS-C (Table 12). Again, these formate should come from contamination of the saturated portlandite solution used to perform the corrosion tests. Again, this contamination could maybe come from the polypropylene vials used to transfer the solution or from the ion chromatograph during the measurement of our sample.

Table 12. Results from ion chromatography (blank value removed from leachate concentration).

Sample ID	Electrolyte / Material	Formate		Acetate		Oxalate	
		mg/L	mmol/L	mg/L	mmol/L	mg/L	mmol/L
Blank-Ca(OH) ₂	Saturated portlandite water solution	0.16	3.55 x10 ⁻³	0.14	2.37 x10 ⁻³	< 0.1	-
Blank-CaCl ₂	Saturated Ca(OH) ₂ water solution + 0.5 M CaCl ₂	< 0.1	-	< 0.1	-	< 0.1	-
Inactive-CS_Ca(OH) ₂	Unirradiated Carbon Steel / Polarised test / Ca(OH) ₂ water solution	0.24	5.33 x10 ⁻³	< 0.1	-	< 0.1	-
Inactive-CS_CaCl ₂	Unirradiated Carbon Steel / Polarised test / Ca(OH) ₂ + CaCl ₂ water solution	< 0.1	-	< 0.1	-	< 0.1	-
Active-CS_Ca(OH) ₂	Irradiated Carbon Steel / Polarised test / Ca(OH) ₂ water solution	< 0.1	-	< 0.1	-	< 0.1	-
Active-CS_CaCl ₂	Irradiated Carbon Steel / Polarised test / Ca(OH) ₂ + CaCl ₂ water solution	< 0.1	-	< 0.1	-	< 0.1	-
Sol-CS-A	Irradiated Carbon Steel / Leaching test / Ca(OH) ₂ water solution	< 0.1	-	< 0.1	-	< 0.1	-
Sol-CS-B	Irradiated Carbon Steel / Leaching test / Ca(OH) ₂ water solution	< 0.1	-	< 0.1	-	< 0.1	-
Sol-CS-C	Irradiated Carbon Steel / Leaching test / Ca(OH) ₂ water solution	< 0.1	-	0.17	2.88 x10 ⁻³	< 0.1	-

In conclusion, the interpretation of the TIC/TOC and ion chromatography analyses is not easy and many hypotheses were formulated to try to explain some unexpected results. To check these hypotheses, more experimental work is still in progress such as the analysis of

possible adsorbed carbon-based molecules on the corrosion cell walls, the release of organic carbon from the resin used to embed the test specimens, ...

3.7.3 ^{14}C activity detection by Liquid Scintillation Counting

To determine the total ^{14}C activity released in solution by corrosion, Liquid Scintillation Counting (LSC) was performed on all leachates of irradiated carbon steel (static and accelerated corrosion tests). Unfortunately, due to the contamination of solutions with other radionuclides (e.g. ^{60}Co) which emit highly energetic radiation, it was not possible to calculate the ^{14}C activity of leachates from static corrosion tests and accelerated test in presence of chloride.

The only measurable solution was the leachate from the accelerated corrosion test in saturated portlandite solution. LSC gave an activity below 12.4 Bq/L, which is considered as the background. This value is not unexpected due to the very low corrosion rate occurring during this test.

Moreover, looking at the ^{14}C concentration in the carbon steel sample calculated in Section 3.4 and the possible weight of carbon steel corroded during static tests (see Appendix 4), the activity of the released ^{14}C should be ~0.02 Bq, which is impossible to detect by LSC.

4 Conclusions

The work at SCK•CEN, in the framework of Work Package 2 of the CAST project, focussed on the release of ¹⁴C from JRQ carbon steel representative for the reactor pressure vessel steel of the Belgian nuclear power plants and the ¹⁴C speciation in a cementitious environment, which is relevant for the Belgian Supercontainer design, as perceived for the geological disposal of high level radioactive waste. To this end, we investigated both unirradiated and irradiated material.

The unirradiated sample was a Charpy-V specimen which was cut into smaller pieces. The nitrogen content in the unirradiated material was approximately 19 µg/g, which is at the lower end of the 20-30 µg/g range mentioned in the literature. Calculations showed that this would lead, after irradiation, to a ¹⁴C activity of about 175 Bq/g in the JRQ steel.

Metallographic analysis was performed on both unirradiated and irradiated material in order to investigate the influence of irradiation on the metallic structure. The grain structure is that of a ferritic-bainitic steel, which is the expected grain structure for a RPV steel. The main defects present in both the unirradiated and irradiated material are line dislocations, with the dislocation density diminishing by irradiation. Another effect of irradiation is the formation of a small amount of dislocation loops. Two types of carbides were found in both materials: Fe₃C and Mo₂C. The concentration of Fe₃C is increased by irradiation.

Measurements of the ⁶⁰Co release of JRQ carbon steel in pure portlandite water suggested that the corrosion rate indeed obeys a parabolic law, as reported in literature. The obtained corrosion rates however are very low, below 10 nm/year. This can be explained by experimental artefacts such as precipitation in the portlandite solution.

To obtain information on the behaviour of JRQ carbon steel in real geological disposal conditions, long-running leaching corrosion tests were performed. Accelerated (polarised) corrosion tests were performed to obtain some indication of the corrosion mechanism and the formation of lower carbon molecules in a shorter reaction time. The electrolyte used was a saturated portlandite Ca(OH)₂ aqueous solution of pH 12.5, representative of the

geological disposal conditions. In addition, for a second batch of accelerated tests, 0.5 M of CaCl₂ was added to the portlandite solution, stimulating pitting corrosion in order to obtain a higher yield of corrosion products.

The accelerated tests were performed in glass test cells equipped with a standard three-electrode setup, using a house-made Ag/AgCl electrode as reference electrode, a platinum mesh as counter electrode, and an embedded and polished JRQ carbon steel sample as working electrode. Gas chromatography after the tests in saturated portlandite water showed no carbon-containing corrosion products. Tests in a portlandite solution with added CaCl₂ revealed a hydrogen peak due to pitting corrosion but no carbon-based molecules were formed.

The static (leaching) tests were performed in PEEK-lined steel vials with an internal volume of 50 cm³ filled with 35 cm³ of electrolyte under a nitrogen atmosphere. After closing the cell gastight with a lid, the whole setup was left behind a lead wall for 231 days. Gas chromatography revealed that during the static tests, hydrogen, methane, ethene, and ethane were produced. Assuming that all carbon released from the metal is transformed into gaseous carbon compounds, this yields a corrosion rate of 68 to 117 nm/year.

References

[DIOMIDIS, 2014] Diomidis, N. [2014]. Scientific basis for the production of gas due to corrosion in a deep geological repository, *NAGRA, Switzerland*, report NAB 14-21.

[FUJISAWA, 1997] Fujisawa, R., Cho, T., Sugahara, K., Takizawa, Y., Horikawa, Y., Shiomi, T. and Hironaga, M. [1997]. The corrosion behavior of iron and aluminium under waste disposal conditions, *Mat. Res. Soc. Symp. Proc.* 465, 675-682.

[FUJIWARA, 2002] Fujiwara, A. [2002]. Gas generation by steel corrosion under reductive conditions – Continuous measurement test, presented at the *GASNET Workshop*, 12-14 November, 2002, Cologne, Germany.

[GRAUER, 1991a] Grauer, R., Knecht, B., Kreis, P. and Simpson, J.P. [1991]. Hydrogen evolution from corrosion of iron and steel in intermediate level waste repositories, *In: Abrajano, T. and Johnson, L.H., eds., Scientific Basis for Nuclear Waste Management XIV, Mat. Res. Soc. Symp. Proc.*, Vol. 212, 295-302.

[GRAUER, 1991b] Grauer, R., Knecht, B., Kreis, P. and Simpson, J.P. [1991]. The long term corrosion rate of passive iron in anaerobic alkaline solutions, *Werkstoffe und Korrosion*, Vol. 42, 637-642.

[HONDA, 2009] Honda, A., Masuda, K., Imakita, T., Kato, O. and Nishimura, T. [2009]. Modelling of chemical transition of nitrate accompanied by corrosion of carbon steel under alkaline conditions, *Corrosion Engineering*, Vol. 58, 219-234.

[IAEA, 2001] IAEA. [2001]. Reference manual on the IAEA JRQ correlation monitor steel for irradiation damage studies, *IAEA, Austria*, IAEA-TECDOC-1230.

[IAEA, 2009] IAEA. [2009]. Integrity of reactor pressure vessels in nuclear power plants: assessment of irradiation embrittlement effects in reactor pressure vessel steels, *IAEA Austria*, IAEA Nuclear Energy Series No. NP-T-3.11.

- [KANEKO, 2004] Kaneko, M., Miura, N., Fujiwara, A. and Yamamoto, M. [2004]. Evaluation of gas generation rate by metal corrosion in the reducing environment, *Radioactive Waste Management Funding and Research Center (RWMC), Japan*, report RWMC-TRE-03003.
- [KREIS, 1991] Kreis, P. [1991]. Hydrogen evolution from corrosion of iron and steel in low/intermediate level waste repositories, *NAGRA, Switzerland*, report NAGRA NTB 91-21.
- [KREIS, 1992] Kreis, P. and Simpson, J.P. [1992]. Hydrogen gas generation from the corrosion of iron in cementitious environments. 57-72 in *Corrosion problems related to nuclear waste disposal, European Federation of Corrosion Publication number 7*. (Institute of Materials, London, U.K.).
- [KURSTEN, 2014] Kursten, B. [2014]. Uniform corrosion rate data of carbon steel in cementitious environments relevant to the Supercontainer design, *SCK•CEN, Belgium*, State-of-the-art report as of December 2013, SCK•CEN Report no. SCK•CEN-ER-94.
- [MIHARA, 2002] Mihara, M., Nishimura, T., Wada, R. and Honda, A. [2002]. Estimation on gas generation and corrosion rates of carbon steel, stainless steel and zircaloy in alkaline solutions under low oxygen condition, *JNC Technical Review*, Vol. 15, 91-101 (in Japanese).
- [NAISH, 1990] Naish, C.C., Balkwill, P.H., O'Brien, T.M., Taylor, K.J. and Marsh, G.P. [1990]. The anaerobic corrosion of carbon steel in concrete, *AEAT Technology, U.K.*, report NSS/R273.
- [NAISH, 1993] Naish, C.C. [1993]. Corrosion Aspects of the Proposed Sellafield Waste Repository, *UK Corrosion '93*.
- [NAISH, 2001] Naish, C.C., Blackwood, D.J., Thomas, M.I. and Rance, A.P. [2001]. The anaerobic corrosion of carbon steel and stainless steel, *AEA Technology, U.K.*, report AEAT/R/ENV/0224.

[NEWMAN, 2010] Newman, R.C. and Wang S. [2010]. Feasibility study of hydrogen monitoring during anaerobic corrosion of carbon steel in grouts, *NAGRA, Switzerland*, report NAB 10-27.

[NEWMAN, 2015] Newman, R.C., Wang, S. and Senior, N. [2015]. Understanding and quantifying the corrosion of carbon steel in grouts relevant to the Swiss L/ILW repository, *NAGRA, Switzerland*, report NAB 15-17.

[NISHIMURA, 2003] Nishimura, T., Wada, R. and Fujiwara, K. [2003]. Evaluation of gas generation rates caused by metal corrosion under the geological repository conditions, *R&D Kobe Steel Engineering Reports*, Vol. 53, 78-83 (in Japanese).

[RWMC, 1998] RWMC [1998]. Verification test on advanced radioactive waste disposal systems, *Radioactive Waste Management Funding and Research Center (RWMC), Japan*, volume 1 and 2 – 1998 report.

[SMART, 2002] Smart, N.R. [2002]. A survey of steel corrosion data for use in the GAMMON computer program, *Serco Assurance, U.K.*, report SERCO/ERRA-0484.

[SMART, 2009] Smart, N.R., Rance, A.P., Winsley, R.J., Fennell, P.A.H., Reddy, B. and Kursten, B. [2009]. The effect of irradiation on the corrosion of carbon steel in alkaline media in *Long-Term Performance of Cementitious Barriers and Reinforced Concrete in Nuclear Power Plants and Waste Management*. L'Hostis, V. Gens, R. and Gallé, C., Eds. NUCPERF 2009, RILEM proceedings PRO 64, 45-52.

[TAIT, 1994] TAIT, W.S. [1994]. *An introduction to electrochemical corrosion testing for practicing engineers and scientists*, (USA: Pair O Docs Publications).

[WALLACE, 1977] WALLACE, D. [1977]. Carbon-14 production in nuclear reactors [online], Oak Ridge National Laboratory, Tennessee, USA, Available from <http://web.ornl.gov/info/reports/1977/3445605743782.pdf>

Appendix 1: Precipitation probability of CaCO_3 (calcite) at a pH of 12.5

What is the solubility of CaCO_3 at 25°C ?

$$K_{\text{sp}} = 4.95 \cdot 10^{-9} \text{ M}^2 = [\text{Ca}^{2+}] \cdot [\text{CO}_3^{2-}]$$

In a $\text{Ca}(\text{OH})_2$ aqueous solution at a pH of 12.5, the concentration of Ca^{2+} is:

Strong base pH formula: $\text{pH} = 14 + \log [\text{base}]$

$$\Rightarrow 12.5 = 14 + \log [\text{OH}^-]$$

$$\Rightarrow [\text{OH}^-] = 0.032 \text{ M}$$

$$\text{So, } [\text{Ca}^{2+}] = [\text{OH}^-]/2 = 0.016 \text{ M}$$

Then, precipitation of CaCO_3 will start when the concentration of CO_3^{2-} reaches:

$$[\text{CO}_3^{2-}] > K_{\text{sp}} / [\text{Ca}^{2+}] = 4.95 \cdot 10^{-9} / 0.016$$

$$[\text{CO}_3^{2-}] > 3.1 \cdot 10^{-7} \text{ M or } 1.86 \cdot 10^{-5} \text{ g/L}$$

Appendix 2: Validation of the measurement of methane, carbon dioxide, ethene, ethane, propene and propane in gas samples by the GC-2010 Plus gas chromatograph

1. Summary

In the table below a summary of the validation results is given. More details can be found in the next chapters.

Reporting limits	Methane: 0.4 $\mu\text{g/g}$ Carbon dioxide: 3 $\mu\text{g/g}$ Ethene: 0.2 $\mu\text{g/g}$ Ethane: 0.2 $\mu\text{g/g}$ Propene: 1.5 $\mu\text{g/g}$ Propane: 0.75 $\mu\text{g/g}$
Linearity	From reporting limit to 10 $\mu\text{g/g}$ (when a regression with weights 1/concentration is used)
Measurement uncertainty^(*)	Methane: 0.2 $\mu\text{g/g}$ or 5% of concentration (largest of both) Carbon dioxide: 2 $\mu\text{g/g}$ or 5% of concentration (largest of both) Other gases: 1/3 of reporting limit or 5% of concentration (largest of both)

(*) Only a rough estimate of the measurement uncertainty can be given.

Note: The measurements for the validation study took place from December 2016 till February 2017 and chromatograms were acquired by means of the method *Method Cast- No headspace.gcm* (see SOP *Measurement of methane, carbon dioxide, ethene, ethane, propene and propane in gas samples by the GC-2010 plus A gas chromatograph* for more information).

2. Detection limits

Initially, detection limits were calculated by means of the noise in the proximity of the peak of interest as follows (Figure A2-1):

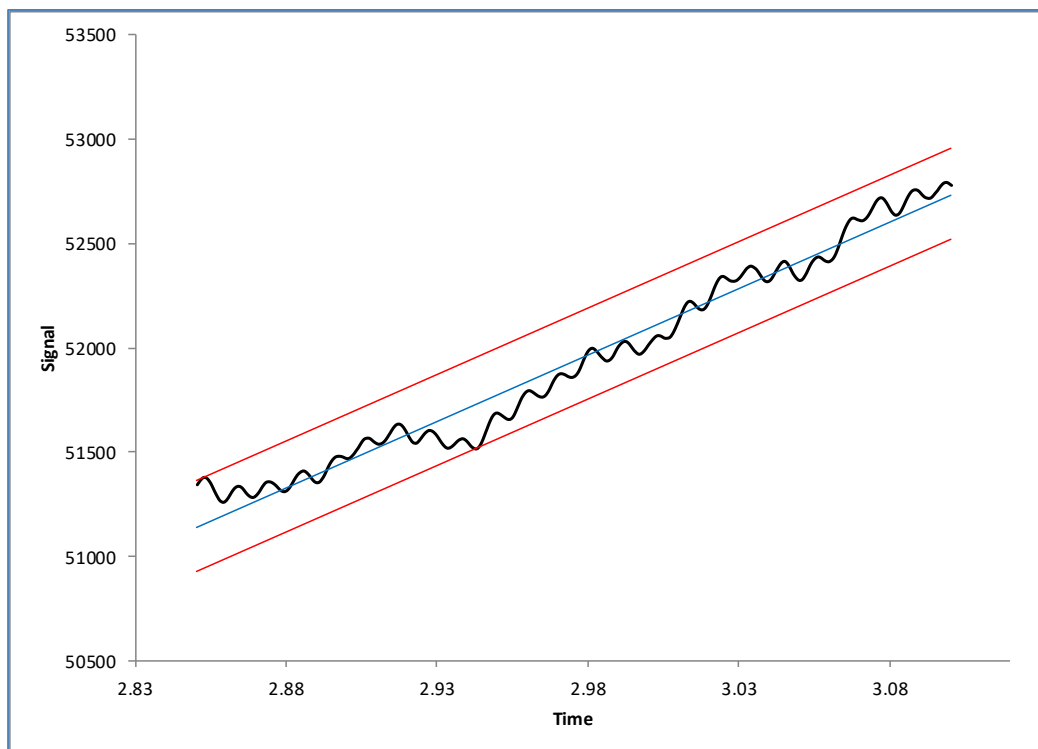


Fig.A2-1 Determination of detection limit by means of noise

- A background section with width (time interval) at least equal to the width of the near peak (peak width at baseline) is determined.
- The slope of the approximated linear line for the data points within this section is calculated by the least square method.
- Two parallel lines are drawn by shifting the slope upward and downward, so that all data points within the section fall between two lines.
- The distance between the two parallel lines in the Y axis direction is the noise width for the section.
- The noise width is multiplied by 3 and this result is transformed to concentration ($\mu\text{g/g}$) via a calibration.

Secondly, detection limits were also determined in a more practical way by measuring standards of successive lower concentrations (difference in concentration between successive standards was maximum a factor 2) until no (clear) peak was observed anymore.

Results of both methods are given in the table below:

	Detection limit (in $\mu\text{g/g}$) determined by means of the noise	Detection limit (in $\mu\text{g/g}$) determined by measuring standards of successive lower concentrations
Methane	0.11	0.10
Carbon dioxide	(0.11)	---
Ethene	0.19	0.10
Ethane	0.17	0.10
Propene	0.65	1.5
Propane	0.61	0.75

For carbon dioxide however, the above methods give no realistic value of the practical detection limit: because a direct injection technique of the sample is used, some air will always enter the column (and the detector), which results in carbon dioxide contamination. This of course influences the practical detection limit of carbon dioxide and must be taken into account.

Therefore, 59 blanks were measured over a period of 2 weeks. These blanks consisted of pure nitrogen or other standard gases in which no carbon dioxide was present.

Approximately half of them were taken directly from the gas bottle and the other half from the gas mouse that was filled with the standard gas. No systematical difference in carbon dioxide concentration was observed between blanks from the bottle as compared to blanks from the gas mouse, from which it can be concluded that use of the gas mouse causes no further carbon dioxide contamination. The observed peak areas of the carbon dioxide in the blanks varied between 62×10^3 and 299×10^3 , the average value was 180×10^3 and the standard deviation 56×10^3 . For the calibration (see also further), all peak areas of the standards are corrected for the mean value of the blank (from all measured peak areas a value of 180×10^3 is subtracted) and also when samples are measured, the carbon dioxide peak areas are corrected by this value. This implies that the detection limit can be defined

CAST
Report on ¹⁴C release speciation from carbon steel under alkaline reducing conditions
(D2.7)

as 3 times the standard deviation of the blank values, which means that the carbon dioxide detection limit equals a peak area of 168×10^3 (3 times 56×10^3), corresponding to a concentration of $3 \mu\text{g/g}$.

Also it was noticed that sometimes a ‘ghost peak’ appears at the retention time of methane. To investigate this further, 15 blanks were taken over a period of two weeks. These blanks were taken directly from the gas bottle with pure nitrogen as well as from the glove bag in which the experimental setups are placed (glove bag filled with nitrogen). Evaluation of these blank measurements revealed no systematic difference between blanks from the bottle compared to blanks from the glove bag, and in blanks corresponding methane concentrations between 0 and $0.40 \mu\text{g/g}$ were found, with an average of $0.13 \mu\text{g/g}$ and a standard deviation of $0.10 \mu\text{g/g}$. As the average blank concentration (coming from the ghost peak) is very low and a ghost peak not always appears, correction for the blank is not advisable. However, the detection limit will be influenced by the (occasional) appearance of a ghost peak and can be taken as the average corresponding methane concentration plus three times the standard deviation of the blank measurements, thus $0.4 \mu\text{g/g}$.

The table below gives the reporting limits, which are taken as the maximum (rounded up) of the detection limits determined by means of the different methods.

	Reporting limits ($\mu\text{g/g}$)
Methane	0.4
Carbon dioxide	3
Ethene	0.2
Ethane	0.2
Propene	1.5
Propane	0.75

Remark concerning samples from the CAST project:

As samples in the framework of the CAST project are taken in a bag placed in a fume hood, that is flushed with pure nitrogen, a possible additional carbon dioxide contamination can occur when the nitrogen does not flush all air out of the bag. This was investigated by taking several samples (blanks) from the flushed bag and the results are given in the table below. From these data we can see that, apart from the first measurement, peak areas do not significantly differ from the ‘environmental/apparatus blank’ that is described above. So,

no additional correction seems needed. However, when it turns out that sample carbon dioxide concentrations around the reporting limit (3 µg/g) are important (depends on the outcome of the CAST experiments), further investigation is advised.

Date of measurement	Carbon dioxide peak area	Corresponding carbon dioxide concentration (µg/g) (*)
2017-01-18	521970	6
2017-01-19	183197	1
2017-02-06	256666	2
2017-02-07	205673	1
2017-02-08	157470	0
2017-02-14	122227	0

(*) Concentrations are calculated using the calibration curve described further in § 2 (peak areas are corrected for ‘environmental/apparatus blank’ of 180414 and concentrations are calculated using the corrected peak areas and an intercept of -57275 and a slope of 67721).

3. Linearity

Of each gas several standards with concentrations from the detection limit up to 10 µg/g were measured.

Different linear regression models were evaluated: unweighted, weighted with weights equal to 1/C (C = concentration) and weighted with weights equal to 1/C². From these evaluations, it appeared that the models with weights equal to 1/C gave the best results, so these will be used for further routine measurements.

In the following figures, the calibration curves are presented and in the tables below some regression statistics are given. From the graphs and the values of the residuals it can be concluded that for all gasses a linear relationship exists from the detection limit to 10 µg/g (when a regression with weights 1/C is used).

Note: All measured peak areas for carbon dioxide are corrected for the average blank (signal of 180 000, see §1). This means that peak areas from samples also have to be corrected for the blank, before the concentration is calculated by means of the calibration curve. For example, a carbon dioxide peak area in a sample of 500 000 corresponds to a concentration of 5.6 µg/g:

CAST

Report on ¹⁴C release speciation from carbon steel under alkaline reducing conditions

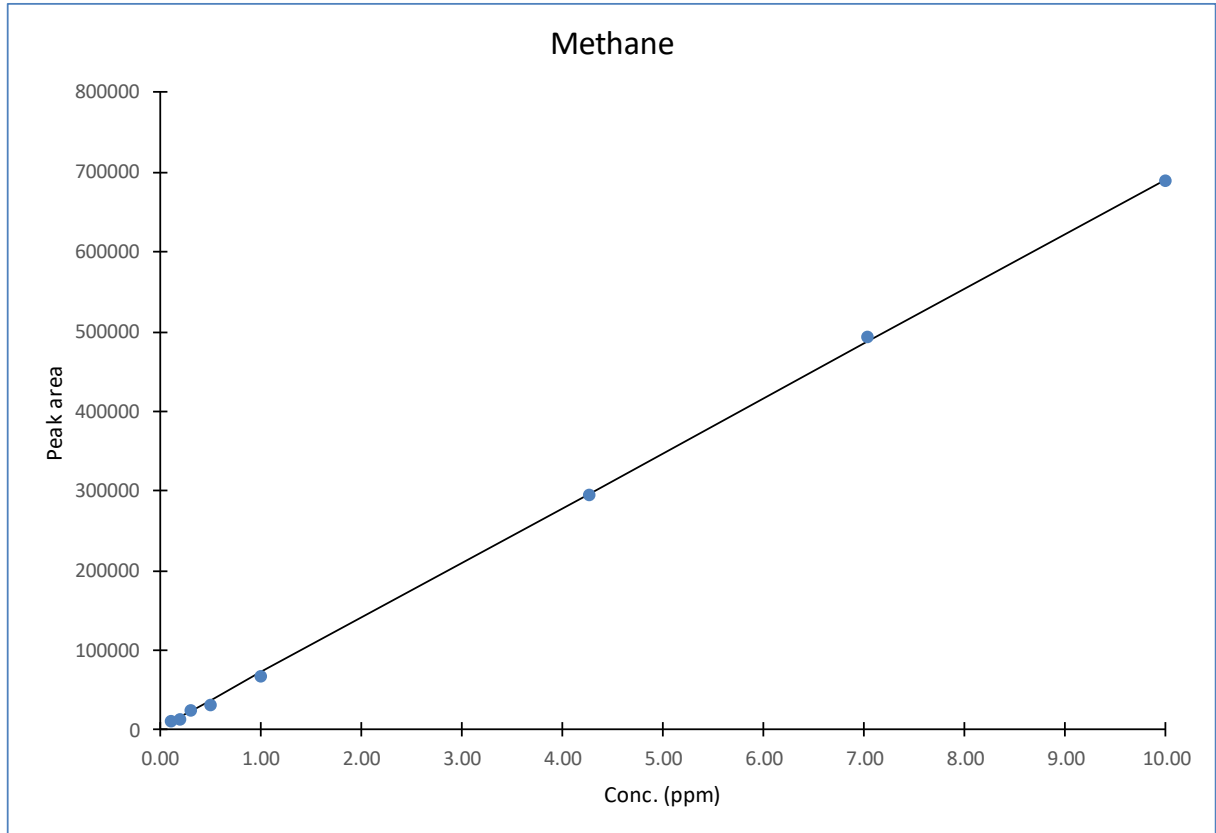
(D2.7)

$[(500\,000 - 180\,000) - (-57275)] / 67721 = 5.6$ (-57275 is the intercept of the calibration curve and 67721 the slope)

CAST

Report on ¹⁴C release speciation from carbon steel under alkaline reducing conditions

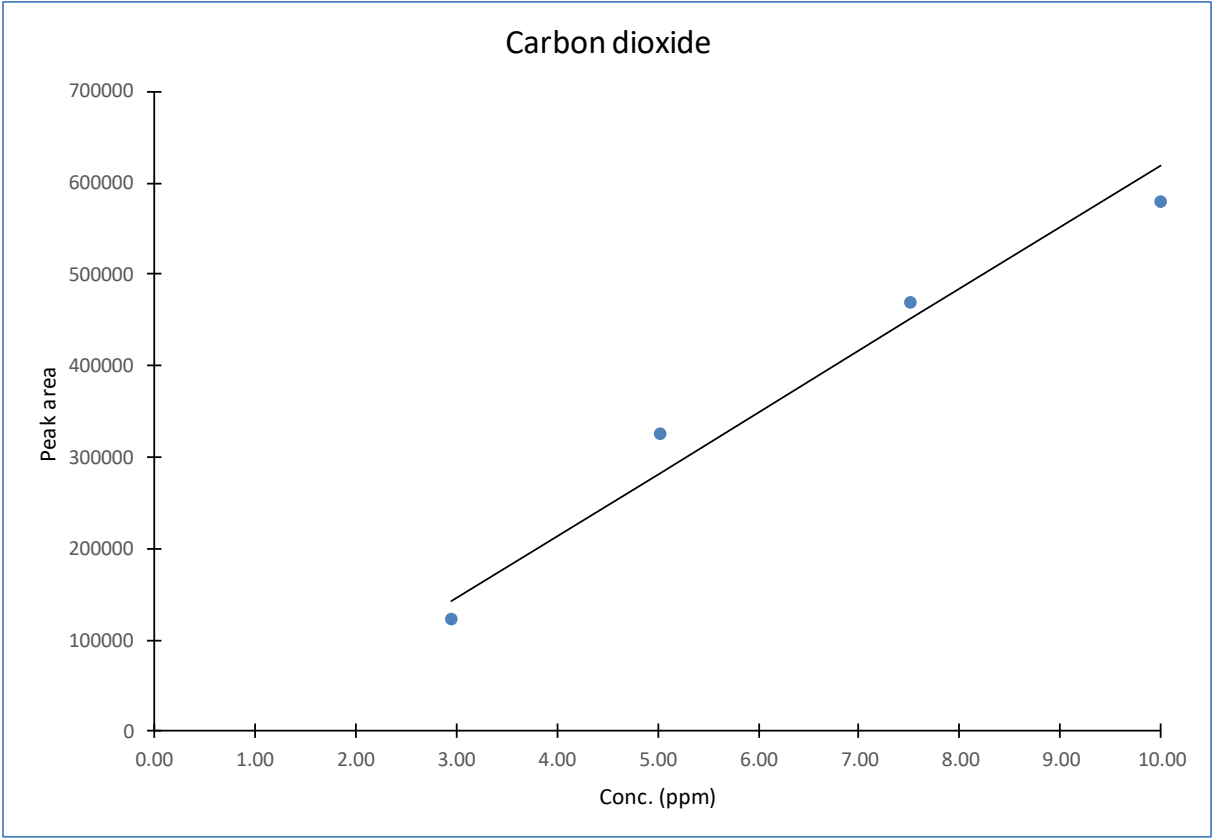
(D2.7)



Methane

Conc. (µg/g)	Measured peak area	Calculated conc.	Residual in µg/g	Residual in %
0.10	12397	0.13	0.03	34
0.20	14171	0.16	-0.04	-21
0.30	24625	0.31	0.02	5
0.50	32860	0.43	-0.07	-14
1.00	67962	0.94	-0.06	-6
4.27	296015	4.27	-0.01	0
7.04	495056	7.17	0.12	2
10.00	689973	10.01	0.01	0
Intercept	3233			
Slope	68640			

CAST
 Report on ¹⁴C release speciation from carbon steel under alkaline reducing conditions
 (D2.7)



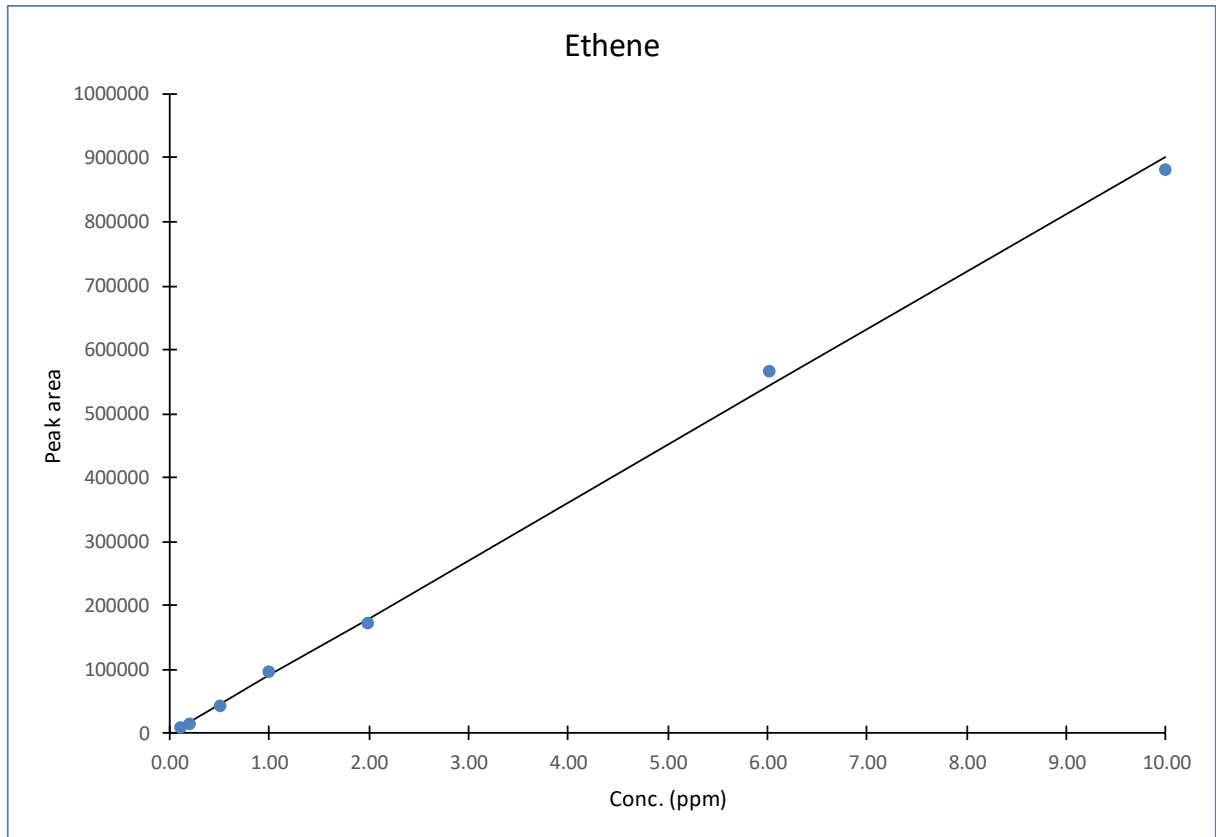
Carbon dioxide

Conc. (µg/g)	Measured peak area (corrected for blank)	Calculated conc.	Residual in µg/g	Residual in %
2.95	122174	2.65	-0.30	-10
5.03	326044	5.66	0.64	13
7.52	470022	7.79	0.27	4
10.00	579125	9.40	-0.60	-6
Intercept	-57275			
Slope	67721			

CAST

Report on ¹⁴C release speciation from carbon steel under alkaline reducing conditions

(D2.7)

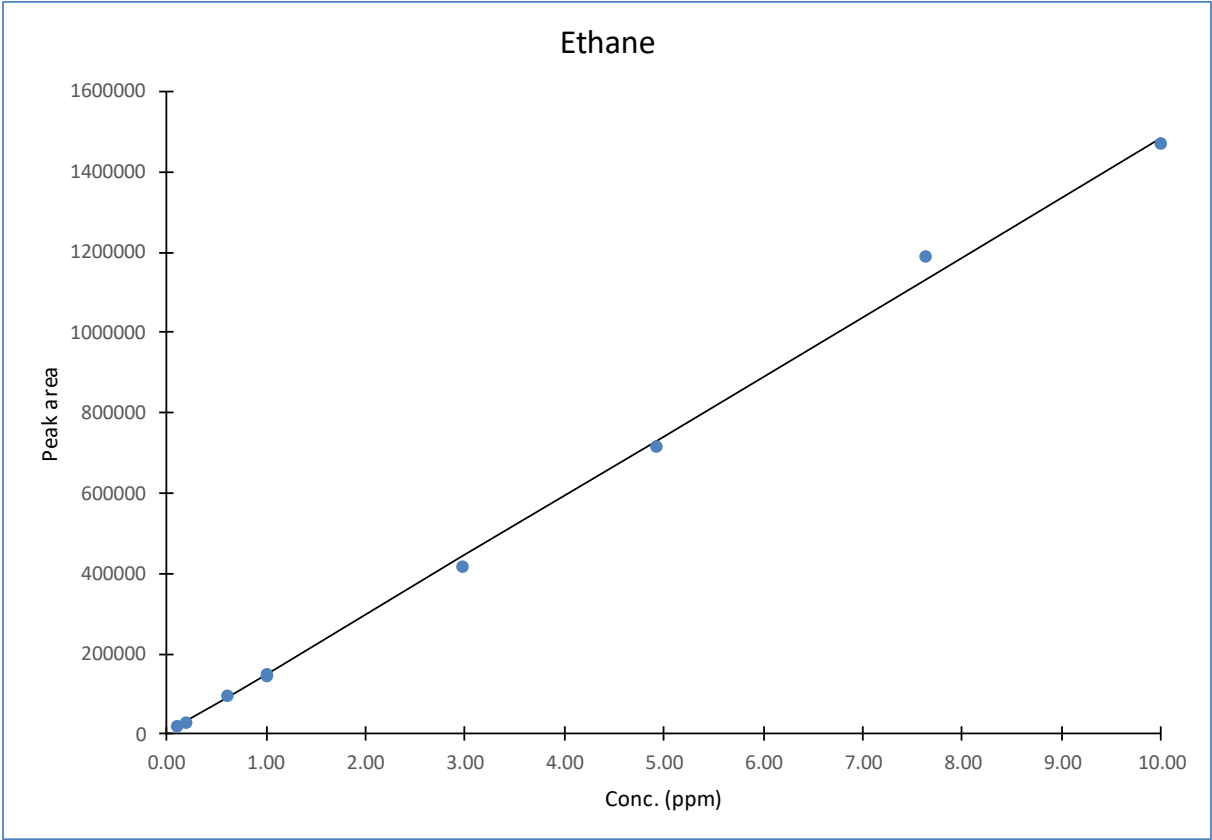


Ethene

Conc. (µg/g)	Measured peak area	Calculated conc.	Residual in µg/g	Residual in %
0.10	10485	0.11	0.01	14
0.20	15204	0.17	-0.03	-16
0.50	43173	0.48	-0.02	-4
1.00	96210	1.07	0.07	7
1.99	173095	1.92	-0.07	-3
6.02	566638	6.29	0.26	4
10.00	880847	9.77	-0.23	-2

Intercept	192
Slope	90093

CAST
 Report on ¹⁴C release speciation from carbon steel under alkaline reducing conditions
 (D2.7)



Ethane

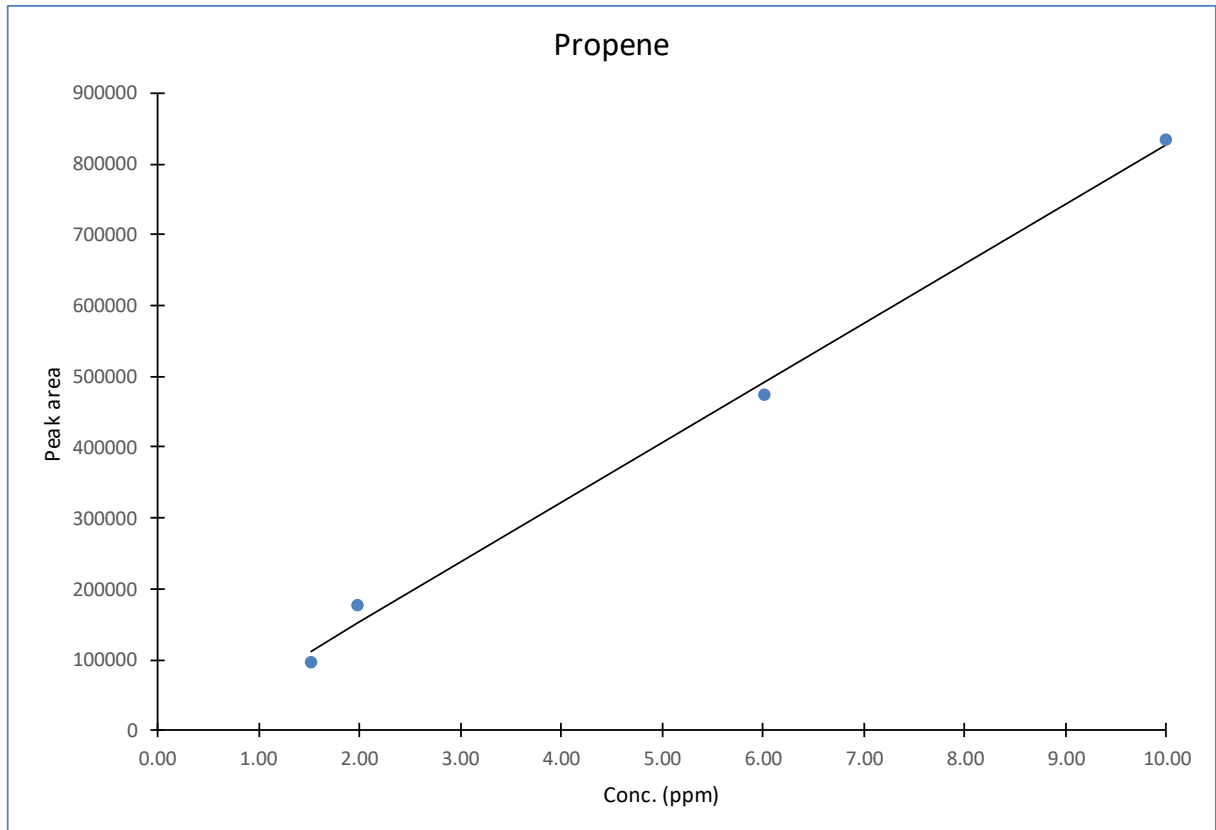
Conc. (µg/g)	Measured peak area	Calculated conc.	Residual in µg/g	Residual in %
0.10	19021	0.11	0.01	15
0.20	30038	0.19	-0.01	-7
0.61	92870	0.61	0.01	1
1.00	143101	0.95	-0.05	-5
1.00	147592	0.98	-0.02	-2
2.98	418263	2.81	-0.16	-5
4.93	717848	4.84	-0.09	-2
7.63	1189578	8.02	0.39	5
10.00	1469406	9.92	-0.08	-1

Intercept	2004
Slope	147990

CAST

Report on ^{14}C release speciation from carbon steel under alkaline reducing conditions

(D2.7)

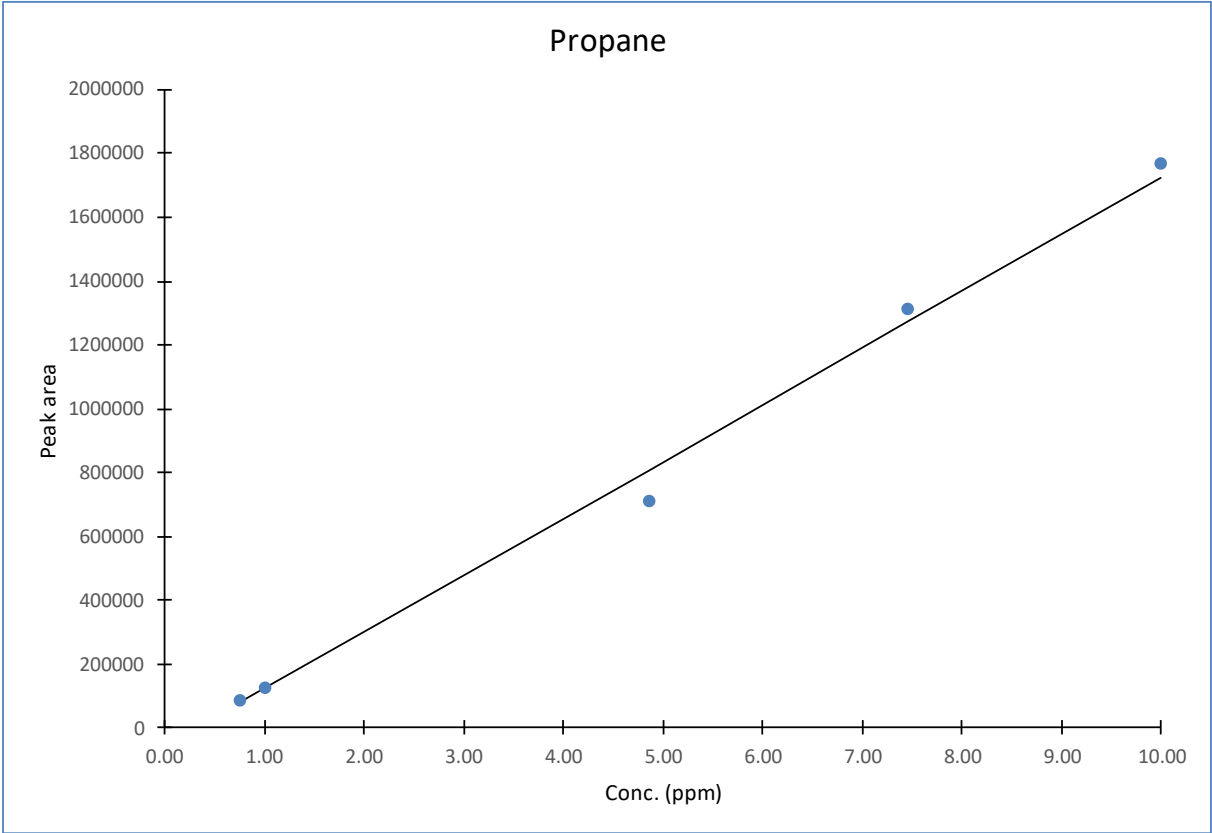


Propene

Conc. ($\mu\text{g/g}$)	Measured peak area	Calculated conc.	Residual in $\mu\text{g/g}$	Residual in %
1.53	96329	1.33	-0.20	-13
1.98	176171	2.28	0.30	15
6.02	474245	5.82	-0.20	-3
10.00	834735	10.10	0.10	1

Intercept	-15991
Slope	84238

CAST
Report on ¹⁴C release speciation from carbon steel under alkaline reducing conditions
(D2.7)



Propane

Conc. (µg/g)	Measured peak area	Calculated conc.	Residual in µg/g	Residual in %
0.76	86775	0.79	0.03	4
1.00	125659	1.01	0.01	1
4.85	709554	4.30	-0.56	-11
7.46	1314673	7.70	0.24	3
10.00	1770776	10.27	0.27	3
Intercept	-53835			
Slope	177640			

4. Measurement uncertainty

The calculated residuals (see § 3) can give us an idea of the measurement uncertainty: apart from one outlier (propane 4.85 $\mu\text{g/g}$), all residuals are less than or equal to one third of the reporting limit or 5 % of the concentration. So these values can be used as a (rough) estimate of the measurement uncertainty (95 % confidence interval).

The above applies to all gases, except to carbon dioxide at low concentrations (less than 40 $\mu\text{g/g}$) and methane at low concentrations (less than 4 $\mu\text{g/g}$):

- As the reporting limit of carbon dioxide is mainly determined by fluctuations in the 'environmental/apparatus blank', we need to take as measurement uncertainty for low concentrations a value of 2 times the standard deviation of the blank measurements, being 2 $\mu\text{g/g}$.
- As the reporting limit of methane is mainly determined by the occasional appearance of a ghost peak, we need to take as measurement uncertainty for low concentrations a value of 2 times the standard deviation of the methane concentrations that correspond to the peak areas of the ghost peak, being 0.2 $\mu\text{g/g}$.

Note: The procedure thus consists of calculating the value of 5 % of the concentration (in $\mu\text{g/g}$) and if this value is larger than 1/3 of the reporting limit (or 2 $\mu\text{g/g}$ for carbon dioxide and 0.2 $\mu\text{g/g}$ for methane), this is the measurement uncertainty. Else, the measurement uncertainty equals 1/3 of the reporting limit (or 2 $\mu\text{g/g}$ for carbon dioxide and 0.2 $\mu\text{g/g}$ for methane).

Example 1: In a sample an ethane peak area of 400 000 is measured. From the calibration is calculated that this peak area corresponds to a concentration of 2.69 $\mu\text{g/g}$. 5 % of 2.69 $\mu\text{g/g}$ is 0.13 $\mu\text{g/g}$, which is larger than 1/3 of the reporting limit of ethane (1/3 of the reporting limit is 0.07 $\mu\text{g/g}$). So, the measurement uncertainty is 0.13 $\mu\text{g/g}$ and the result is expressed as: 2.69 $\mu\text{g/g} \pm 0.13 \mu\text{g/g}$.

Example 2: In a sample a propene peak area of 200 000 is measured. From the calibration is calculated that this peak area corresponds to a concentration of 2.56 $\mu\text{g/g}$. 5 % of 2.56 $\mu\text{g/g}$ is 0.13 $\mu\text{g/g}$, which is lower than 1/3 of the reporting limit of propene (1/3 of the reporting limit is 0.5 $\mu\text{g/g}$). So, the measurement uncertainty is 0.5 $\mu\text{g/g}$ and the result is expressed as: 2.6 $\mu\text{g/g} \pm 0.5 \mu\text{g/g}$.

Example 3: In a sample a carbon dioxide peak area of 500 000 is measured. This value is corrected for the blank (180 000, see § 1), which gives a corrected peak area of 320 000. From the calibration is calculated that a (corrected) peak area of 320 000 corresponds to a concentration of 5.6 $\mu\text{g/g}$. 5 % of 5.6 $\mu\text{g/g}$ is 0.28 $\mu\text{g/g}$, which is lower than 2 $\mu\text{g/g}$. So, the measurement uncertainty is 2 $\mu\text{g/g}$ and the result is expressed as: 5.6 $\mu\text{g/g} \pm 2.0 \mu\text{g/g}$.

Important to remark is that the above derived measurement uncertainties strictly speaking only apply to standards (only measurements of standards were used). This however is the best we can do: determination of the measurement uncertainties for real samples requires at least multiple measurements of the same samples, which is impossible as we have very little amounts of the real samples. On the other hand, because it is known that in gas chromatography matrix effects are very limited, the measurement uncertainties of standards can be considered as representative for real samples (to a certain extent).

Appendix 3. Corrosion rate calculation from the I vs. t plot

Hypotheses:

- All the recorded current come from the corrosion of the carbon steel sample
- Only the oxydation of Fe^o in Fe²⁺ is considered

Taking into account:

Parameter	Parameter symbol	Values
Corrosion time, unirradiated carbon steel	$t_{\text{corr,unirr}}$	516210 seconds
Corrosion time, irradiated carbon steel	$t_{\text{corr,irr}}$	603000 seconds
Density of carbon steel	ρ_{CS}	7.77 g/cm ³
Mean specific surface of unirradiated Carbon Steel	$A_{\text{corr,unirr}}$	1.96 cm ²
Mean specific surface of irradiated Carbon Steel	$A_{\text{corr,irr}}$	0.6 cm ²
Molecular weight	MM_{Fe}	55.845 g/mol
Avogadro number	N_{A}	$6.023 \times 10^{23} \text{ mol}^{-1}$

Unirradiated carbon steel sample

Thanks to the potentiostatic I vs. t plot, the mean current ($\langle I \rangle$) was calculated:

$$\langle I \rangle = 2.5 \times 10^{-5} \text{ A}$$

Knowing the corrosion time ($t_{\text{corr,unirr}}$), it is possible to calculate the total charge (Q):

$$Q = \langle I \rangle \times t_{\text{corr,unirr}} = 2.5 \times 10^{-5} \times 516210 = 12.98 \text{ C}$$

Knowing that 1C is equivalent to the charge of approximately 6.2415×10^{18} electrons, the number of electrons involved (N_{e^-}) is:

$$N_{e^-} = Q \times 6.2415 \times 10^{18} = 12.98 \times 6.2415 \times 10^{18} = 8.1 \times 10^{19} e^-$$

Two electrons are involved in the corrosion of one atom of iron ($\text{Fe}^0 \rightarrow \text{Fe}^{2+} + 2\text{e}^-$). So, the number of iron atoms involved (N_{Fe}) is:

$$N_{\text{Fe}} = N_{\text{e}^-} / 2 = 8.1 \times 10^{19} / 2 = 4.1 \times 10^{19} \text{ iron atoms}$$

And the number of mol of iron (n_{Fe}) is:

$$n_{\text{Fe}} = N_{\text{Fe}} / N_{\text{A}} = 4.1 \times 10^{19} / 6.023 \times 10^{23} = 6.7 \times 10^{-5} \text{ mol of Fe}$$

Making the approximation that the carbon steel is only composed of iron, the weight of corroded carbon steel (W_{CS}) is:

$$\begin{aligned} W_{\text{CS}} &= n_{\text{Fe}} \times \text{MM}_{\text{Fe}} = 6.7 \times 10^{-5} \times 55.845 = 3.8 \times 10^{-3} \text{ g of iron} \\ &= 3.8 \times 10^{-3} \text{ g of carbon steel} \end{aligned}$$

Finally, knowing the specific surface of carbon steel ($A_{\text{corr,unirr}}$) and the carbon steel density (ρ_{CS}), the corrosion depth (Corr. Depth) is:

$$\text{Corr. Depth} = (W_{\text{CS}} / \rho_{\text{CS}}) / A_{\text{corr}} = (3.8 \times 10^{-3} / 7.77) / 1.96 = 2.4 \times 10^{-4} \text{ cm} = 2.4 \text{ } \mu\text{m}$$

And the corrosion rate (per year) is:

$$2.4 / 516210 \times (365.25 \times 24 \times 60 \times 60) = \mathbf{150.8 \text{ } \mu\text{m/year}}$$

Irradiated carbon steel sample

The same calculation was made for the corrosion of the irradiated carbon steel sample and the corrosion rate is **63.4 $\mu\text{m/year}$** .

Clearly, the main part of the recorded current during the accelerated corrosion tests came from the water hydrolysis.

Appendix 4. Corrosion rate calculation from the carbon-based gas production during the leaching tests

Hypotheses:

- All the carbon is used to form methane, ethene or ethane during corrosion.
- The carbon is homogeneously present in the bulk

Taking into account:

Parameter	Parameter symbol	Values
Concentration of carbon in Carbon Steel	C_{content}	0.1-0.17 wt.%
Density of Carbon Steel	$\rho_{\text{C-Steel}}$	7.77 g/cm ³
Density of methane	ρ_{CH_4}	6.56 x10 ⁻⁴ g/cm ³
Density of ethene	$\rho_{\text{C}_2\text{H}_4}$	1.18 x10 ⁻³ g/cm ³
Density of ethane	$\rho_{\text{C}_2\text{H}_6}$	1.36 x10 ⁻³ g/cm ³
Mean specific surface of Carbon Steel	A_{corr}	1.98 cm ²
Head Space volume	V_{HS}	15 cm ³
Molecular weight of methane	MW_{CH_4}	16.043 g/mol
Molecular weight of ethene	$MW_{\text{C}_2\text{H}_4}$	28.054 g/mol
Molecular weight of ethane	$MW_{\text{C}_2\text{H}_6}$	30.07 g/mol
Molecular weight of carbon	MW_{C}	12.011 g/mol
Mean concentration of methane	C_{CH_4}	10.44 µg/g (µL/L)
Mean concentration of ethene	$C_{\text{C}_2\text{H}_4}$	1.74 µg/g (µL/L)
Mean concentration of ethane	$C_{\text{C}_2\text{H}_6}$	0.63 µg/g (µL/L)

Calculation:

Methane:

The volume of methane (V_{CH_4}) produced during corrosion equals:

$$V_{\text{CH}_4} = C_{\text{CH}_4} \times V_{\text{HS}} = 10.44 \times 0.015 = 0.157 \mu\text{L} = 1.57 \times 10^{-4} \text{ cm}^3$$

But knowing the density of methane (ρ_{CH_4}), the weight of methane (W_{CH_4}) produced equals:

$$W_{\text{CH}_4} = V_{\text{CH}_4} \times \rho_{\text{CH}_4} = 1.57 \times 10^{-4} \times 6.56 \times 10^{-4} = 1.03 \times 10^{-7} \text{ g}$$

Which correspond to a number of moles (n_{CH_4}) of:

$$n_{\text{CH}_4} = W_{\text{CH}_4} / MW_{\text{CH}_4} = 1.03 \times 10^{-7} / 16.043 = 6.42 \times 10^{-9} \text{ moles of CH}_4 = 6.42 \times 10^{-9} \text{ moles of carbon}$$

Ethene:

The volume of ethene ($V_{\text{C}_2\text{H}_4}$) produced during corrosion equals:

$$V_{\text{C}_2\text{H}_4} = C_{\text{C}_2\text{H}_4} \times V_{\text{HS}} = 1.74 \times 0.015 = 0.0261 \mu\text{L} = 2.61 \times 10^{-5} \text{ cm}^3$$

But knowing the density of ethene ($\rho_{\text{C}_2\text{H}_4}$), the weight of ethene ($W_{\text{C}_2\text{H}_4}$) produced equals:

$$W_{\text{C}_2\text{H}_4} = V_{\text{C}_2\text{H}_4} \times \rho_{\text{C}_2\text{H}_4} = 2.61 \times 10^{-5} \times 1.18 \times 10^{-3} = 3.08 \times 10^{-8} \text{ g}$$

Which corresponds to a number of mole ($n_{\text{C}_2\text{H}_4}$) of:

$$n_{\text{C}_2\text{H}_4} = W_{\text{C}_2\text{H}_4} / MW_{\text{C}_2\text{H}_4} = 3.08 \times 10^{-8} / 28.054 = 1.098 \times 10^{-9} \text{ moles of C}_2\text{H}_4 = 2.196 \times 10^{-9} \text{ moles of carbon}$$

Ethane:

The volume of ethane ($V_{\text{C}_2\text{H}_6}$) produced during corrosion equals:

$$V_{\text{C}_2\text{H}_6} = C_{\text{C}_2\text{H}_6} \times V_{\text{HS}} = 0.63 \times 0.015 = 0.00945 \mu\text{L} = 9.45 \times 10^{-6} \text{ cm}^3$$

But knowing the density of ethane ($\rho_{\text{C}_2\text{H}_6}$), the weight of ethane ($W_{\text{C}_2\text{H}_6}$) produced equals:

$$W_{\text{C}_2\text{H}_6} = V_{\text{C}_2\text{H}_6} \times \rho_{\text{C}_2\text{H}_6} = 9.45 \times 10^{-6} \times 1.36 \times 10^{-3} = 1.285 \times 10^{-8} \text{ g}$$

Which corresponds to a number of mole ($n_{\text{C}_2\text{H}_6}$) of:

$n_{\text{C}_2\text{H}_6} = W_{\text{C}_2\text{H}_6} / MW_{\text{C}_2\text{H}_6} = 1.285 \times 10^{-8} / 30.07 = 4.274 \times 10^{-10}$ moles of $\text{C}_2\text{H}_6 = 8.548 \times 10^{-10}$ moles of carbon

Taking into account the above calculations, the total amount of mole of carbon released (C_{released}) is:

$C_{\text{released}} = n_{\text{CH}_4} + n_{\text{C}_2\text{H}_4} + n_{\text{C}_2\text{H}_6} = 6.42 \times 10^{-9} + 2.196 \times 10^{-9} + 8.548 \times 10^{-10} = 9.47 \times 10^{-9}$ moles

Considering the molecular weight of carbon (MW_C), it is possible to calculate the weight of carbon released (W_C)

$W_C = C_{\text{released}} \times MW_C = 9.47 \times 10^{-9} \times 12.011 = 1.138 \times 10^{-7} \text{ g} = 113.8 \text{ ng}$

And with the concentration of carbon in the carbon steel bulk (C_{content}), it is possible to calculate the weight of corroded steel ($W_{\text{CS-corr}}$):

$W_{\text{CS-corr}} = W_C / C_{\text{content}} = 1.138 \times 10^{-7} / 0.1 \% = 1.138 \times 10^{-4} \text{ g} = 113.8 \text{ }\mu\text{g}$

or $= 1.138 \times 10^{-7} / 0.17 \% = 6.69 \times 10^{-5} \text{ g} = 66.9 \text{ }\mu\text{g}$

Finally, knowing the specific surface of carbon steel (A_{corr}) and the carbon steel density ($\rho_{\text{C-Steel}}$), the corrosion depth (Corr. Depth) after 231 days is:

$\text{Corr. Depth} = (W_{\text{CS-corr}} / \rho_{\text{C-Steel}}) / A_{\text{corr}} = (6.69 \times 10^{-5} / 7.77) / 1.98 = 4.35 \times 10^{-6} \text{ cm} = 43.5 \text{ nm}$

or $= (1.138 \times 10^{-4} / 7.77) / 1.98 = 7.40 \times 10^{-6} \text{ cm} = 74.0 \text{ nm}$

And the corrosion rate (per year) is:

$43.5 / 231 \times 365 = \mathbf{68.7 \text{ nm/year}}$

$74.0 / 231 \times 365 = \mathbf{117.0 \text{ nm/year}}$

These corrosion rate values are in the range of 0.1 $\mu\text{m/year}$ of expected corrosion rate calculated by Kursten et al. [KURSTEN, 2014].

Appendix 5. Total inorganic / organic carbon content and ion chromatography results

Table A5-1 and A5-2 present the results of respectively the total inorganic / organic carbon content and the concentration of carboxylic acids (formate, acetate and oxalate) realised on blank electrolytes and on all leachate solutions after static and accelerated corrosion tests without subtraction of the blank values.

Table A5-1. Results from total organic / inorganic carbon analysis of blank electrolytes and the carbon steel leachates.

Sample-ID	Electrolyte/Material	TIC		TOC	
		mg/L	mmol/L	mg/L	mmol/L
Blank-Ca(OH) ₂	Saturated portlandite water solution	6.4 ± 0.8	0.53 ± 0.07	4.4 ± 0.5	0.37 ± 0.04
Blank-CaCl ₂	Saturated Ca(OH) ₂ water solution + 0.5 M CaCl ₂	7.4 ± 0.7	0.62 ± 0.06	7.4 ± 0.7	0.62 ± 0.06
Inactive-CS_ Ca(OH) ₂	Unirradiated Carbon Steel / Polarised test / Ca(OH) ₂ water solution	5.1 ± 0.5	0.42 ± 0.04	8.5 ± 0.8	0.71 ± 0.07
Inactive-CS_ CaCl ₂	Unirradiated Carbon Steel / Polarised test / Ca(OH) ₂ + CaCl ₂ water solution	18.5 ± 0.5	1.54 ± 0.04	14.5 ± 1.4	1.21 ± 0.12
Active-CS_ Ca(OH) ₂	Irradiated Carbon Steel / Polarised test / Ca(OH) ₂ water solution	< 0.5	-	27.2 ± 2.8	2.26 ± 0.23
Active-CS_ CaCl ₂	Irradiated Carbon Steel / Polarised test / Ca(OH) ₂ + CaCl ₂ water solution	< 0.5	-	1.5 ± 0.5	0.12 ± 0.04
Sol-CS-A	Irradiated Carbon Steel / Leaching test / Ca(OH) ₂ water solution	< 0.5	-	1.6 ± 0.5	0.13 ± 0.04
Sol-CS-B	Irradiated Carbon Steel / Leaching test / Ca(OH) ₂ water solution	< 0.5	-	1.6 ± 0.5	0.13 ± 0.04
Sol-CS-C	Irradiated Carbon Steel / Leaching test / Ca(OH) ₂ water solution	< 0.5	-	1.9 ± 0.5	0.16 ± 0.04

Table A5-2. Carboxylic acid content analysis by ion chromatography results of the carbon steel leachates and blank electrolytes.

Sample ID	Electrolyte / Material	Formate		Acetate		Oxalate	
		mg/L	mmol/L	mg/L	mmol/L	mg/L	mmol/L
Blank-Ca(OH) ₂	Saturated portlandite water solution	0.16	3.55 x10 ⁻³	0.14	2.37 x10 ⁻³	< 0.1	-
Blank-CaCl ₂	Saturated Ca(OH) ₂ water solution + 0.5 M CaCl ₂	< 0.1	-	< 0.1	-	< 0.1	-
Inactive-CS_ Ca(OH) ₂	Unirradiated Carbon Steel / Polarised test / Ca(OH) ₂ water solution	0.40	8.89 x10 ⁻³	0.19	3.22 x10 ⁻³	< 0.1	-
Inactive-CS_ CaCl ₂	Unirradiated Carbon Steel / Polarised test / Ca(OH) ₂ + CaCl ₂ water solution	< 0.1	-	< 0.1	-	< 0.1	-
Active-CS_ Ca(OH) ₂	Irradiated Carbon Steel / Polarised test / Ca(OH) ₂ water solution	0.10	2.22 x10 ⁻³	< 0.1	-	< 0.1	-
Active-CS_ CaCl ₂	Irradiated Carbon Steel / Polarised test / Ca(OH) ₂ + CaCl ₂ water solution	< 0.1	-	< 0.1	-	< 0.1	-
Sol-CS-A	Irradiated Carbon Steel / Leaching test / Ca(OH) ₂ water solution	< 0.1	-	< 0.1	-	< 0.1	-
Sol-CS-B	Irradiated Carbon Steel / Leaching test / Ca(OH) ₂ water solution	0.11	2.44 x10 ⁻³	< 0.1	-	< 0.1	-
Sol-CS-C	Irradiated Carbon Steel / Leaching test / Ca(OH) ₂ water solution	< 0.1	-	0.31	5.25 x10 ⁻³	< 0.1	-